

REVIEW ARTICLE

Few-body physics with ultracold atomic and molecular systems in traps

D. Blume

Department of Physics and Astronomy, Washington State University, Pullman,
Washington 99164-2814, USA

Abstract. Few-body physics has played a prominent role in atomic, molecular and nuclear physics since the early days of quantum mechanics. It is now possible—thanks to tremendous progress in cooling, trapping, and manipulating ultracold samples—to experimentally study few-body phenomena in trapped atomic and molecular systems with unprecedented control. This review summarizes recent studies of few-body phenomena in trapped atomic and molecular gases, with an emphasis on small trapped systems. We start by introducing the free-space scattering properties and then investigate what happens when two particles, bosons or fermions, are placed in an external confinement. Next, various three-body systems are treated analytically in limiting cases. Our current understanding of larger two-component Fermi systems and Bose systems is reviewed, and connections with the corresponding bulk systems are established. Lastly, future prospects and challenges are discussed. Throughout this review, commonalities with other systems such as nuclei or quantum dots are highlighted.

PACS numbers: 34.50.-s,67.85.-d

1. Introduction

Although few-body physics plays an important role in all or nearly all branches of physics, few-body phenomena are often only covered briefly, if at all, in a typical undergraduate or graduate core curriculum. Only selected few-body problems such as the celestial three-particle Kepler problem and the quantum mechanical treatment of the helium atom, which becomes a three-body problem if the nucleus is treated as a point-particle, can be found in modern textbooks. One of the reasons is that few-body problems do not, in general, reduce to an effective one-body problem. Instead, the dynamics typically depend in non-trivial ways on all or nearly all degrees of freedom, making the analytical and numerical treatment of few-body systems in many cases challenging. This review discusses few-body aspects of trapped atomic and molecular Bose and Fermi gases, which are ideal model systems with which to study few-body physics. These systems exhibit a variety of few-body phenomena that are amenable to analytical treatments and that can, in certain cases, even be interpreted within an effective one-body framework despite the presence of strong interactions and multiple degrees of freedom.

Degenerate Bose and Fermi gases are nowadays being produced routinely in laboratories all over the world. Most experimental set-ups work with alkali atoms (Li [1, 2], Na [3], K [4, 5], Rb [6, 7], Cs [8]), which have one outer valence electron. At ultracold temperatures, i.e., in the regime where the de Broglie wave length λ_{dB} is larger than the range r_0 of the two-body interaction potential, the interactions of the atomic gas are dominated by isotropic s -wave collisions. The net effect of an s -wave collision can be parametrized through the s -wave scattering length $a_0(0)$, which, in many instances, is the only microscopic parameter that enters into the description of larger systems [9, 10]. A well-known example of this type of description is the mean-field Gross-Pitaevskii equation [11, 12, 13, 14, 15], which depends on the product of the number of particles N (or more precisely, $N - 1$ [16]) and the s -wave scattering length $a_0(0)$. The Gross-Pitaevskii equation has been proven to predict accurately a variety of aspects of dilute bosonic gases, including a mechanical instability for negative $a_0(0)$. Besides alkalis, atoms with a more complicated valence electron structure such as Ca [17], He* [18, 19], Cr [20], Yb [21, 22] and Sr [23, 24] have been condensed. The atom-atom collisions between two Cr atoms, e.g., are anisotropic and long-ranged [25, 26]. These characteristics give rise to exciting beyond s -wave physics that depends on the strength of the dipole moment in addition to the s -wave scattering length [25, 26].

This review summarizes our current understanding of trapped few-atom systems that interact through isotropic short-range potentials. The quantized energy spectrum of the trapped system is the result of the interplay of the particle-particle interactions and the external trapping geometry. In fact, the external confinement can be viewed as quantizing the scattering continuum that is characteristic for the free-space system. Experimentally, trapped few-particle systems can be realized by loading so-called microtraps with just a few particles [27]. Alternatively, arrays of few-particle systems can be realized by loading a deep optical lattice, i.e., an optical lattice where tunneling between different lattice sites is strongly suppressed and where nearest-neighbor interactions can be neglected, with multiple atoms per lattice site [28, 29, 30].

A distinct characteristic of cold atom systems is that the atom-atom interactions can be tuned through the application of an external magnetic field in the vicinity of a Fano-Feshbach resonance [31]. A Fano-Feshbach resonance occurs when the two-body

energy of a closed channel molecule coincides with the scattering threshold of the open channel. Fano-Feshbach resonances in ultracold atomic gases were first observed experimentally in 1998 [32, 33, 34]. Their existence paves the way to perform detailed comparisons between theory and experiment as a function of the interaction strength.

Trapped few-atom systems—together with quantum dots, nuclei, atomic and molecular clusters, and certain nano-particles—fall into the category of mesoscopic systems. Quite generally, the study of mesoscopic systems provides a bridge between the microscopic and macroscopic worlds. This review discusses several links between small and large systems, and illustrates how the treatment of mesoscopic systems can provide an interpretation of the physics of large systems that is complementary to that derived within effective many-body frameworks. In this context, two-component Fermi gases with infinitely large s -wave scattering length provide a particularly rich example [35, 36, 37, 38, 39]. In this system, the underlying two-body interactions do not define a meaningful length scale, thereby making the system scale invariant. This scale invariance implies that the few-body system and the many-body system share the same or related universal features [40, 41, 42, 43, 44]. Moreover, the scale invariance implies that atomic two-component Fermi gases share certain characteristics with nuclear and neutron matter, despite the fact that the typical energy and length scales of these systems are vastly different.

A particularly interesting few-body phenomenon, which is discussed in Subsecs. 3.3, 4.3 and 5.3, is the Efimov effect. In the early 1970s, Vitaly Efimov [45, 46, 47] considered a two-body system in free space with infinitely large s -wave scattering length that supports exactly one zero-energy bound state and no other weakly-bound states. Efimov found the surprising and, at first sight, counterintuitive result that the corresponding three-body system, obtained by adding a third particle and assuming pairwise interactions, supports infinitely many weakly-bound three-body states. Efimov's prediction, known as the three-body Efimov effect, stimulated much theoretical and experimental efforts [48, 49], and continues to be one of the flagships of few-body physics today. Signatures of the three-body Efimov effect and associated Efimov resonances have been searched for in the helium trimer [50] and in nuclear systems [51], among others. However, it was not till recently that the three-body Efimov effect has been confirmed conclusively experimentally via loss measurements of cold trapped atomic gases [52, 53, 54, 55, 56, 57, 58, 59]. This review summarizes the key features of the Efimov effect, or more generally of Efimov physics, and its modifications when the three-body system is placed in an external trap. Extensions of the Efimov scenario to larger systems are also considered.

The present review article aims at providing an introduction to the field of trapped few-atom and few-molecule systems. Readers who would like to place this topic into a broader context are directed to a number of other review articles. Experimental and theoretical aspects of cold and ultracold collisions have been reviewed by Weiner *et al.* in 1999 [60]. The topic of Fano-Feshbach resonances has been reviewed by Chin *et al.* in 2010 [31] (see also Refs. [61, 62]). The Efimov effect in free-space has been reviewed by Braaten and Hammer in 2006 and 2007 [48, 49]. A related “Trend” was authored by Ferlaino and Grimm [63], and a Physics Today article by Greene [64] in 2010. The broad subjects of Bose and Fermi gases are covered in reviews by Dalfovo *et al.* from 1998 [15] and Giorgini *et al.* from 2008 [39], respectively. Many-body aspects of cold atom gases have been reviewed by Bloch *et al.* in 2008 [65]. Various reviews have focused on specific few-body systems: Jensen *et al.* discuss the physics of halo systems [66], Carlson and Schiavilla that of few-nucleon systems [67], Reiman

et al. that of vortices in few-particle droplets [68], and Nielsen *et al.* that of three-body systems with short-range interactions [69]. Lastly, the treatment of few-particle systems within the hyperspherical framework, which is utilized at various places in the present work, has been reviewed by Lin in 1995 [70] and Rittenhouse *et al.* in 2011 [71].

The remainder of this article is structured as follows. Section 2 discusses the underlying two-body physics, both without and with confinement, while Sec. 3 considers the physics of three interacting particles under external spherically symmetric confinement. Section 4 discusses various aspects of trapped Fermi gases, focusing primarily on *s*-wave interacting two-component Fermi gases. Section 5 summarizes the key characteristics of *s*-wave interacting Bose gases under external confinement. Lastly, Sec. 6 comments on a number of present and future frontiers.

2. Underlying two-body physics

2.1. Free-space two-particle scattering in three-dimensional space

This subsection considers the two-particle system in free space while the next subsection treats the trapped two-particle system. For two neutral atoms, the two-body potential at large interparticle distances r is dominated by the van der Waals tail that falls off as $-C_6/r^6$ (C_6 denotes the van der Waals coefficient). The characteristic length or range l_{char} of the two-body interaction potential is defined as the distance at which the kinetic and potential energies are approximately equal, $l_{\text{char}} = (2\mu C_6/\hbar^2)^{1/4}$ [60], where μ denotes the reduced mass of the two interacting particles. For alkali atoms, l_{char} is of the order of $100a_{\text{bohr}}$, where a_{bohr} denotes the Bohr radius, $a_{\text{bohr}} = 5.292 \times 10^{-11}m$.

The potentials that describe diatomic alkali systems support many two-body bound states in free space. For example, the number of vibrational bound states in the rotational ground state is respectively 66 and 16 for the electronic ground and excited state $X^1\Sigma_g^+$ and $a^3\Sigma_u^+$ potential curves of $^{23}\text{Na}_2$ [72]. Throughout this review, we are concerned with the low-temperature regime, i.e., we are interested in physics that occurs at energy scales that are much smaller than E_{char} , where $E_{\text{char}} = \hbar^2/(2\mu l_{\text{char}}^2)$, or equivalently, length scales that are much larger than l_{char} . This includes at most a few weakly-bound two-body states as well as the energetically low-lying scattering continuum (or “quantized scattering continuum”) but excludes deeply bound two-body states and the high-energy scattering continuum. Generally speaking, the low-energy physics is independent of the details of the underlying two-body potential and is determined by a few parameters such as the two-body scattering length and the effective range. Thus, low-energy phenomena can be described by replacing the true or full interaction potential by a model potential that is characterized by the same parameters as the true potential (e.g., the same scattering length and effective range), or by effective theories such as an effective range expansion approach or an effective field theory approach. Effective range and effective field theory approaches have been applied to a variety of systems, ranging from the scattering of atoms at ultracold temperatures [48] to the low-energy scattering of two nucleons in free-space [73] and on a lattice [74, 75, 76] to the description of particle physics phenomena such as narrow charmonium resonances [77]. The effective pseudopotential description, frequently employed in this review, goes back to Fermi, who treated the scattering between slow neutrons and hydrogen atoms [78].

In the following, we assume that the two particles of mass m_1 and m_2 (with position vectors \vec{r}_1 and \vec{r}_2) interact through a spherically symmetric two-body potential $V_{\text{tb}}(r)$, where r denotes the distance coordinate between the two particles, $r = |\vec{r}_1 - \vec{r}_2|$. Separating off the center-mass degrees of freedom, the relative scattering wave function $\psi_k(\vec{r})$ can be decomposed into partial waves, $\psi_k(\vec{r}) = \sum_l R_{lk}(r) P_l(\vartheta)$, where ϑ denotes the polar angle and P_l the Legendre polynomial of degree l .

Asymptotically, i.e., in the regime where the interaction potential can be neglected, the radial wave functions are given by [79]

$$R_{lk}^{\text{out}}(r) = N_l(k) \{j_l(kr) - \tan[\delta_l(k)] n_l(kr)\}, \quad (1)$$

where k is related to the scattering energy E through $k = \sqrt{2\mu E}/\hbar$ and where j_l and n_l denote the spherical Bessel function and the Neumann function, respectively. In the small kr limit, $j_l(kr)$ and $n_l(kr)$ behave as $(kr)^l$ and $(kr)^{-(l+1)}$, respectively [79]. Correspondingly, j_l and n_l are referred to as regular and irregular solutions. In Eq. (1), $N_l(k)$ denotes a normalization constant. The scattering phase shifts $\delta_l(k)$ are determined by matching the asymptotic solution $R_{lk}^{\text{out}}(r)$, Eq. (1), to the inner solution $R_{lk}^{\text{in}}(r)$, which depends on the details of the potential $V_{\text{tb}}(r)$. The phase shifts accumulate in the inner region and quantify the admixture of the irregular solutions $n_l(kr)$. A vanishing phase shift δ_l indicates an effectively non-interacting system, i.e., the asymptotic solution of the l^{th} partial wave channel is identical to that of the corresponding non-interacting system (differences can exist, though, in the inner region). A small positive phase shift indicates that the asymptotic solution of the l^{th} partial wave channel is shifted to smaller kr (“pulled inward”) compared to that of the non-interacting system, thus indicating an effectively attractive interaction. A small negative phase shift, in contrast, indicates that the asymptotic solution of the l^{th} partial wave channel is shifted to larger kr (“pushed outward”) compared to that of the non-interacting system, thus indicating an effectively repulsive interaction. The phase shifts $\delta_l(k)$ can be used to define the energy-dependent generalized scattering lengths $a_l^{2l+1}(k)$ [79] (note that the opposite sign convention is sometimes employed in nuclear and particle physics),

$$a_l^{2l+1}(k) = -\frac{\tan[\delta_l(k)]}{k^{2l+1}}. \quad (2)$$

For short-range potentials, i.e., for potentials that fall off faster than $1/r^{2l+3}$ asymptotically, the energy-dependent scattering lengths approach a constant in the zero-range limit [60], $a_l^{2l+1}(0) = \lim_{k \rightarrow 0} a_l^{2l+1}(k)$ (for long-range potentials, see Subsec. 2.3). For the lowest partial wave, i.e., for $l = 0$, $a_0(0)$ is the usual s -wave scattering length, which dominates, away from higher partial wave resonances, the low-energy cross sections of bosonic gases, two-component Fermi gases and Bose-Fermi mixtures. In the zero-energy limit, the scaled outside wave function $rR_{00}^{\text{out}}(r)$ becomes $N_0(0) [r - a_0(0)]$. The leading-order energy-dependence of the s -wave scattering length can be written in terms of the effective range r_{eff} [79],

$$\frac{1}{a_0(k)} \approx \frac{1}{a_0(0)} - \frac{1}{2} r_{\text{eff}} k^2; \quad (3)$$

the validity of Eq. (3) requires that the potential falls off faster than $1/r^{2l+5}$ asymptotically. For identical fermions, the Pauli exclusion principle forbids s -wave scattering, making the p -wave channel with generalized scattering length or scattering volume $a_1^3(k)$ dominant.

Figure 1 illustrates the behavior of the scattering lengths and wave functions for

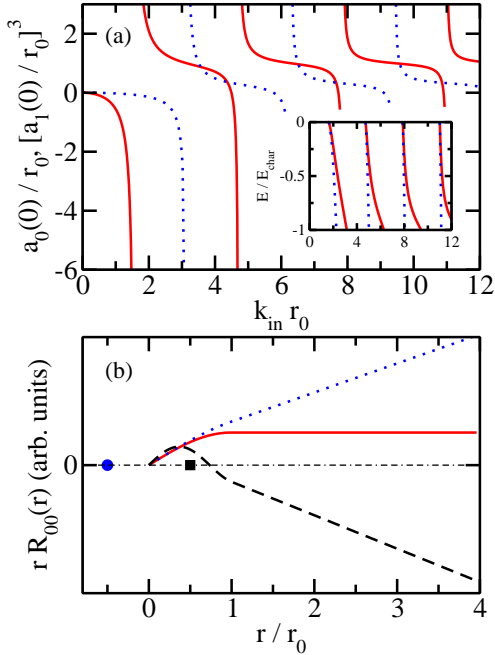


Figure 1. (Color online) Illustration of two-body scattering for an attractive square well model potential with depth V_0 and range r_0 . (a) Solid and dotted lines show the zero-energy scattering lengths $a_0(0)$ and $a_1^3(0)$ as a function of $k_{\text{in}} r_0$, where $k_{\text{in}}^2 = 2\mu V_0/\hbar^2$. Inset: Solid lines show the energy of the most weakly-bound s -wave state for the square well potential as a function of $k_{\text{in}} r_0$. For comparison, dotted lines show Eq. (7) with $a_0(k)$ approximated by $a_0(0)$ of the square well potential. (b) Solid, dotted and dashed lines show the scaled s -wave scattering wave function $r R_{00}(r)$ as a function of r/r_0 for $[a_0(0)]^{-1} = 0$ (one zero-energy s -wave bound state), $a_0(0) = -r_0/2$ [no s -wave bound state; $a_0(0)$ is marked by a circle] and $a_0(0) = r_0/2$ [one s -wave bound state; $a_0(0)$ is marked by a square], respectively.

an attractive square well potential with depth V_0 and range r_0 . This or similarly simplistic model potentials suffice to describe generic low-energy features of cold atom systems. Solid and dotted lines in Fig. 1(a) show the scattering lengths $a_0(0)$ and $a_1^3(0)$ as a function of the dimensionless “strength parameter” $k_{\text{in}} r_0$, where $k_{\text{in}} = \sqrt{2\mu V_0}/\hbar$. The scattering lengths $a_0(0)$ and $a_1^3(0)$ vanish for vanishing V_0 , and decrease with increasing $k_{\text{in}} r_0$. The s - and p -wave scattering lengths diverge when $k_{\text{in}} r_0 = \pi/2$ and $k_{\text{in}} r_0 = \pi$, respectively. As $k_{\text{in}} r_0$ increases further, the scattering lengths decrease from large positive to large negative values. When the scattering lengths $a_0(0)$ and $a_1^3(0)$ diverge, the square well potential supports a new s -wave or a new p -wave bound state, respectively. Dashed, dotted and solid lines in Fig. 1(b) show the scaled s -wave scattering wave function $r R_{00}(r)$ for finite positive, finite negative and infinitely large $a_0(0)$, respectively. The linear behavior of $r R_{00}(r)$ for $r > r_0$ is clearly visible. For finite $a_0(0)$, the scattering length can be “read off” by extrapolating the linear behavior to $r < r_0$ [see symbols in Fig. 1(b)]. By construction, the wave functions

for the same zero-energy scattering length but different depth or number of bound states (not shown) agree in the large r limit. Differences, however, exist in the small r region. These short-range features are typically not probed at low temperatures, making the scattering length the only relevant quantity. This can be intuitively understood by realizing that the de Broglie wave length λ_{dB} increases with decreasing temperature, thereby setting a resolution limit, i.e., the collision energy (which is in typical experiments set by a combination of the temperature and the particle statistics) is too small to probe features at small length scales. Correspondingly, the low temperature regime is known as the long wave length limit.

Mathematically, it can be advantageous to replace the true interaction potential or shape-dependent model potential by a zero-range pseudopotential that acts only when the two particles sit on top of each other [78, 80, 81]. Using the quantum defect language (see, e.g., Refs. [82, 83, 84]), the pseudopotential can be thought of as enforcing a particular value of the logarithmic derivative at $r = 0$. In three spatial dimensions, the regularized s -wave Fermi-Huang pseudopotential V_0^{PP} reads [81]

$$V_0^{\text{PP}}(r) = g_0(k)\delta(\vec{r})\frac{\partial}{\partial r}r, \quad (4)$$

where the interaction strength $g_0(k)$ is chosen such that V_0^{PP} reproduces the energy-dependent s -wave scattering length $a_0(k)$ of the true interaction potential,

$$g_0(k) = \frac{2\pi\hbar^2 a_0(k)}{\mu}. \quad (5)$$

The regularization operator $(\partial/\partial r)r$ in Eq. (4) ensures that the pseudopotential is well behaved as r goes to 0 [81]. The pseudopotential imposes a boundary condition on the relative wave function $\psi_k(\vec{r})$ at $r = 0$ [85, 86],

$$\left[\frac{\frac{\partial}{\partial r} (r\psi_k(\vec{r}))}{r\psi_k(\vec{r})} \right]_{r \rightarrow 0} = \frac{-1}{a_0(k)}. \quad (6)$$

This so-called Bethe-Peierls boundary condition serves as an alternative parametrization of $V_0^{\text{PP}}(r)$. The pseudopotential V_0^{PP} supports no two-body bound state for negative s -wave scattering length $a_0(k)$ and a single two-body s -wave bound state with binding energy E_{bound} ,

$$E_{\text{bound}} = \frac{-\hbar^2}{2\mu[a_0(k)]^2}, \quad (7)$$

for positive $a_0(k)$. Equation (7) is an implicit equation for the bound state energy, which requires knowing $a_0(k)$ for imaginary k . The size of the bound state of V_0^{PP} is determined by $a_0(k)$, i.e., $\sqrt{\langle r^2 \rangle} = a_0(k)/\sqrt{2}$. We note that Eq. (7) also describes the s -wave bound states of finite-range potentials. This can be seen by analytically continuing Eq. (1) to negative energies or by analyzing the poles of the energy-dependent S-matrix [79]. In the low-energy limit, Eq. (7) provides a good description of the bound state energies if $a_0(k)$ is approximated by $a_0(0)$ (see also below). In fact, it should be noted that the original formulation of the pseudopotential (or corresponding boundary condition) employed the zero-energy scattering length $a_0(0)$ instead of $a_0(k)$. In the cold atom context, the energy-dependent scattering length $a_0(k)$ was first introduced in Refs. [87, 88].

It is important to note that V_0^{PP} only acts on the lowest partial wave. The partial waves R_{lk}^{out} with $l \geq 1$ have vanishing amplitude at $r = 0$, and are thus not affected by V_0^{PP} . This implies that Eq. (6) remains valid if ψ_k is replaced by R_{0k}^{out} and

that $R_{lk}^{\text{out}}(r) = N_l(k)j_l(kr)$ for $l \geq 1$. Pseudopotentials V_l^{PP} for higher partial wave scattering have been developed in the literature [81, 89, 90, 91, 92, 93, 94, 95]. Similar to the s -wave pseudopotential, the higher partial wave pseudopotentials, applicable to spherically symmetric systems, can be parameterized in terms of a boundary condition at $r = 0$,

$$\frac{\Gamma(l+1/2)}{\sqrt{\pi}\Gamma(l+1)} \left[\frac{\frac{\partial^{2l+1}}{\partial r^{2l+1}} \left(r^{l+1} \int \psi_k(\vec{r}) P_l(\cos \vartheta) d \cos \vartheta \right)}{r^{l+1} \int \psi_k(\vec{r}) P_l(\cos \vartheta) d \cos \vartheta} \right]_{r \rightarrow 0} = \frac{-1}{a_l^{2l+1}(k)} \quad (8)$$

Solid lines in the inset of Fig. 1(a) show the energy of the most weakly-bound s -wave state of the square well potential as a function of $k_{\text{in}}r_0$. As discussed in the context of the main figure, a new s -wave bound state is being supported when $k_{\text{in}}r_0 = n\pi/2$, where $n = 1, 3, \dots$. For comparison, dotted lines show the bound state energy E_{bound} , Eq. (7), with $a_0(k)$ approximated by the zero-energy scattering length $a_0(0)$ of the square well potential. For $|E|/E_{\text{char}} \ll 1$, where $E_{\text{char}} = \hbar^2/(2\mu r_0^2)$ (i.e., in the low-energy regime), the agreement between the solid and dotted lines is good. However, as $|E|/E_{\text{char}}$ increases, deviations between the two data sets are visible. This can be attributed to the fact that the energy-dependence of $a_0(E)$ becomes stronger as $|E|$ increases.

Typical interactions between alkali atoms involve two electronic energy curves, the singlet and the triplet Born-Oppenheimer (BO) potential curves labeled $X^1\Sigma_g^+$ and $a^3\Sigma_u^+$, respectively, which are coupled through a hyperfine Hamiltonian. The coupling is responsible for the multi-channel nature of the scattering process. Multi-channel scattering is reviewed in detail in Refs. [60, 79]. For our purposes, it is important that the coupling between the channels can give rise to Fano-Feshbach resonances [31]. A Fano-Feshbach resonance in the l th partial wave arises when the scattering energy coincides with the energy of a bound state in the l th partial wave. Since the ‘‘detuning’’ between the open and closed channels in the large r regime is determined by the difference in magnetic moments, the thresholds of the two channels can be varied through the application of an external magnetic field. If the topology of the potential energy surfaces is such that the variation of the external field allows for the bound state energy and the scattering energy to coincide, then the system exhibits a resonance. Varying the strength B of the external magnetic field in the vicinity of a Fano-Feshbach resonance allows the coupled-channel l -wave scattering length $a_l^{2l+1}(k)$ to be tuned to essentially any value.

Assuming no overlapping Fano-Feshbach resonances exist and higher partial wave contributions are negligible, the magnetic field-dependent coupled-channel s -wave scattering length $a_0(B)$ can be parameterized by three effective parameters, the background scattering length a_{bg} , the resonance width ΔB and the resonance position B_{res} [72],

$$a_0(B) = a_{\text{bg}} \left(1 - \frac{\Delta B}{B - B_{\text{res}}} \right). \quad (9)$$

This effective description has been confirmed by coupled-channel calculations and experimental data; it can, for example, be derived using a simple coupled-channel zero-range or square well model [96, 97]. The parameters ΔB , B_{res} and a_{bg} are extracted from experimental data or full coupled-channel calculations. The solid line in Fig. 2(a) shows the magnetic field dependence of the scattering length for the magnetic Fano-Feshbach resonance for two ^{85}Rb atoms in the $(F, M_F) = (2, -2)$ state near 155G (here, F denotes the hyperfine quantum number and M_F the corresponding

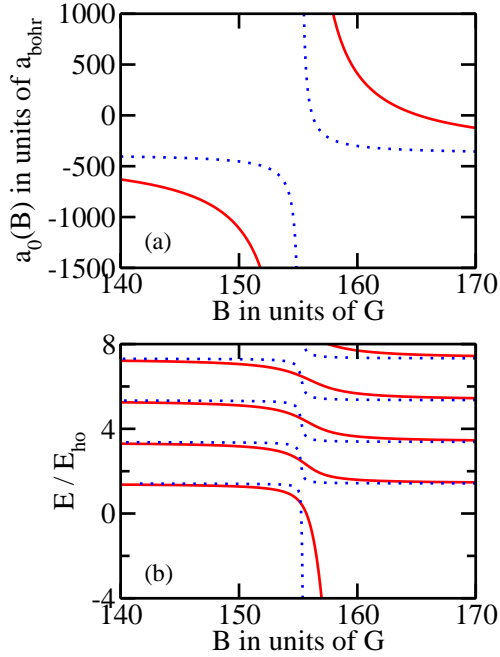


Figure 2. (Color online) (a) The solid line shows the field-dependent scattering length $a_0(B)$, Eq. (9), for the Fano-Feshbach resonance around 155G for two ^{85}Rb atoms in the $(F, M_F) = (2, -2)$ state as a function of B ; the parameters adopted are $\Delta B = 10\text{G}$, $B_{\text{res}} = 155.2\text{G}$ and $a_{\text{bg}} = -380a_{\text{bohr}}$ [97]. For comparison, the dotted line shows the effective scattering length for a “mock resonance” with $\Delta B = 1\text{G}$ but the same a_{bg} and B_{res} as for the ^{85}Rb resonance. (b) Solid and dotted lines show the s -wave energy spectra, calculated using Eqs. (17) and (9), for two atoms under harmonic confinement with $a_{\text{ho},\mu} = 5000a_{\text{bohr}}$.

projection quantum number). It is often useful to write the field-dependent scattering length in terms of the energy width Γ_E [72],

$$a_0(B) = a_{\text{bg}} \left(1 + \frac{\Gamma_E}{E + (B - B_{\text{res}}) \frac{\partial E_{\text{res}}(B)}{\partial B}} \right), \quad (10)$$

where $\Gamma_E = 2ka_{\text{bg}}\Delta B[\partial E_{\text{res}}(B)/\partial B]$ and where $E_{\text{res}}(B)$ denotes the field-dependent bound state energy of the coupled-channel system. Here, E and k denote, as above, the two-body scattering energy and corresponding wave vector, respectively. We note that the E -term in the denominator of Eq. (10) can often be neglected. In this case, Eq. (10) reduces to Eq. (9). The quantity $\partial E_{\text{res}}(B)/\partial B$ is known from experiment and/or theory. The energy width Γ_E can be used to define broad and narrow resonances [39, 98, 99, 100, 101, 102]. If Γ_E is larger (smaller) than the characteristic energy scale of the system, the resonance is called broad (narrow). The characteristic energy scale depends on the system under investigation. For the BCS-BEC crossover problem, for example, the characteristic energy scale in the low temperature regime is set by the Fermi energy when $|a_0(B)|$ is small and $a_0(B) < 0$,

and by the two-body binding energy when $a_0(B)$ is small and $a_0(B) > 0$ [99]. As a rule of thumb, broad resonances can be modeled quite accurately within a single-channel model; narrow resonances, in contrast, require a coupled-channel treatment.

2.2. Two particles in a spherically symmetric harmonic trap

This subsection considers two particles interacting through a spherically symmetric potential V_{tb} under external confinement, i.e., we consider what happens to the scattering continuum and the weakly-bound states when the asymptotic boundary conditions are modified by the external confinement. Throughout, we consider the regime where the confinement length is much larger than the range of the underlying particle-particle interaction potential. Experimentally, trapped systems can be realized by loading atoms into an optical lattice created by counterpropagating standing light waves. The atom-light interaction creates a periodic potential felt by the atoms. Near the bottom of each well, the confining potential is approximately harmonic. Furthermore, for atoms with short-range interactions, the spacing between the lattice sites is so large that “off-site” interactions can be neglected. Assuming that tunneling between neighboring lattice sites can also be neglected, the lattice sites are independent from each other and each lattice site hosts an independent few-body system. Experimentally, the number of atoms per lattice site can be controlled. Here, we treat the two-body system; larger systems are discussed in Secs. 3-5.

We assume that the external confinement is harmonic, i.e., that the i^{th} particle feels the external potential $m_i\omega^2\vec{r}_i^2/2$ ($i = 1$ or 2), where ω denotes the angular trapping frequency and \vec{r}_i the position vector of the i^{th} particle measured with respect to the trap center. For this system, the center of mass motion separates, i.e., $E_{\text{tot}} = E_{\text{cm}} + E$, where the center of mass energy is given by $E_{\text{cm}} = (2Q_{\text{cm}} + L_{\text{cm}} + 3/2)\hbar\omega$ with $Q_{\text{cm}} = 0, 1, \dots$ and $L_{\text{cm}} = 0, 1, \dots$, and E denotes the relative energy. Assuming a spherically symmetric interaction potential $V_{\text{tb}}(r)$, the relative Hamiltonian for the two-body system reads

$$H = -\frac{\hbar^2}{2\mu}\nabla_{\vec{r}}^2 + \frac{1}{2}\mu\omega^2r^2 + V_{\text{tb}}(r), \quad (11)$$

where μ denotes, as above, the reduced two-body mass. The relative eigen functions $\psi_{lq}(\vec{r})$ separate, $\psi_{lq}(\vec{r}) = r^{-1}u_{lq}(r)Y_{lm}(\vartheta, \varphi)$. $u_{lq}(r)$ solves the radial Schrödinger equation

$$\left[\frac{-\hbar^2}{2\mu} \frac{\partial^2}{\partial r^2} + \frac{\hbar^2 l(l+1)}{2\mu r^2} + \frac{1}{2}\mu\omega^2r^2 + V_{\text{tb}}(r) \right] u_{lq}(r) = E_{lq}u_{lq}(r), \quad (12)$$

where $E_{lq} = E = (2q + l + 3/2)\hbar\omega$. The non-integer quantum number q labels the radial solutions for a given relative orbital angular momentum l . Equation (12) can be solved numerically for essentially any $V_{\text{tb}}(r)$. Here, we seek analytical solutions for the l -wave zero-range pseudopotentials V_l^{PP} .

The linearly independent solutions f_{lq} and g_{lq} of the radial Schrödinger equation with $V_{\text{tb}} = V_l^{\text{PP}}$ for $r > 0$ are identical to those for an isotropic harmonic oscillator with mass μ . Introducing the harmonic oscillator length $a_{\text{ho},\mu}$, $a_{\text{ho},\mu} = \sqrt{\hbar/(\mu\omega)}$, and defining the dimensionless variable x , $x = r/a_{\text{ho},\mu}$, f_{lq} and g_{lq} can be written as

$$f_{lq}(x) = x^{l+1} \exp\left(-\frac{x^2}{2}\right) {}_1F_1(-q, l + 3/2, x^2) \quad (13)$$

and

$$g_{lq}(x) = x^{-l} \exp\left(\frac{-x^2}{2}\right) {}_1F_1(-q-l-1/2, -l+1/2, x^2), \quad (14)$$

where ${}_1F_1$ denotes the confluent hypergeometric function of the first kind. We write $u_{lq}(x) = c_l(q)f_{lq}(x) + d_l(q)g_{lq}(x)$ and choose the ratio $c_l(q)/d_l(q)$ such that $u_{lq}(x)$ vanishes in the large x limit, i.e., so that the exponentially increasing pieces of $f_{lq}(x)$ and $g_{lq}(x)$ cancel as $x \rightarrow \infty$. Using the $x \rightarrow \infty$ behavior of ${}_1F_1$ [103], we find

$$\frac{\Gamma(l+3/2)}{\Gamma(-q)} c_l(q) = -\frac{\Gamma(-l+1/2)}{\Gamma(-q-1/2-l)} d_l(q). \quad (15)$$

Using Eq. (15) in $u_{lq}(x)$, we find

$$u_{lq}(x) = N_l(q) \exp\left(\frac{-x^2}{2}\right) x^{l+1} U(-q, l+3/2, x^2), \quad (16)$$

where U denotes the confluent hypergeometric function of the second kind and $N_l(q)$ a normalization constant. Next, we ensure that $r^{-1}u_{lq}$ obeys the boundary condition in the small x limit, i.e., we enforce Eq. (8). The resulting quantization condition reads

$$\frac{(-1)^l 2^{2l+1} \Gamma\left(\frac{-E_{lq}}{2\hbar\omega} + \frac{l}{2} + \frac{3}{4}\right)}{\Gamma\left(\frac{-E_{lq}}{2\hbar\omega} - \frac{l}{2} + \frac{1}{4}\right)} = \frac{a_{\text{ho},\mu}^{2l+1}}{a_l^{2l+1}(k)}. \quad (17)$$

The transcendental equation, Eq. (17), determines the eigenspectrum for any l and $a_l^{2l+1}(k)$. The eigenenergies E_{lq} can be obtained straightforwardly using a simple rootfinding routine. For $l=0$, this eigenequation was first derived by Busch *et al.* [104]. For $l>0$, the solutions can be found in Refs. [84, 91, 92, 94, 105]. The wave function u_{lq} is normalizable for $l=0$ but not for $l>0$. This issue has been discussed in detail in Refs. [95, 106, 107] and will not be elaborated on here.

Figures 3(a) and 3(b) show the energy spectra for $l=0$ and $l=1$, respectively, as a function of the inverse scattering lengths. Solid lines show the energy spectra obtained from Eq. (17) using $a_l^{2l+1}(k) = a_l^{2l+1}(0)$. For comparison, dotted lines show the eigenspectra obtained for a square well potential with a fairly large range r_0 , $r_0 = 0.1a_{\text{ho},\mu}$. The s -wave spectrum for the square well potential is fairly well reproduced by the zero-range model for all $a_0(0)$; the deviations are largest for negative energies where the short-range physics plays a non-negligible role. For $l=1$, the square well spectrum is qualitatively reproduced for $E \gtrsim 5\hbar\omega/2$ and large $|a_{\text{ho},\mu}/a_1(0)|^3$. In other parameter regimes, significant deviations are visible. A significantly improved description is obtained by treating the energy-dependence of the generalized scattering length explicitly. To this end, we solve Eq. (17) self-consistently [87, 88], i.e., we seek solutions for which the energy on the left hand side of Eq. (17) is the same as that at which the generalized free-space scattering length $a_l^{2l+1}(k)$ for the square well potential with $r_0 = 0.1a_{\text{ho},\mu}$ is being evaluated. The resulting eigenenergies [not shown in Figs. 3(a) and 3(b)] are in excellent agreement with the eigenenergies for the square-well potential for both $l=0$ and $l=1$. In general, it is found that the use of the energy-dependent scattering length is crucial for the description of higher partial wave physics within the zero-range pseudopotential framework [91, 92, 94].

Figure 4 shows the $l=0$ wave function $u_{0q}(r)$ for several $a_0(0)$ corresponding to the lowest energy branch. In the small $|a_0(0)|$ limit, $a_0(0) < 0$, $u_{0q}(r)$ approaches the non-interacting wave function. In the small $a_0(0)$ limit, $a_0(0) > 0$, in contrast, $u_{0q}(r)$

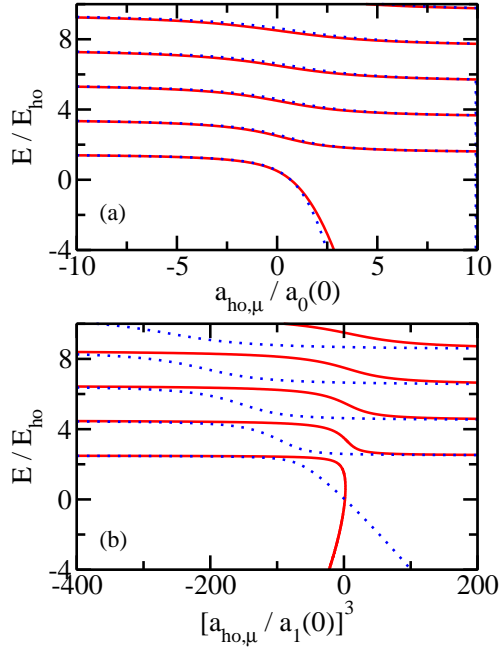


Figure 3. (Color online) Illustration of the energy spectrum of the trapped two-particle system for (a) $l = 0$ and (b) $l = 1$. Solid lines show the eigenenergies E_{lq} obtained by solving Eq. (17) with $a_l^{2l+1}(k)$ approximated by $a_l^{2l+1}(0)$. Dotted lines show the eigenenergies obtained for a square well potential with $r_0 = 0.1a_{\text{ho},\mu}$ and V_0 adjusted to obtain the desired $a_l^{2l+1}(0)$ [and such that the free-space system supports no (one) l -wave bound state for $a_l^{2l+1}(0) < 0$ ($a_l^{2l+1}(0) > 0$)].

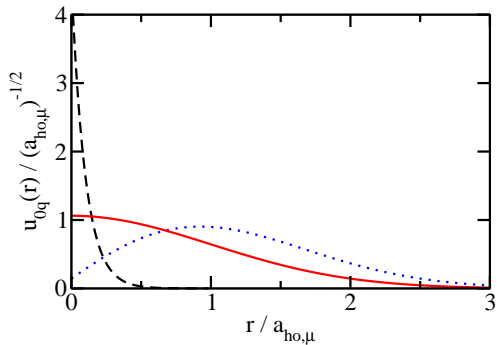


Figure 4. (Color online) Dotted, solid and dashed lines show the relative $l = 0$ wave function $u_{0q}(r)$, Eq. (16), corresponding to the lowest energy branch of the trapped two-body system with $a_0(0)/a_{\text{ho},\mu} = -0.1, \infty$ and 0.1 , respectively.

approaches the wave function of a tightly bound molecule in free-space. At unitarity, the admixture of the irregular solution is maximal, leading to a wave function that has vanishing derivative at $r = 0$. Formally, this wave function is identical to the relative even-parity wave function of two non-interacting harmonically trapped particles in one dimension.

We now discuss the dependence of the s -wave energy spectrum on the external magnetic field strength B . Solid and dotted lines in Fig. 2(a) show the magnetic field dependent scattering length $a_0(B)$, Eq. (9), for two resonances with the same a_{bg} and B_{res} but different widths ΔB , i.e., $\Delta B = 10G$ and $1G$, respectively. Solid and dotted lines in Fig. 2(b) show the s -wave energy spectra obtained from Eq. (17) corresponding to the resonances shown in Fig. 2(a). To this end, the scattering length $a_0(0)$ in Eq. (17) is converted to B via Eq. (9). Figure 2(b) shows that the energy spectrum for $\Delta B = 10G$ is characterized by broader avoided crossings than that for $\Delta B = 1G$. The coupling between the resonance state (or the closed molecular channel) and the trap states increases with increasing ΔB . A Landau-Zener analysis [72] shows that the energy width Γ_E , Eq. (10), determines the probability to make a transition from the trapped state to the molecular state. In particular, it is found that the transition probability decreases exponentially with increasing Γ_E for the same ramp speed. Correspondingly, the closed molecular channel plays a negligible role for resonances with relatively large ΔB and a non-negligible role for those with relatively small ΔB . Thus, broad resonances can, generally, be described within a single channel framework while narrow resonances require a two-channel description (see also Subsec. 2.1).

2.3. Beyond spherical symmetry

The previous subsection discussed the physics of two atoms interacting through a spherically symmetric potential under spherically symmetric confinement. This confining geometry is fairly easy to treat both numerically and analytically, and is directly relevant to on-going cold atom experiments. This subsection considers systems for which the spherical symmetry is broken either due to a non-spherically symmetric confinement, a non-spherically symmetric interaction potential or both. In all three cases, new two-body resonances arise that can be tuned by varying the confinement (thus motivating the term confinement-induced resonance [108, 109]) or by changing the admixture of the non-spherical contribution to the interaction potential. These tunable two-body resonances pave the way for investigations of intriguing few- and many-body phenomena.

Table 1 lists confinement geometries that have been considered in the literature. As an example, we consider two particles interacting through a spherically symmetric potential V_{tb} under cylindrically-symmetric confinement in more detail [94, 108, 109, 110, 111, 112, 113, 114]. As in Subsec. 2.2, the center-of-mass degrees of freedom separate off and the confinement in the relative coordinate becomes $V_{\text{trap}} = \mu(\lambda^2\omega_z^2\rho^2 + \omega_z^2z^2)/2$, where $z = z_1 - z_2$ and $\rho = \sqrt{(x_1 - x_2)^2 + (y_1 - y_2)^2}$. The aspect ratio λ is defined in terms of the angular trapping frequencies ω_ρ and ω_z along the ρ - and z -directions, $\lambda = \omega_\rho/\omega_z$. Intuitively, one expects that a tight confinement in one spatial dimension ($\lambda \ll 1$) leads to an effectively two-dimensional system in which the motion along the tight confinement direction, or high energy coordinate, is frozen out. Correspondingly, a tight confinement in two spatial dimensions ($\lambda \gg 1$) is expected to lead to an effectively one-dimensional system. This argument can be formalized by

Table 1. Selected trapping geometries considered in the literature for two-particle systems. Other geometries such as double well geometries and optical lattice type potentials have also been considered.

Trapping geometry	References
hardwall at $r = R$ (three-dimensional)	[81]
$\frac{1}{2}\mu\omega^2 r^2$ (three-dimensional)	[84, 91, 92, 104, 105]
$\frac{1}{2}\mu\omega^2 \rho^2$ (two-dimensional)	[115]
$\frac{1}{2}\mu\omega^2 z^2$ (one-dimensional)	[91, 104]
$\frac{1}{2}\mu(\omega_\rho^2 \rho^2 + \omega_z^2 z^2)$	[94, 108, 109, 110, 111, 112, 113, 114]
$\frac{1}{2}m \sum_{i=1,2}(\omega_x^2 x_i^2 + \omega_y^2 y_i^2 + \omega_z^2 z_i^2)$	[116, 117, 118]
$\frac{1}{2}(m_1\omega_1^2 r_1^2 + m_2\omega_2^2 r_2^2)$	[119, 120, 121]
cubic box; periodic boundary condition	[75]
box with lengths L_x, L_y, L_z ; periodic boundary condition	[122]

defining effective one- and two-dimensional interaction potentials.

We exemplarily consider the $\lambda \gg 1$ case with s -wave interactions [108, 109]. To start with, we assume that the motion in the ρ - and z -directions separates and, further, that the motion along the ρ -coordinate is frozen in the harmonic oscillator ground state $\phi_{\text{ho},0}(\rho)$. Modeling the two-body interaction potential through V_0^{PP} , we define an effective one-dimensional potential $V_{\text{eff}}^{\text{1d}}(z)$ through

$$V_{\text{eff}}^{\text{1d}}(z) = 2\pi \int_0^\infty \phi_{\text{ho},0}^*(\rho) V_0^{\text{PP}}(\vec{r}) \phi_{\text{ho},0}(\rho) \rho d\rho. \quad (18)$$

The integral evaluates to $V_{\text{eff}}^{\text{1d}}(z) = g_{\text{eff}}^{\text{1d}} \delta(z)$ with $g_{\text{eff}}^{\text{1d}} = 2\hbar^2 a_0(0)/(\mu a_{\text{ho},\rho}^2)$, where $a_{\text{ho},\rho}$ denotes the transverse confinement length, $a_{\text{ho},\rho} = \sqrt{\hbar/(\mu\omega_\rho)}$. So far, we have assumed that the motion along the ρ -coordinate is frozen in the harmonic oscillator ground state $\phi_{\text{ho},0}(\rho)$. This is, however, not the case since the pseudopotential V_0^{PP} couples the ρ and z degrees of freedom. Thus, the cylindrically symmetric outside solution (valid for $r > 0$) needs to be projected onto the spherically symmetric inside solution (valid for $r = 0$), thereby leading to an admixture of excited state harmonic oscillator wave functions $\phi_{\text{ho},j}(\rho)$; here, j collectively denotes the quantum numbers associated with the motion in the xy -plane. For finite-range potentials, the outside and inside solutions can, using a frame transformation approach, be connected at a finite r value [112]. A full microscopic calculation for the zero-range potential gives [108],

$$g_{\text{eff}}^{\text{1d}} = \frac{2\hbar^2 a_0(0)}{\mu a_{\text{ho},\rho}^2} \left[1 - |\zeta(1/2)| \frac{a_0(0)}{a_{\text{ho},\rho}} \right]^{-1}, \quad (19)$$

where $\zeta(1/2) = -1.4604$. For small $|a_0(0)|/a_{\text{ho},\rho}$, Eq. (19) reduces to the naive estimate discussed above. For large $|a_0(0)|/a_{\text{ho},\rho}$, however, the strong transverse confinement modifies the effective one-dimensional coupling constant. In particular, a diverging one-dimensional coupling constant, and thus a one-dimensional resonance, is found for $a_0(0)/a_{\text{ho},\rho} = |\zeta(1/2)|^{-1}$. Effectively one-dimensional many-body systems are, in many cases, well described by strictly one-dimensional Hamiltonian such as the Lieb-Liniger or Gaudin-Yang Hamiltonian [123, 124, 125, 126]. For cold atom realizations of these Hamiltonian, the coupling constant is given by $g_{\text{eff}}^{\text{1d}}$, Eq. (19). Since $g_{\text{eff}}^{\text{1d}}$ can be tuned by varying $a_{\text{ho},\rho}$ or $a_0(0)$, Eq. (19) forms the basis for studying strongly correlated one-dimensional systems. One-dimensional systems have attracted a great deal of attention from mathematicians and physicists since they are more amenable to analytical treatments than two- or three-dimensional systems.

Strictly one-dimensional systems with contact interactions, e.g., are integrable. Deviations from a strictly one-dimensional geometry may lead to deviations from integrability. Thus, important questions regarding integrability, near-integrability and thermalization can be investigated by studying highly-elongated quasi-one-dimensional Bose and Fermi gases [127, 128, 129, 130, 131].

Similar analyses have been conducted for higher partial waves as well as for geometries with $\lambda \ll 1$ [94, 110, 112]. In all cases, confinement induced resonances, i.e., diverging effective low-dimensional coupling constants, are found for finite three-dimensional scattering lengths. The study of small quasi-two-dimensional trapped Fermi gases is partially motivated by analogous studies of two-dimensional quantum dot systems [132, 133]. In the context of cold Fermi gases, the filling of energy levels has been analyzed using Hund's rules [134]. An alternative trapping geometry consists of a periodic optical lattice, which also gives rise to confinement induced resonances that can be tuned by varying the lattice height or other system parameters [135, 136, 137, 138].

The energy spectrum of two-particle systems in a cubic box with periodic boundary conditions has been analyzed extensively in the context of lattice QCD calculations [74, 75, 139]. For this confining geometry, the center of mass of the system does not decouple and two-body interactions lead to a modification of the plane wave solutions applicable to the non-interacting system. In analogy to Eq. (17), the two-body energy spectrum for the box-confinement has been related to the phase shifts. The corresponding equation is termed Lüscher's formula [75] and has found applications in QCD and other lattice simulation studies. An analysis of the energy spectrum determined from Lüscher's formula shows that the relationship between the phase shifts and eigenenergies is notably different from that found for the spherically symmetric harmonic confining potential treated in Subsec. 2.2. This shows exemplarily that the energy spectrum depends in non-trivial ways on the geometry of the external confinement.

Lastly, we comment briefly on two particles that interact through a non-spherically symmetric dipole-dipole potential V_{dd} under spherically symmetric confinement. For simplicity, we assume that the electric or magnetic point dipoles are aligned along the z -axis, $V_{\text{dd}}(r) = d^2(1 - 3\cos^2\vartheta)/r^3$, where d denotes the strength of the dipole moment and ϑ the angle between the z -axis and \vec{r} . For $r < r_0$, we assume a spherically symmetric potential $V_{\text{sr}}(r)$. The dipole-dipole potential introduces a new length scale, the dipole length d_* , $d_* = 2\mu d^2/\hbar^2$. Since the angle-dependence of the dipole-dipole potential leads to the coupling of different partial waves, the scattering framework discussed in Subsec. 2.1 requires modifications. One of the consequences is that one now has to consider a scattering matrix with elements $a_{\nu l}$, where $a_{\nu l}(k) = -\tan[\delta_{\nu l}(k)]/k$ [60, 140, 141, 142]. Compared to short-range potentials [see Eq. (2)], the dipole-dipole interaction potential leads to a modified threshold behavior, i.e., $a_{\nu l}(0) = \lim_{k \rightarrow 0} a_{\nu l}(k)$ approaches a constant [60]. V_{dd} connects the incoming partial wave labeled by l with the outgoing partial wave labeled by l' . The multi-channel nature of the dipole-dipole potential gives rise to novel two-body resonances, which can be tuned by varying the dipole moment d [140, 142, 143, 144, 145, 146]. For electric dipoles, this can be achieved through the application of an external electric field. Similarly to the case of purely spherically-symmetric two-body interaction potentials, the energy spectrum of two dipoles under spherically symmetric harmonic confinement can be determined analytically if the dipole length d_* is smaller than the harmonic oscillator length $a_{\text{ho},\mu}$ [115]. This review

will not discuss the few-body physics of trapped dipolar systems further.

3. Hyperspherical coordinate treatment of trapped three-particle system

This section considers three-particle systems with short-range interactions under external spherically symmetric harmonic confinement. For this confinement geometry, the center-of-mass degrees of freedom \vec{R}_{cm} separate off, leaving six relative coordinates. The trapped three-body system can be analyzed by a variety of techniques including those developed by chemists and nuclear physicists. This section focuses on the hyperspherical coordinate approach, which provides an intuitive picture for understanding three-body systems with bosonic, fermionic or mixed symmetry. Subsection 3.1 introduces the formalism, while Subsecs. 3.2 and 3.3 discuss selected aspects of the non-interacting and large scattering length regimes and the Efimov regime, respectively. Implications of three-body physics for larger systems are discussed in Secs. 4 and 5.

3.1. General framework

The hyperspherical coordinate approach transforms the coordinates of the system into a single length, the hyperradius R , and a set of hyperangles, collectively denoted by $\vec{\Omega}$ [41, 70, 71, 147, 148, 149, 150, 151]. For the three-body system in the center of mass frame, $\vec{\Omega}$ consists of five hyperangles [152]. The hyperspherical coordinate approach has been employed in many contexts such as in the description of autoionizing states of the He atom [147] and the Efimov effect [153]. It has also been applied successfully to systems consisting of more than three particles [41, 149, 151] (see, e.g., Subsec. 4.2). The hyperradial dynamics can be visualized and interpreted in much the same way as that of a diatomic molecule described by a set of coupled BO potential curves.

To define the hyperspherical coordinates for three-body systems with masses m_i and position vectors \vec{r}_i ($i = 1, 2, 3$), we introduce Jacobi vectors $\vec{\rho}_i$,

$$\vec{\rho}_1 = \vec{r}_1 - \vec{r}_2 \quad (20)$$

and

$$\vec{\rho}_2 = \frac{m_1\vec{r}_1 + m_2\vec{r}_2}{m_1 + m_2} - \vec{r}_3. \quad (21)$$

The Jacobi vector $\vec{\rho}_3$ coincides with \vec{R}_{cm} . The hyperradius R , which can be interpreted as measuring the overall size of the system, is defined through

$$\mu_R R^2 = \mu_1 \rho_1^2 + \mu_2 \rho_2^2, \quad (22)$$

where μ_R denotes the hyperradial mass (a scaling factor that can be chosen conveniently), and where μ_1 and μ_2 denote the reduced masses associated with $\vec{\rho}_1$ and $\vec{\rho}_2$, respectively, $\mu_1 = m_1 m_2 / (m_1 + m_2)$ and $\mu_2 = (m_1 + m_2) m_3 / (m_1 + m_2 + m_3)$. The hyperangle α , $0 \leq \alpha \leq \pi/2$, is defined as

$$\alpha = \arctan \left(\frac{\sqrt{\mu_1} \rho_1}{\sqrt{\mu_2} \rho_2} \right). \quad (23)$$

The other four hyperangles are given by the angles (ϑ_1, φ_1) and (ϑ_2, φ_2) , which describe the orientation of the unit vectors $\hat{\rho}_1$ and $\hat{\rho}_2$, respectively. In these coordinates, the volume element becomes $R^5 dR d\vec{\Omega}$, where $d\vec{\Omega} = \sin(2\alpha) d\alpha d\vec{\Omega}_1 d\vec{\Omega}_2$ with $d\vec{\Omega}_j = \sin \vartheta_j d\vartheta_j d\varphi_j$. We note that the definition of the hyperangular coordinates

is not unique. The “optimal set of coordinates” depends on the choice of the analytical or numerical technique employed.

In the hyperspherical framework, the relative wave function $\psi(R, \vec{\Omega})$ is expanded in terms of a set of channel functions $\Phi_\nu(R; \vec{\Omega})$ that depend parametrically on the hyperradius R and a set of weight functions $F_{\nu q}(R)$ [69, 147],

$$\psi(R, \vec{\Omega}) = \frac{1}{R^{5/2}} \mathcal{S} \left(\sum_{\nu q} F_{\nu q}(R) \frac{\Phi_\nu(R; \vec{\Omega})}{\sin(2\alpha)} \right), \quad (24)$$

where \mathcal{S} denotes the symmetrization operator, which can be written in terms of permutation operators P_{jk} that exchange the j^{th} and the k^{th} particle. For three identical bosons, e.g., \mathcal{S} can be written as $3^{-1/2}(1 + P_{23} + P_{31})$. The channel functions $\Phi_\nu(R; \vec{\Omega})$ are eigenfunctions of the fixed- R hyperangular Hamiltonian H_{adia} ,

$$H_{\text{adia}} \Phi_\nu(R; \vec{\Omega}) = \frac{\hbar^2 s_\nu^2(R)}{2\mu_R R^2} \Phi_\nu(R; \vec{\Omega}), \quad (25)$$

where

$$H_{\text{adia}} = \frac{\hbar^2 \Lambda^2}{2\mu_R R^2} + V_{\text{int}}(R, \vec{\Omega}). \quad (26)$$

For each fixed hyperradius R , the channel functions form an orthonormal set, i.e., $\int \Phi_\nu^*(R; \vec{\Omega}) \Phi_{\nu'}(R; \vec{\Omega}) d\vec{\Omega} = \delta_{\nu\nu'}$. In Eq. (26), Λ^2 denotes the square of the grand angular momentum operator, which contains the contributions of the hyperangular motion to the kinetic energy operator [148]. For the purpose of this review, the functional form of Λ^2 is not needed. The potential energy surface V_{int} accounts for the particle-particle interactions, $V_{\text{int}} = \sum_{j < k} V_{\text{tb}}(r_{jk})$.

The weight functions $F_{\nu q}(R)$ are solutions to the coupled equations

$$\begin{aligned} & \left[H_R - \frac{\hbar^2}{2\mu_R} W_{\nu\nu'}(R) - E_{\nu q} \right] F_{\nu q}(R) = \\ & \frac{\hbar^2}{2\mu_R} \sum_{\nu' \neq \nu} \left[W_{\nu\nu'}(R) + 2P_{\nu\nu'}(R) \frac{\partial}{\partial R} \right] F_{\nu' q}(R), \end{aligned} \quad (27)$$

where

$$H_R = \frac{-\hbar^2}{2\mu_R} \frac{\partial^2}{\partial R^2} + \frac{\hbar^2 [s_\nu^2(R) - 1/4]}{2\mu_R R^2} + \frac{1}{2} \mu_R \omega^2 R^2. \quad (28)$$

The last term on the right hand side of Eq. (28) represents the external spherically symmetric confining potential V_{trap} in the relative coordinates, $V_{\text{trap}} = \sum_i m_i \omega^2 \vec{r}_i^2 / 2 - M_{\text{cm}} \omega^2 \vec{R}_{\text{cm}}^2 / 2$ with $M_{\text{cm}} = \sum_i m_i$. The coupling elements $P_{\nu\nu'}(R)$ and $W_{\nu\nu'}(R)$ are defined through

$$P_{\nu\nu'}(R) = \int \Phi_\nu(R; \vec{\Omega}) \frac{\partial \Phi_{\nu'}(R; \vec{\Omega})}{\partial R} d\vec{\Omega} \quad (29)$$

and

$$W_{\nu\nu'}(R) = \int \Phi_\nu(R; \vec{\Omega}) \frac{\partial^2 \Phi_{\nu'}(R; \vec{\Omega})}{\partial R^2} d\vec{\Omega}. \quad (30)$$

No approximations have been made, and Eqs. (25) and (27) are equivalent to the relative Schrödinger equation.

Note that V_{trap} enters into the hyperradial Schrödinger equation, Eq. (27), but not into the hyperangular Schrödinger equation, Eq. (25). This implies that the

three-body system under spherically symmetric harmonic confinement shares many properties with the corresponding free-space system. In particular, the hyperangular eigenvalues $\hbar^2 s_\nu^2(R)/(2\mu_R R^2)$ are the same for the free-space and trapped systems. On the other hand, the weight functions $F_{\nu q}(R)$ of the free-space system obey, depending on the threshold, either bound state or scattering boundary conditions at large R , while all $F_{\nu q}(R)$ of the trapped system obey bound state boundary conditions at large R . A comparison of the two-body and three-body systems reveals that the three-body hyperradius R plays a role analogous to the two-body interparticle distance r , and that the hyperangles $\vec{\Omega}$ play a role analogous to the angles that describe the direction of \vec{r} .

In general, the coupled equations in the hyperradial coordinate R , see Eq. (27), have to be solved numerically. However, certain approximations can be made that lead to strict upper and lower variational bounds [69, 154, 155]. An upper bound to the energies can be obtained by neglecting the coupling matrix elements $W_{\nu\nu'}$ and $P_{\nu\nu'}$ with $\nu \neq \nu'$, i.e., by setting the right hand side of Eq. (27) to zero. The energies obtained by solving the radial equation in this approximation, the so-called adiabatic approximation, provide an upper bound to the exact eigenenergies. A lower bound to the exact ground state energy can be obtained by additionally neglecting the diagonal coupling element or so-called adiabatic correction $W_{\nu\nu}$.

If V_{int} is given by a sum of two-body zero-range potentials, i.e., $V_{\text{int}} = \sum_{j < k} V_0^{\text{PP}}(\vec{r}_{jk})$, the eigenvalues $\hbar^2 s_\nu^2(R)/(2\mu_R R^2)$ of the hyperangular Schrödinger equation can be obtained by finding the roots of a transcendental equation [156] for any combination of masses m_i , any combination of s -wave scattering lengths $a_0^{(jk)}(0)$, and any symmetry (for earlier work see, e.g., Refs. [69, 153, 157, 158, 159]). For this review, the BBB system (three identical bosons) and the FFX system (two identical fermions and a third particle, either boson or fermion) are the most relevant. The FFX system with mass ratio $\kappa = 1$ can be realized by occupying two different hyperfine states of ${}^6\text{Li}$ or ${}^{40}\text{K}$. FFX systems with unequal masses of current experimental interest include ${}^6\text{Li}$ - ${}^{84}\text{Sr}$ ($\kappa \approx 0.071$), ${}^6\text{Li}$ - ${}^{87}\text{Rb}$ ($\kappa \approx 0.069$), ${}^{40}\text{K}$ - ${}^{84}\text{Sr}$ ($\kappa \approx 0.48$), ${}^{173}\text{Yb}$ - ${}^{40}\text{K}$ ($\kappa \approx 4.3$), ${}^{40}\text{K}$ - ${}^6\text{Li}$ ($\kappa \approx 6.7$), and ${}^{87}\text{Sr}$ - ${}^6\text{Li}$ ($\kappa \approx 14.5$).

For the BBB system with relative angular momentum $L = 0$ and s -wave scattering length $a_0(0)$ [i.e., all $a_0^{(jk)}(0)$ are identical], the transcendental equation reads [153, 156, 160]

$$s_\nu(R) \cos \left[s_\nu(R) \frac{\pi}{2} \right] - \frac{8}{\sqrt{3}} \sin \left[s_\nu(R) \frac{\pi}{6} \right] = \sqrt{\frac{\mu_R}{m}} \frac{R}{a_0(0)} \sqrt{2} \sin \left[s_\nu(R) \frac{\pi}{2} \right]. \quad (31)$$

Equation (31) is written in terms of $\sqrt{\mu_R}R$ as opposed to R since the definition of R^2 , Eq. (22), contains the scaling factor μ_R ; in other words, $\mu_R R^2$ is an invariant. Figure 5 shows the quantity $s_\nu(R)$ for the BBB system with $L = 0$ as a function of $\sqrt{\mu_R}R/[\sqrt{m}a_0(0)]$. $s_\nu(R)$ is either purely real or purely imaginary. In particular, the lowest $s_\nu(R)$ value becomes imaginary at $\sqrt{\mu_R}R/[\sqrt{m}a_0(0)] \approx -0.6385$. Although s_ν changes from being purely real to being purely imaginary, the quantity s_ν^2 , which enters into the hyperradial Schrödinger equation [see Eqs. (27) and (28)], changes smoothly (it simply changes sign). The purely imaginary root has profound implications on the system properties. As discussed in more detail in Subsec. 3.3, the imaginary root in the large $|a_0(0)|$ regime gives rise to Efimov physics. Expressions analogous to Eq. (31) can

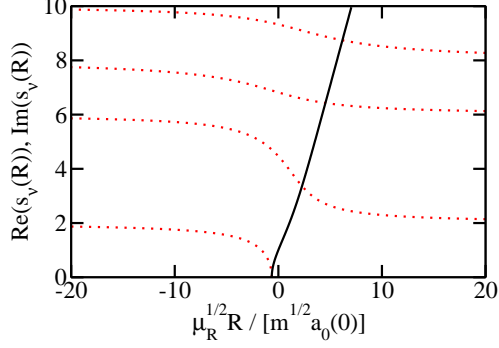


Figure 5. (Color online) $s_\nu(R)$ values for the BBB system with $L = 0$. Dotted and solid lines show the purely real and purely imaginary roots $s_\nu(R)$, obtained by solving Eq. (31), as a function of $\sqrt{\mu_R}R/[\sqrt{m}a_0(0)]$.

be obtained for other L values, i.e., there exists a sequence of hyperangular eigenvalues $s_\nu(R)$ for each L . Efimov physics is absent for BBB systems with $L > 0$.

The FFX system contains two s -wave interactions, one for each of the two FX pairs. The implicit eigenequations for $s_\nu(R)$ read [156]

$$\frac{s_\nu(R)\kappa^{1/2}\cos\left[s_\nu(R)\frac{\pi}{2}\right]}{(1+\kappa)^{1/2}} + \frac{(1+\kappa)^{3/2}\sin\left[s_\nu(R)\sin^{-1}\left(\frac{\kappa}{1+\kappa}\right)\right]}{[\kappa(1+2\kappa)]^{1/2}} = \sqrt{\frac{\mu_R}{m}}\frac{R}{a_0(0)}\sin\left[s_\nu(R)\frac{\pi}{2}\right] \quad (32)$$

for $L = 0$ and [156, 157]

$$\frac{\kappa^{3/2}[s_\nu^2(R) - 1] {}_2F_1\left(\frac{3-s_\nu(R)}{2}, \frac{3+s_\nu(R)}{2}, \frac{5}{2}, \frac{\kappa^2}{(1+\kappa)^2}\right)}{3(1+\kappa)^{3/2}} - \frac{[s_\nu^2(R) - 1]\kappa^{1/2}\sin\left[s_\nu(R)\frac{\pi}{2}\right]}{s_\nu(R)(1+\kappa)^{1/2}} = \sqrt{\frac{\mu_R}{m}}\frac{R}{a_0(0)}\cos\left[s_\nu(R)\frac{\pi}{2}\right] \quad (33)$$

for $L = 1$, where κ denotes the ratio between the mass of the F and X atoms and m denotes the mass of the X atom. Similar expressions can be obtained for $L > 1$. Figure 6 shows the effective potentials $\hbar^2 s_\nu^2(R)/(2\mu_R R^2)$ for the FFX system ($\kappa = 1$) with $L = 0$ and 1 as a function of $\sqrt{\mu_R}R/[\sqrt{m}a_0(0)]$, where $a_0(0)$ is positive. For the three-body system, a large hyperradius R corresponds to one of two scenarios. Either all particles are far apart from each other or one particle is far apart from the other two. The former is associated with the atom-atom-atom continuum while the latter is associated with the atom-dimer continuum. The hyperradial potential curves that

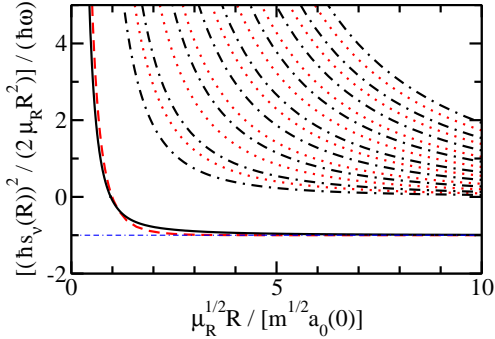


Figure 6. (Color online) Hyperradial potential curves $\hbar^2 s_\nu^2(R)/(2\mu_R R^2)$ for the FFX system ($\kappa = 1$) as a function of $\sqrt{\mu_R}R/[\sqrt{m}a_0(0)]$ for $a_0(0) > 0$. Dashed and solid lines show the potential curves that asymptotically approach the atom-dimer threshold for $L = 0$ and $L = 1$, respectively. Dotted and dash-dotted lines show the potential curves that asymptotically approach the atom-atom-atom threshold for $L = 0$ and $L = 1$, respectively. As a reference, the thin dash-dash-dotted line indicates the atom-dimer threshold.

approach the atom-dimer threshold are shown by dashed and solid lines for $L = 0$ and $L = 1$, respectively. Figure 6 shows that the $L = 0$ curve approaches the atom-dimer threshold (thin dash-dash-dotted line) faster than the $L = 1$ curve. The ordering of the hyperspherical potential curves in the small $R/a_0(0)$ regime reflects the values of s_ν at unitarity [$R/a_0(0) = 0$ corresponds to the infinite scattering length or unitary limit]. As elaborated on further in Subsec. 3.2 (see Fig. 7), the lowest s_ν value for $L = 1$ lies below that for $L = 0$ at unitarity. The fact that Fig. 6 contains only a single atom-dimer threshold is unique to the zero-range potential model employed. More realistic two-body potentials support several two-body bound states, and the corresponding three-body hyperradial potential curves contain as many atom-dimer thresholds as the two-body potential supports bound states. The fact that the lowest hyperradial potential curves for $L = 0$ and $L = 1$ are purely repulsive for $\kappa = 1$ signals the absence of three-body bound states for the FFX system with zero-range interactions.

3.2. Analytical solutions in the non-interacting and large scattering length limits

This subsection applies the hyperspherical framework to non-interacting three-body systems and three-body systems with large scattering length. Throughout this subsection, we assume that V_{int} is given by a sum of two-body potentials $V_{\text{tb}}(r_{jk})$, which are characterized by zero-energy s -wave scattering lengths $a_0^{(jk)}(0)$. If all $a_0^{(jk)}$ are either zero or infinity, the scattering lengths do not define meaningful length scales. In the zero-range limit, the hyperradial and hyperangular degrees of freedom decouple, i.e., the coupling matrix elements $W_{\nu\nu'}$ and $P_{\nu\nu'}$ vanish identically [41, 156, 160], and Φ_ν and s_ν are independent of R . For finite-range two-body interactions with infinite scattering lengths, the decoupling is approximate. In this case, the zero-range solutions apply in the regime where R and $a_0(0)$ are much greater than r_0 , where r_0 denotes

the range of V_{tb} [or, if the $V_{\text{tb}}(r_{jk})$ are not the same for the different pairs, the largest of the ranges of the $V_{\text{tb}}(r_{jk})$].

For now, we assume that the s_ν are known [see, e.g., Eqs. (31) through (33)] and independent of R . The hyperradial Schrödinger equation then reads

$$\left[\frac{-\hbar^2}{2\mu_R} \frac{\partial^2}{\partial R^2} + V_{\text{eff}}(R) + \frac{1}{2}\mu_R\omega^2 R^2 \right] F_{\nu q}(R) = E_{\nu q} F_{\nu q}(R), \quad (34)$$

where

$$V_{\text{eff}}(R) = \frac{\hbar^2(s_\nu^2 - 1/4)}{2\mu_R R^2}. \quad (35)$$

Here, q is the hyperradial quantum number [see Eqs. (27) and (28)]. Equations (34) and (35) are identical to Eq. (12) with $V_{\text{tb}} = 0$ if the identifications $R = r$, $\mu_R = \mu$ and $s_\nu - 1/2 = l$ are made. This subsection assumes that s_ν is real and greater than zero; the next subsection discusses the case where s_ν is purely imaginary. The two linearly independent solutions of Eq. (34) are thus identical to those given in Eqs. (13) and (14) if the appropriate substitutions are made. The main difference between Eq. (34) and Eq. (12) with $V_{\text{tb}} = 0$ is that the quantity $s_\nu - 1/2$ can take non-integer values ($s_\nu - 1/2 > -1/2$) while the orbital angular momentum quantum number l takes the values $0, 1, \dots$. Enforcing the bound state boundary condition at large R , the hyperradial wave function is given by Eq. (16) with the substitutions introduced above.

To determine the quantization condition for q , we investigate the small R behavior of the two linearly independent functions $f_{\nu q}(R)$ and $g_{\nu q}(R)$ (here and in the following, the first subscript is written as ν as opposed to $s_\nu - 1/2$ for notational convenience). Using $\lim_{x \rightarrow 0} ({}_1F_1(a, b, x^2)) = 1$ [103] in Eqs. (13) and (14), we find $f_{\nu q}(x) \rightarrow x^{s_\nu+1/2}$ and $g_{\nu q}(x) \rightarrow x^{-s_\nu+1/2}$ as $x \rightarrow 0$, where $x = R/a_{\text{ho},R}$ with $a_{\text{ho},R} = \sqrt{\hbar/(\mu_R\omega)}$. $f_{\nu q}(x)$ is normalizable for all $s_\nu + 1/2 > -1/2$ while $g_{\nu q}(x)$ is only normalizable if s_ν is less than one [161]. The latter follows from the fact that $\int_0^\epsilon |g_{\nu q}(x)|^2 dx = \ln x|_0^\epsilon + C$ for $s_\nu = 1$, where C is an integration constant and ϵ denotes a small positive quantity; thus, the integral shows divergent (convergent) behavior in the $x \rightarrow 0$ limit for $s_\nu > 1$ ($s_\nu < 1$). Correspondingly, the irregular function $g_{\nu q}(x)$ must be eliminated for $s_\nu > 1$ [41, 161, 162]. Enforcing the boundary condition $F_{\nu q}(x) \rightarrow 0$ on the exponentially decaying piece of $f_{\nu q}(x)$, one finds $q = 0, 1, \dots$ for $s_\nu > 1$. For $0 < s_\nu < 1$, the irregular solution is normalizable and the hyperradial solution is given by a linear combination of the regular and irregular solutions. The ratio between the two solutions is determined by the logarithmic derivative or hyperradial boundary condition at small R , which can be thought of as being imposed by an effective hyperradial three-body potential. If the irregular solution is suppressed naturally, which is expected to be the case for “generic interactions”, the properties of the system with $1 > s_\nu > 0$ are fully determined by $a_0(0)$ [161, 162]. However, as discussed in Refs. [163, 164, 165] and Subsec. 4.3, intriguing physics emerges if both the regular and irregular solutions contribute. Table 2 summarizes the dependence of the quantization condition on the value of s_ν .

We now apply the outlined formalism to the BBB and FFX systems [158, 160]. For three identical bosons, the wave function has to be fully symmetric under the exchange of any pair of bosons. This symmetry constraint reduces the density of states compared to that of a XYZ system, which consists of three distinguishable particles that interact through the same potential energy surface as the BBB system. Since the hyperradius R is unchanged under the exchange of any pair of particles, the symmetrization operator

Table 2. Dependence of the solutions to the hyperradial Schrödinger equation with R -independent s_ν , Eqs. (27) and (28), on the value of s_ν .

s_ν real, $s_\nu > 1$	$q = 0, 1, \dots$
s_ν real, $1 > s_\nu > 0$	q depends on hyperradial boundary condition
s_ν imaginary	q depends on hyperradial boundary condition (Efimov physics)

\mathcal{S} only affects $\vec{\Omega}$ and, correspondingly, only the hyperangular channel functions. The ground state energy of the non-interacting BBB system, which has vanishing relative angular momentum and natural parity (i.e., $L^\Pi = 0^+$), corresponds to a situation in which all bosons occupy the lowest single particle state. Since each single particle state has an energy of $3\hbar\omega/2$, the relative ground state energy E is $E = 3\hbar\omega$ (or $s_0 = 2$) and the center of mass energy is $E_{\text{cm}} = 3\hbar\omega/2$. The allowed s_ν values of the excited non-interacting states can be found by solving Eq. (31) for $a_0(0) = 0$ (see also asymptotic values in Fig. 5). For $L = 0$, we find $s_\nu = 2, 6, 8, 10, 12, 14, 16, 18, \dots$ ($s_\nu = 4$ is forbidden due to symmetry constraints), with degeneracies $1, 1, 1, 1, 1, 2, 1, 2, \dots$; the s_ν values for 18 and higher are doubly-degenerate [166]. This non-interacting $L = 0$ example shows that the s_ν values do not necessarily follow a simple, easy to guess pattern. For each s_ν (which depends on L), q takes the values $q = 0, 1, \dots$.

Next, we consider the BBB system with infinite scattering lengths [158, 160]. The lowest few s_ν values for $L = 0$ are $s_\nu \approx 1.00624i, 4.46529, 6.81836$ and 9.32469 (see Fig. 5). To connect the allowed s_ν values for vanishing and infinitely large scattering lengths, we follow the dotted lines in Fig. 5 from the left to the right. As $\sqrt{\mu_R}R/[\sqrt{m}a_0(0)]$ increases from $-\infty$ to -0.6385 , the lowest s_ν value decreases from 2 to 0. At $\sqrt{\mu_R}R/[\sqrt{m}a_0(0)] \approx -0.6385$, the lowest s_ν value becomes purely imaginary and the dotted line “goes over” to the solid line. The s_ν values corresponding to excited hyperangular states decrease as $\sqrt{\mu_R}R/[\sqrt{m}a_0(0)]$ increases from $-\infty$ to 0 to ∞ . The overall behavior of the s_ν values (s_ν real) as a function of $\sqrt{\mu_R}R/[\sqrt{m}a_0(0)]$ is similar to that of the eigenenergies of the two-body system as a function of $a_{\text{ho},\mu}/a_0(0)$ [see Fig. 3(a)]. However, the amount by which s_ν drops when going from the non-interacting to the large scattering length limits depends, unlike in the two-body case, on the state under consideration. Furthermore, it must be kept in mind that the s_ν values are related to the hyperangular eigenvalues and that coupling between the different hyperangular channels modifies the energy spectrum for finite $a_0(0)$.

Next, we consider FFX systems with $\kappa = 1$ and $\kappa > 1$. Figure 7 shows the s_ν coefficients for the FFX system ($\kappa = 1$) as a function of L for $a_0(0) = \infty$ [158]. The s_ν coefficients are purely real and greater than 1 for all L and correspondingly q takes the values $0, 1, \dots$ for each s_ν (see Table 2). In Fig. 7, dotted lines show the approximate semi-classically derived s_ν values for $a_0(0) = \infty$ [158], $s_\nu = 2\nu + 3$ for $L = 0$ and $s_\nu = 2\nu + L + 1$ for $L \geq 1$ ($\nu = 0, 1, \dots$). These expressions, which have also been deduced using an “atom-dimer type picture” [167, 168], become more accurate with increasing ν and/or L . The s_ν coefficients at unitarity constitute a key ingredient for determining the finite temperature equation of state of strongly-interacting two-component Fermi gases in the bulk limit via a high temperature virial expansion approach (see Subsec. 4.4 and Refs. [169, 170]).

Figure 8 shows the real part of the lowest s_ν coefficients of the FFX system for $a_0(0) = \infty$ as a function of the mass ratio κ for $L = 0 - 3$. The s_ν coefficient for

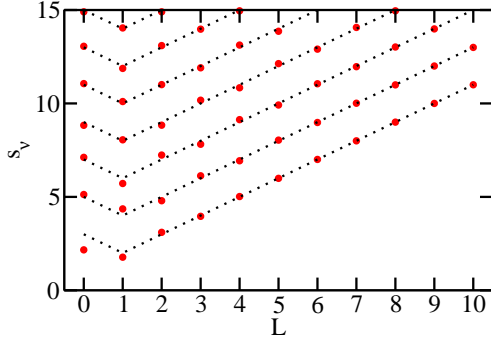


Figure 7. (Color online) Symbols show the s_ν coefficients for the FFX system ($\kappa = 1$) as a function of L for $a_0(0) = \infty$. Note that the s_ν values are purely real for all L . The s_ν values have been obtained by solving Eq. (17) of Ref. [158] [for $L = 0$ and 1, see Eqs. (32) and (33)]. Dotted lines show approximate semi-classically derived expressions (see text).

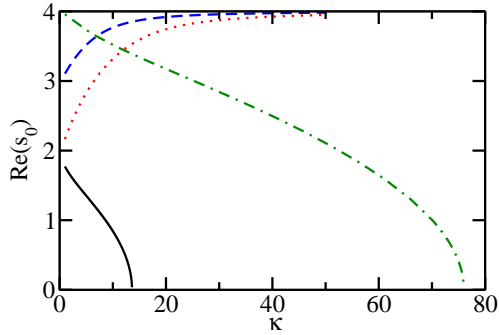


Figure 8. (Color online) Dotted, solid, dashed and dash-dotted lines show the lowest s_0 value as a function of κ for the FFX system at unitarity for $L = 0, 1, 2$ and 3, respectively, and $\Pi = (-1)^L$. The s_0 values are obtained by solving the equations given in Sec. III of Ref. [156] [for $L = 0$ and 1, see Eqs. (32) and (33)].

$L = 1$, which is lower than that for $L = 0, 2$ and 3, decreases from 1.773 to 1 to 0 as κ increases from 1 to 8.619 to 13.607. For $\kappa > 13.607$, the lowest s_ν coefficient for $L^\Pi = 1^-$ becomes purely imaginary, indicating that Efimov physics plays a role for two-component Fermi systems with $\kappa > 13.607$. Applying the results from Table 2 to the FFX system with $L^\Pi = 1^-$, q takes integer values for $\kappa < 8.619$, depends on the short-range hyperradial boundary condition for $8.619 < \kappa < 13.607$, and depends on the three-body Efimov parameter for $\kappa > 13.607$. The fact that the lowest s_ν coefficient of the FFX system for $L = 1$ decreases with increasing κ can be attributed to an effective attraction between the two heavy fermions, which is induced by the light particle. This interpretation emerges within a BO treatment [162], in which the

light particle (“electron”) moves in an effective potential created by the two heavy particles (“nuclei”); thus, the FFX system with large κ can be interpreted in much the same way as, for example, the H_2^+ molecule.

3.3. Efimov physics

As already alluded to, the Efimov effect arises if two or more of the s -wave scattering lengths that characterize the two-body subsystems diverge and if s_ν is purely imaginary. Examples include the BBB system with $L^\Pi = 0^+$ symmetry and the FFX system with $\kappa > 13.607$ and $L^\Pi = 1^-$ symmetry. In the limit that $r_0 \rightarrow 0$, the hyperradial potential V_{eff} , Eq. (35), takes the form $\hbar^2(-\bar{s}_\nu^2 - 1/4)/(2\mu_R R^2)$, where \bar{s}_ν is purely real, i.e., $\bar{s}_\nu = \text{Im}(s_\nu)$. The bound state solution of the free-space hyperradial Schrödinger, Eq. (34) with $\omega = 0$ and V_{eff} given above, reads $F_{\nu\bar{\kappa}}(R) = (\bar{\kappa}R)^{1/2}K_{i\bar{s}_\nu}(\bar{\kappa}R)$, where $\bar{\kappa} = \sqrt{2\mu_R|E|/\hbar}$ and where $K_{i\bar{s}_\nu}$ denotes the modified Bessel function of the second kind with imaginary index [48]. Here, the hyperradial solution is labeled by $\bar{\kappa}$ and not by k , as done in Subsec. 2.1, since we are considering bound states and not scattering states. To be consistent with our previously introduced conventions, our $\bar{\kappa}$ includes an extra factor of $\sqrt{2}$ compared to Eq. (152) of Ref. [48]. An analysis of the solution shows that the three-body system supports an infinite number of three-body bound states. While the bound state energies $E^{(n)}$ depend on the short range boundary condition, the ratio between two consecutive bound state energies $E^{(n)}$ and $E^{(n+1)}$ is independent of the three-body parameter and fully determined by \bar{s}_ν ,

$$\frac{E^{(n+1)}}{E^{(n)}} = \exp\left(-\frac{2\pi}{\bar{s}_\nu}\right). \quad (36)$$

For the BBB system in free space, for example, the spacing between the $(n+1)^{\text{th}}$ and n^{th} bound state is approximately $1/515$. This geometric spacing reflects a discrete scale invariance and is the key characteristic of the Efimov effect. Other observables such as the three-body recombination rate K_3 to weakly bound dimers and scattering resonances also carry signatures of the discrete scale invariance. For example, K_3 can be written as $f\hbar|a_0(0)|^4/m$, where the “amplitude” f depends on the two-body s -wave scattering length $a_0(0)$ and the three-body phase θ_b , which is—in turn—related to $E^{(n)}$ [171, 172, 173, 174]. The short-range phase θ_b can thus be determined by fitting the experimentally determined three-body recombination rate, measured over a wide range of s -wave scattering lengths [52], to the known functional form of K_3 . Although the discussion so far is, strictly speaking, only valid in the $r_0 \rightarrow 0$ and $a_0(0) \rightarrow \infty$ limits, the key features survive as long as $r_0/|a_0(0)| \ll 1$. See, e.g., Refs. [175, 176, 177] for a discussion of finite-range effects.

We now investigate how the external spherically symmetric confinement modifies the Efimov spectrum [158, 160, 178, 179]. In particular, we seek solutions to Eqs. (34) and (35) for purely imaginary and R -independent s_ν . As before, the hyperradial solutions are given by Eq. (16) with l replaced by $i\bar{s}_\nu - 1/2$ and x equal to $R/a_{\text{ho},R}$. The radial solutions can be conveniently written in terms of the Whittaker function W [103, 158], $F_{\nu\kappa}(x) = N_{i\bar{s}_\nu}(\kappa)x^{-1/2}W_{E/2, i\bar{s}_\nu/2}(x^2)$, where κ is used instead of q to label the hyperradial solutions and where $N_{i\bar{s}_\nu}(\kappa)$ denotes a normalization constant. In the small x limit, the radial solutions become

$$F_{\nu\kappa}(x) \rightarrow N_{i\bar{s}_\nu}(\kappa)\sqrt{x}(bx^{i\bar{s}_\nu} - b^*x^{-i\bar{s}_\nu}), \quad (37)$$

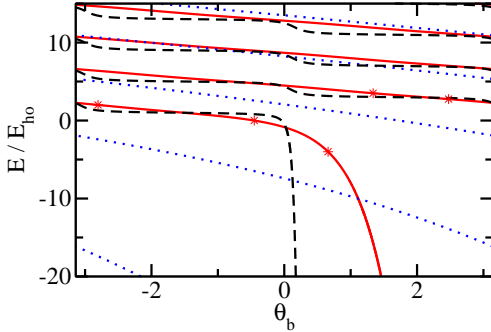


Figure 9. (Color online) The solid lines show the relative eigenenergies E , calculated using Eq. (40), as a function of θ_b for the BBB system with $L^\Pi = 0^+$ at unitarity ($\bar{s}_\nu \approx 1.00624$). For comparison, dashed and dotted lines show the eigenenergies for a 10 times smaller and a 10 times larger \bar{s}_ν value, corresponding to the FFX system with $L^\Pi = 1^-$ and κ just larger than 13.607 and very large, respectively. Asterisks mark the (θ_b, E) values for which Fig. 10 shows the radial wave functions.

where [160]

$$b = \frac{\Gamma\left(\frac{1}{2} - \frac{E}{2\hbar\omega} + \frac{i\bar{s}_\nu}{2}\right)}{\Gamma(1 + i\bar{s}_\nu)}. \quad (38)$$

We emphasize that the quantity b depends on the energy of the trapped three-body system. Thus, for a given three-body system, b can be varied by changing the angular trapping frequency. Defining $b = |b| \exp(i\theta_b)$, Eq. (37) becomes

$$F_{\nu\kappa}(x) \rightarrow N_{i\bar{s}_\nu}(\kappa) \sqrt{x} \sin(\bar{s}_\nu \ln x + \theta_b) \quad (39)$$

with

$$\theta_b = \arg(b). \quad (40)$$

For a fixed θ_b , the allowed energy eigenvalues are determined by Eq. (40).

Figure 9 shows the three-body eigenenergies as a function of the three-body phase θ_b at unitarity for three different \bar{s}_ν values, i.e., $\bar{s}_\nu = 1.00624$, 0.100624 , and 10.0624 . It can be seen that the energy spectrum depends quite strongly on θ_b . In particular, the energy spacing between consecutive eigenenergies varies notably with θ_b for fixed \bar{s}_ν . For negative energies, the spectrum looks Efimov-like; by this we mean that the spacing between consecutive energy levels follows, very roughly, that of the free-space system. For positive energies, in contrast, the spectrum shows similarities with the gas-like spectrum of three-body systems for which Efimov physics is absent. We emphasize that the three-body phase θ_b is not determined by the zero-range model and needs to be extracted from experimental data or *ab initio* calculations. Spectroscopic measurements for the trapped three-body system may, e.g., allow one to extract the three-body phase θ_b [179].

The short-range phase θ_b determines the small R hyperradial boundary condition. The limiting behavior of $F_{\nu\kappa}(x)$, Eq. (39), indicates that the radial eigenfunction shows oscillatory behavior at small R . Figure 10 shows the radial solutions $F_{\nu\kappa}(x)$ for the

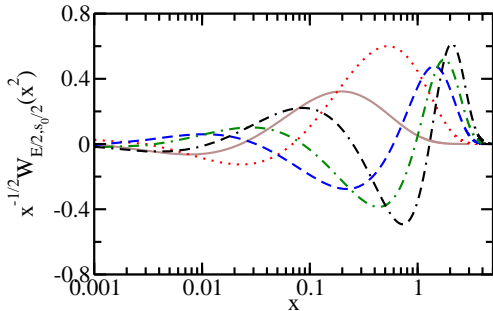


Figure 10. (Color online) Solid, dotted, dashed, dash-dotted and dash-dash-dotted lines show the radial wave function $W_{E/2, s_0/2}(x^2)/\sqrt{x}$ for the BBB system at unitarity ($\bar{s}_0 = 1.00624$) for $E = -4\hbar\omega$, 0 , $2\hbar\omega$, $11\hbar\omega/4$ and $7\hbar\omega/2$, respectively.

BBB system at unitarity ($\bar{s}_\nu = 1.00624$) for five different relative energies $E/(\hbar\omega)$ or, alternatively, for five different three-body phases θ_b . The corresponding (θ_b, E) values are marked by asterisks in Fig. 9. It can be seen that the wave length of the oscillations decreases with decreasing x and that the wave function extends to larger hyperradii with increasing energy.

A more detailed discussion of Efimov physics can be found in Refs. [48, 49]. The key point for the discussion of larger systems is that the three-body energy spectrum in the Efimov regime depends, in addition to the scattering length, on a three-body parameter (parameterized through θ_b above). Although the behavior at unitarity is particularly transparent since the channel coupling vanishes, the three-body phase also plays a role for systems with finite scattering lengths. As shown in Subsec. 5.3, the energy of weakly-interacting trapped Bose gases also depends—although in a rather different manner—on the three-body parameter.

4. Fermi gases under external confinement

This section discusses the behavior of s -wave interacting Fermi gases under external confinement. Subsection 4.1 provides a qualitative and, where possible, quantitative description of the crossover from the weakly-attractive atomic Fermi gas to the weakly-repulsive molecular Bose gas regime of equal-mass systems and introduces a perturbative description of the weakly-interacting regimes. Subsection 4.2 focuses on the unitary regime, where the s -wave scattering length diverges. Subsection 4.3 extends the discussion of equal-mass Fermi gases to unequal-mass Fermi gases. Lastly, Subsec. 4.4 shows that the microscopic few-body energy spectra can be used to predict the thermodynamic properties of inhomogeneous and homogeneous equal-mass two-component Fermi gases via a high temperature virial expansion approach, which—somewhat surprisingly—remains valid down to about half the Fermi temperature.

4.1. Microscopic description of BCS-BEC crossover of trapped two-component Fermi gas with equal masses

This subsection considers two-component Fermi gases with N_1 atoms of the first species and N_2 atoms of the second species ($N = N_1 + N_2$). We assume that like fermions are non-interacting and that unlike fermions interact through a spherically symmetric short-range two-body potential $V_{\text{tb}}(r_{jk})$, where $r_{jk} = |\vec{r}_j - \vec{r}_k|$ [\vec{r}_j denotes the position vector of the j^{th} fermion ($j = 1, \dots, N$) measured with respect to the trap center]. Restricting ourselves to spherically symmetric harmonic confining potentials with angular trapping frequency ω , the model Hamiltonian H reads

$$H = \sum_{j=1}^N \left(\frac{-\hbar^2}{2m} \nabla_{\vec{r}_j}^2 + \frac{1}{2} m \omega^2 \vec{r}_j^2 \right) + \sum_{j=1}^{N_1} \sum_{k=N_1+1}^N V_{\text{tb}}(r_{jk}), \quad (41)$$

where m denotes the atom mass. The Hamiltonian given in Eq. (41) describes equal-mass two-component Fermi gases such as ^6Li atoms in two different hyperfine states or ^{40}K atoms in two different hyperfine states. The Hamiltonian is single-channel in nature, which—following the discussion of Subsec. 2.1—implies that our treatment applies to Fermi gases near broad but not near narrow Fano-Feshbach resonances. This subsection discusses the properties of systems governed by H , Eq. (41), as functions of the number of particles N (throughout, we use $N_1 \geq N_2$) and the s -wave scattering length $a_0(0)$ of the two-body potential V_{tb} .

Equal-mass two-component Fermi gases are fully universal, i.e., the system behavior is fully determined by $a_0(0)$, provided the range r_0 of the two-body potential V_{tb} is much smaller than the s -wave scattering length $a_0(0)$, the average interparticle spacing $\langle r_{ij} \rangle$ and the harmonic oscillator length a_{ho} , where $a_{\text{ho}} = \sqrt{\hbar/(m\omega)}$. The evidence for universality comes from studies that show that the system behavior remains essentially unchanged when the shape of the two-body interaction potential is varied in the regime $r_0 \ll a_{\text{ho}}$ and $r_0 \ll \langle r_{ij} \rangle$. This characteristic is closely linked to the fact that the $(2, 1)$ system does not support a weakly-bound three-body state [162, 180] (see Subsecs. 3.1 and 3.2). Furthermore, weakly-bound four-body or higher-body bound states are absent in the zero-range limit [37, 38, 181, 182, 183], and dilute two-component Fermi gases are stable even for infinitely large s -wave scattering length. The Pauli exclusion principle can be thought of as producing an effective repulsive force that stabilizes the system with attractive interactions against collapse. This is reminiscent of the stabilization of white dwarfs against gravitational collapse by the electron degeneracy pressure [184].

We start our analysis of the Hamiltonian H , Eq. (41), by considering the $(N_1, N_2) = (2, 1)$ system. The energy spectrum of the $(2, 1)$ system can be obtained using the hyperspherical framework outlined in Subsec. 3.1. Here, we instead employ an approach based on the Lippmann-Schwinger equation, which allows for the determination of the energy spectrum of the equal-mass three-fermion system with zero-range interactions with comparatively little computational effort [185]. The success of this technique rests in the fact that two-body correlations are built into the three-body wave function from the outset. Figure 11 shows the energy spectra for the two lowest relative angular momenta, i.e., for $L = 0$ and 1, of the three-fermion system as a function of $a_{\text{ho}}/a_0(0)$. In determining the eigenenergies, we assumed that the center-of-mass degrees of freedom are in the ground state, i.e., that $E_{\text{cm}} = 3\hbar\omega/2$. The key characteristics of the three-fermion spectra can be summarized as follows:

- (i) In the $a_0(0) \rightarrow 0^-$ limit, the three-fermion system behaves like a non-

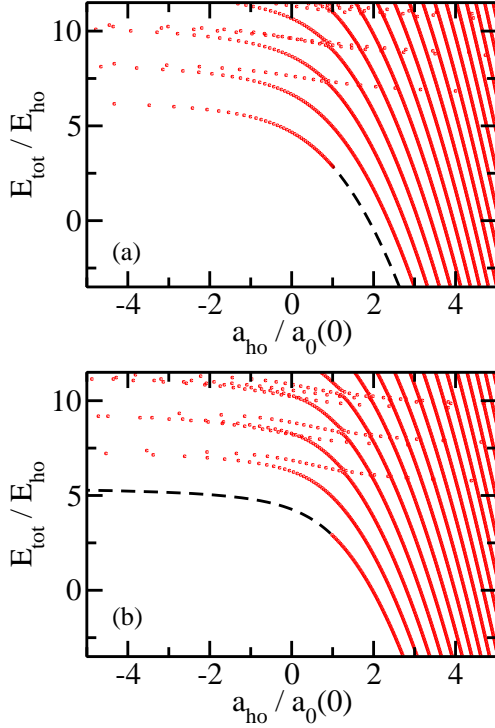


Figure 11. (Color online) Energy spectra for the FFX system with $\kappa = 1$ for (a) $L^{\text{II}} = 0^+$ and (b) $L^{\text{II}} = 1^-$ as a function of the inverse scattering length $[a_0(0)]^{-1}$ (E_{tot} includes the center-of-mass energy of $3\hbar\omega/2$). The BCS-BEC crossover curve is shown by dashed lines. The energy spectra are calculated numerically following the formulation introduced in Ref. [185].

interacting atomic Fermi gas. The energy of the lowest $L = 0$ and 1 states is $E_{\text{tot}} = 13\hbar\omega/2$ and $11\hbar\omega/2$, respectively. The fact that the lowest $L = 1$ state has a lower energy than the lowest $L = 0$ state can be understood readily by considering the non-interacting limit, where the wave function separates into a component that depends on \vec{r}_{12} and a component that depends on the second Jacobi vector (when the interactions are turned on, the wave functions no longer separate and the argument needs to be modified accordingly). The three-fermion wave function is antisymmetric under the exchange of the two spin-up atoms, implying that the wave function component along the \vec{r}_{12} vector carries one unit of angular momentum. For the lowest state with $L = 1$, the wave function component along the second Jacobi vector carries no angular momentum (implying that the wave function component along the second Jacobi vector contributes an energy of $3\hbar\omega/2$). For the lowest state with $L = 0$, in contrast, the wave function component along the second Jacobi vector carries one unit of angular momentum, which couples to the angular momentum associated with the \vec{r}_{12} coordinate such that $L = 0$ (implying that the wave function component along the second Jacobi vector contributes an energy of $5\hbar\omega/2$).

(ii) In the $a_0(0) \rightarrow 0^+$ limit, the three-fermion spectra consist of two different energy families. The first energy family “dives down” as $a_0(0)$ approaches 0^+ (this is the “molecule+atom family”) while the second energy family, the so-called “atom+atom+atom family”, approaches the energy spectrum of the non-interacting atomic Fermi gas [i.e., the atom+atom+atom part of the spectrum is the same as that in the $a_0(0) \rightarrow 0^-$ limit (see above)]. The lowest energy level of the $(2, 1)$ system belongs to the molecule+atom family, for which the system consists of a tightly-bound s -wave molecule and a spare atom that carries the angular momentum L of the three-body system. The energies of states belonging to the molecule+atom family approach $E_{\text{tot}} = E_{\text{bound}} + (2n_{\text{eff}} + L + 3)\hbar\omega$, where $n_{\text{eff}} = 0, 1, \dots$ and where E_{bound} denotes the energy of the tightly-bound s -wave molecule [see Eq. (7)], as $a_0(0) \rightarrow 0^+$. Thus, the lowest $L = 0$ state has an energy that is approximately $\hbar\omega$ below that of the lowest $L = 1$ state. The energy shift due to the effective interaction between the molecule and the atom is discussed below [see Eq. (44)].

(iii) As discussed in (i) and (ii), the lowest energy of the $(2, 1)$ system has angular momentum $L = 1$ in the $a_0(0) \rightarrow 0^-$ limit and $L = 0$ in the $a_0(0) \rightarrow 0^+$ limit. The lowest $L = 1$ and $L = 0$ states cross at $a_{\text{ho}}/a_0(0) \approx 1$ [185, 186, 187]. The energy branch shown by dashed lines in Figs. 11(a) and 11(b) corresponds to the trap analog of the BCS-BEC crossover curve. While the BCS-BEC crossover curve of the homogeneous system depends on two dimensionless parameters, i.e., $k_F a_0(0)$ (k_F denotes the Fermi vector) and the population imbalance p , $p = (N_1 - N_2)/N$, that of the harmonically trapped system depends on three dimensionless parameters, i.e., $a_0(0)/a_{\text{ho}}$, N and $N_1 - N_2$. The system properties of the $(4, 2)$ and $(6, 3)$ systems, for example, differ somewhat, despite the fact that both are characterized by $p = 1/3$.

(iv) The $(2, 1)$ energy spectra show sequences of avoided crossings in the strongly-interacting regime, i.e., for $a_{\text{ho}}/|a_0(0)| \lesssim 1$. These avoided crossings have been analyzed within a Landau-Zener framework [188] and play a crucial role in time-dependent studies. One can, for example, prepare an initial state at equilibrium and analyze the system response to slow (adiabatic) and fast (non-adiabatic) magnetic field ramps, modeled using a time-dependent s -wave scattering length. At the end of the field ramp, the occupation of the energy families, and branches within the energy families, can be monitored. Calculations along these lines are of direct relevance to ongoing experiments. On the one hand, these calculations provide insights into the characteristic time scales that may be extrapolated to larger systems. On the other hand, these calculations describe the dynamics of an isolated optical lattice site. Knowledge of the single optical lattice site dynamics constitutes a crucial building block for understanding the dynamics of systems in which lattice sites are coupled.

The features pointed out in (i)-(iv) for the $(2, 1)$ equal-mass system apply, with appropriate modifications, also to larger trapped two-component Fermi gases. In particular, for small $|a_0(0)|$, $a_0(0) < 0$, the ground state of the trapped (N_1, N_2) system behaves like a weakly-attractive atomic Fermi gas. For small $|a_0(0)|$, $a_0(0) > 0$, the ground state of the trapped system behaves like a weakly-repulsive molecular Bose gas consisting of N_2 diatomic s -wave molecules and $N_1 - N_2$ impurity fermions (if $N_1 \gg N_2$, it is more appropriate to refer to the molecules as impurities immersed in a Fermi sea). In both regimes [negative and positive $a_0(0)$], perturbative treatments reveal the leading order behavior of the energy levels.

For small $a_0(0)$, the unperturbed eigenstates of the N -atom family are given by the non-interacting gas-like atomic states and the sum of atom-atom potentials between unlike fermions is treated as the perturbation. The non-interacting wave

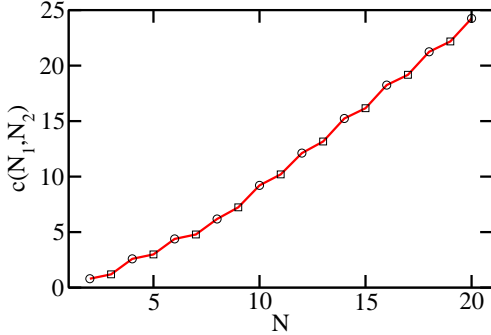


Figure 12. (Color online) Coefficients $c(N_1, N_2)$ that determine the energy shift of the energetically lowest lying state of the weakly-interacting N -atom family [see Eq. (43)] as a function of N . Circles and squares correspond to $N_1 - N_2 = 0$ and 1, respectively; the solid line serves as a guide to the eye. The values of the coefficients are taken from Table I of Ref. [187].

functions can be written as a product of two Slater determinants (one for each component), which are constructed from the single particle harmonic oscillator orbitals [187, 189]. If the atom-atom interaction potential is approximated by the Fermi pseudopotential V_F with s -wave scattering length $a_0(0)$ [78],

$$V_F(\vec{r}_{jk}) = \frac{2\pi\hbar^2 a_0(0)}{\mu} \delta(\vec{r}_{jk}), \quad (42)$$

where μ denotes the reduced mass of the two colliding bodies, the leading order energy shifts can be calculated semi-analytically within first order degenerate perturbation theory. Note that V_F is identical to V_0^{PP} , Eq. (4), without the regularization operator $(\partial/\partial r_{jk})r_{jk}$. Diagonalization of the perturbation matrix results in the approximate expression for $E_{\text{tot}}(N_1, N_2)$ [187, 189],

$$E_{\text{tot}}(N_1, N_2) \approx E_{\text{tot}}^{\text{NI}}(N_1, N_2) + c(N_1, N_2) \frac{a_0(0)}{a_{\text{ho}}} \hbar\omega, \quad (43)$$

where $E_{\text{tot}}^{\text{NI}}(N_1, N_2)$ denotes the total energy of the unperturbed (non-interacting) atomic state under consideration and $c(N_1, N_2)$ a coefficient. Figure 12 shows the coefficients $c(N_1, N_2)$ corresponding to the lowest energy state for systems with $N \leq 20$ and $N_1 - N_2 = 0$ or 1. Interestingly, the $c(N_1, N_2)$ coefficients show distinct even-odd oscillations, with c being larger for even N than for odd N . If $a_0(0)$ is negative, as in the weakly-interacting BCS regime, then a larger c coefficient corresponds to a lower energy. Thus, the perturbative energy expression predicts the existence of a finite energy gap $\Delta E(N)$ in the weakly-interacting regime [see Sec. 4.2, Eq. (49), for the definition of $\Delta E(N)$].

For small and positive $a_0(0)$, the perturbative description of the lowest energy family is based on the assumption that N_2 s -wave molecules, consisting of one spin-up and one spin-down atom, form and that the remaining $N_1 - N_2$ spin-up fermions are unpaired. Effectively, the Fermi gas consists of two constituents (fermions of mass m and molecules of mass $2m$) and the system properties are governed by the molecule-

Table 3. Summary of selected studies that determined the three-dimensional atom-dimer and dimer-dimer scattering lengths a_{ad} and a_{dd} , respectively.

$a_{\text{ad}}/a_0(0)$	method
$\kappa = 1$: $a_{\text{ad}}/a_0(0) = 1.2$	free-space scattering [180]
any κ	free-space scattering [162]
$\kappa = 1$: $a_{\text{ad}}/a_0(0) = 1.1790662349$	free-space scattering [42]
$\kappa = 1$: $a_{\text{ad}}/a_0(0) = 1.18(1)$	trap spectrum [187]
$a_{\text{dd}}/a_0(0)$	method
$\kappa = 1$: $a_{\text{dd}}/a_0(0) = 0.6^{(a)}$	free space scattering (four-body) [182]
$\kappa = 1$: $a_{\text{dd}}/a_0(0) = 0.60^{(b)}$	free space scattering [190]
$\kappa = 1$: $a_{\text{dd}}/a_0(0) = 0.60^{(b)}$	diagrammatically [191, 192]
$1 \leq \kappa \leq 13.607$	free-space scattering [99]
$\kappa = 1$: $a_{\text{dd}}/a_0(0) = 0.608(2)$	trap spectrum [187, 189]
$1 \leq \kappa \leq 20$	trap spectrum [187, 189]
$\kappa = 1$: $a_{\text{dd}}/a_0(0) = 0.62(1)$	homogeneous system [38]
$\kappa = 1$: $a_{\text{dd}}/a_0(0) = 0.605(5)$	free-space scattering [193]

^(a)The accuracy is reported to be 2 %. ^(b)No errorbar is reported.

molecule (or dimer-dimer) scattering length a_{dd} and the atom-molecule (or atom-dimer) scattering length a_{ad} . Following this logic, the unperturbed wave function is written as a product of a permanent, constructed from N_2 harmonic oscillator orbitals with width $\sqrt{\hbar/(2m\omega)}$ that depend on the center of mass vectors of the molecules, and a Slater determinant, constructed from $N_1 - N_2$ single particle harmonic oscillator orbitals with width $\sqrt{\hbar/(m\omega)}$. The interaction between an atom and a molecule (between two molecules) is parameterized by Eq. (42) with $a_0(0)$ replaced by a_{ad} (a_{dd}) and μ replaced by $\mu_{\text{ad}} = 2m/3$ ($\mu_{\text{dd}} = m$). For the lowest energy family, the perturbative treatment gives [187, 189]

$$E_{\text{tot}}(N_1, N_2) \approx N_2 E_{\text{dimer}} + E_{\text{tot}}^{\text{NI}}(N_1 - N_2, 0) + \frac{N_2(N_2 - 1)}{2} \sqrt{\frac{2}{\pi}} \frac{a_{\text{dd}}}{a_{\text{ho}, \mu_{\text{dd}}}} \hbar\omega + N_2(N_1 - N_2) c_{\text{ad}} \frac{a_{\text{ad}}}{a_{\text{ho}, \mu_{\text{ad}}}} \hbar\omega, \quad (44)$$

where $a_{\text{ho}, \mu_i} = \sqrt{\hbar/(\mu_i\omega)}$ with $i = \text{ad}$ or dd . In Eq. (44), E_{dimer} denotes the ground state energy of the trapped dimer interacting through V_0^{PP} with scattering length $a_0(0)$ [i.e., the lowest $l = 0$ eigenenergy of Eq. (17), with the center of mass energy of $3\hbar\omega/2$ added]. The coefficient c_{ad} depends on how many unpaired fermions there are and which single-particle states the unpaired fermions occupy. For the ground state of systems with $N_1 - N_2 = 0$ and 1, we have $c_{\text{ad}} = 0$ and $c_{\text{ad}} = \sqrt{2/\pi}$, respectively.

For the (2, 2) system, for example, Eq. (44) describes the energies of the molecule+molecule family [$a_0(0)$ small and positive] while Eq. (43) describes those of the four-atom family [$|a_0(0)|$ small and either positive or negative]. The (2, 2) system additionally contains a molecule+atom+atom family, whose limiting $a_0(0) \rightarrow 0^+$ behavior can be obtained by assuming that only one dimer forms.

Table 3 summarizes the values obtained for a_{ad} and a_{dd} in the literature by a variety of means. Here, we discuss the determination of the dimer-dimer scattering length in more detail. In the first Born approximation, the dimer-dimer scattering length a_{dd} equals $2a_0(0)$. Microscopic free-space scattering calculations confirm that a_{dd} is directly proportional to the atom-atom scattering length and that no other parameter enters but find that the proportionality factor is ≈ 0.6 as opposed to 2 [182]. The microscopically derived proportionality factor has, for example, been

confirmed using a diagrammatic approach [191, 192] and by analyzing the equation of state of the homogeneous two-component Fermi gas, calculated using Monte Carlo techniques [38], within a perturbative framework analogous to that given in Eq. (44). Here, we show that the dimer-dimer scattering length can alternatively be extracted from the energies of states corresponding to the dimer-dimer family of the trapped (2, 2) system [187, 189].

We start our discussion with the normalized energy crossover curve Λ_{N_1, N_2} [187, 189, 194],

$$\Lambda_{N_1, N_2} = \frac{E_{\text{tot}}(N_1, N_2) - N_2 E_{\text{dimer}} - \frac{3(N_1 - N_2)\hbar\omega}{2}}{E_{\text{tot}}^{\text{NI}}(N_1, N_2) - \frac{3}{2}N\hbar\omega}, \quad (45)$$

which depends on N_1 , N_2 and $a_0(0)$. For the BCS-BEC branch, Λ_{N_1, N_2} changes from 1 to 0 as $1/a_0(0)$ changes from $-\infty$ to ∞ . In addition to providing a convenient means to plot the energies throughout the crossover, Λ_{N_1, N_2} significantly reduces the dependence on the underlying two-body potential [187, 189, 194].

The solid line in Fig. 13 shows $\Lambda_{2,2}$ as a function of $1/a_s(0)$. For $a_s(0) \rightarrow 0^-$, $E_{\text{tot}}(N_1, N_2)$ equals $E_{\text{tot}}^{\text{NI}}(N_1, N_2)$ and E_{dimer} equals $3\hbar\omega$ (we have two fermions with energy $3\hbar\omega/2$ each), yielding $\Lambda_{2,2} = 1$. For $a_s(0) \rightarrow 0^+$, the total energy can be thought of as being due to N_2 dimers (with relative energy $3\hbar\omega/2$ and center of mass energy $3\hbar\omega/2$), yielding $\Lambda_{2,2} = 0$. Inserting Eq. (44) into Eq. (45), we find that $\Lambda_{2,2} \approx (2\pi)^{-1/2} a_{\text{dd}}/a_{\text{ho}, \mu_{\text{dd}}}$ in the $a_0(0) \rightarrow 0^+$ regime. Thus, a_{dd} can be extracted from the full four-particle energy spectrum by fitting the crossover curve to the limiting expression. One arrives at the same result by expanding the eigenenergy of the lowest energy branch of Eq. (17) with $l = 0$ and μ and $a_{\text{ho}, \mu}$ replaced by μ_{dd} and $a_{\text{ho}, \mu_{\text{dd}}}$, respectively, around $a_0(0) = 0^+$ (in this approach, the internal dimer energy and the center-of-mass energy need to be added). The analysis can be refined by using the full two-body energy spectrum as opposed to the Taylor-expanded expression and by allowing a_{dd} to be energy-dependent via Eq. (3). The refined analysis gives $a_{\text{dd}} = 0.608(2)a_0(0)$ [187, 189] in good agreement with the microscopic free-space results (see Table 3) and also provides an estimate of the dimer-dimer effective range $r_{\text{eff}, \text{dd}}$, $r_{\text{eff}, \text{dd}} = 0.13(2)a_0(0)$ [187, 189]. The positive value of $r_{\text{eff}, \text{dd}}$ is consistent with the conclusion by Petrov *et al.* [182] that the two dimers interact through an effective potential with soft core repulsion. Dotted and dashed lines show $\Lambda_{2,2}$ obtained using the perturbative energy expressions, i.e., Eqs. (43) and (44). It can be seen that the perturbative treatment provides a fairly accurate description for $a_{\text{ho}}/a_0(0) \lesssim -4$ and $a_{\text{ho}}/a_0(0) \gtrsim 1.5$, respectively.

The energy spectra and crossover curve shown in Figs. 11 and 13 are for the (2, 1) and (2, 2) systems. Crossover studies for systems with $N > 4$ can be found in Refs. [189, 194, 196]. The energies of the (2, 2) system were obtained using the stochastic variational approach [197], a basis set expansion approach that results in stable and highly accurate results for trapped systems with up to $N = 6$ fermions throughout the entire crossover regime [167, 183, 187, 188, 189, 196, 198]. This numerical approach cannot, at least at present, be applied to significantly larger systems since the computational effort increases notably with increasing N . Alternative numerical microscopic approaches include an effective field theory approach [186, 199, 200], an effective interaction approach [201], and Monte Carlo approaches. The applicability of the effective field theory approach is presently also limited to relatively small particle numbers ($N \leq 4$) while Monte Carlo methods have been applied to larger systems. The Monte Carlo techniques can, for the purpose of

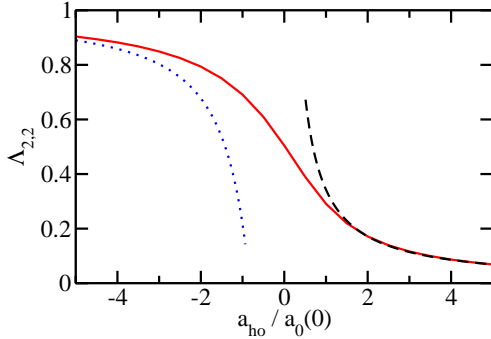


Figure 13. (Color online) Normalized energy crossover curve $\Lambda_{2,2}$ for $\kappa = 1$ as a function of $a_{\text{ho}}/a_0(0)$. The solid line shows $\Lambda_{2,2}$ derived from the $L = 0$ extrapolated zero-range ground state energies reported in the supplemental material of Ref. [167]. The dotted and dashed lines are obtained using the perturbative expressions [Eqs. (43) and (44)] in Eq. (45).

this review, be divided into two classes. The first class, which includes the diffusion Monte Carlo (DMC, sometimes also referred to as Green’s function Monte Carlo) and variational Monte Carlo (VMC) approaches, is applicable to essentially any interaction strength [183, 187, 189, 194, 208]. These techniques employ the fixed node approximation and result in variational upper bounds to the exact eigenenergies [195]. Note that the accuracy may diminish for certain regions of interaction strengths. The second class of Monte Carlo approaches such as the lattice MC approach from Refs. [202, 203] have thus far only been applied to the unitary regime.

4.2. Large scattering length regime: Unitarity

This subsection considers two-component equal-mass Fermi gases with infinitely large s -wave scattering length under external spherically-symmetric harmonic confinement. As discussed in Subsec. 3.2, an infinitely large s -wave scattering length does not define a meaningful length scale for the system. Thus, two-component Fermi gases with infinite $a_0(0)$ and zero-range interactions are characterized by the same number of length scales as the non-interacting system. This implies, as in the three-body case, that the hyperradial and hyperangular degrees of freedom separate in the limit of zero-range interactions with infinitely large $a_0(0)$ [41, 204]. Correspondingly, the hyperradial Schrödinger equation is given by Eq. (34) with R and μ_R now denoting the hyperradius and the hyperradial mass of the N -body system (i.e., $\mu_R R^2 = \sum_{i=1}^{N-1} \mu_i \vec{\rho}_i^2$, where the $\vec{\rho}_i$ denote the Jacobi vectors—excluding the center of mass vector—and the μ_i denote the associated Jacobi masses). Thus, the hyperradial solutions discussed in Subsec. 3.2 apply to two-component Fermi gases with arbitrary (N_1, N_2) . For equal mass systems with zero-range interactions, the s_ν are all greater than 1. This implies that the energies $E_{\text{tot}}^{\text{unit}}$ at unitarity can be written as [41, 204]

$$E_{\text{tot}}^{\text{unit}} = (2q + s_\nu + 1)\hbar\omega + E_{\text{cm}}, \quad (46)$$

where the hyperradial quantum number q takes the values $0, 1, \dots$ and where the s_ν , which depend on N_1 and N_2 , are determined from the solution of the $3N - 4$ dimensional hyperangular differential equation. The separability of the hyperradial and hyperangular degrees of freedom implies that the dynamics of the N -body system is governed by a set of uncoupled effective one-dimensional hyperradial potential curves. Thus, the strongly-interacting N -body problem reduces to an effective one-dimensional problem.

Equation (46) predicts the existence of energy ladders with spacing $2\hbar\omega$ [41, 204]. Correspondingly, the energy spectrum contains breathing mode frequencies at integer multiples of $2\hbar\omega$, in addition to frequencies that are associated with transitions between different hyperradial potential curves. The latter class of frequencies depends on $s_\nu - s_{\nu'}$, since frequencies in this class arise due to transitions between two different hyperradial potential curves. These predictions are a direct consequence of the scale-invariance [40, 41, 204] and can be verified experimentally.

The characterization of strongly-interacting Fermi gases is non-trivial. Various approaches, including those discussed at the end of the previous subsection, have been applied. Unlike in the three-body case, for which analytical solutions to the hyperangular Schrödinger equation are known (see Subsec. 3.1), no analytical solutions are known for larger systems and one generally has to resort to solving the hyperangular equation or the full Schrödinger equation numerically. For systems with $L = 0$ and up to $N = 4$ particles, the hyperangular Schrödinger equation has been solved by adopting a hyperspherical correlated Gaussian approach [205], a variant of the stochastic variational approach discussed earlier. For larger systems, in contrast, obtaining the solution to the hyperangular Schrödinger equation (which would result in the s_ν) is more challenging than obtaining that to the full Schrödinger equation (which results in $E_{\text{tot}}^{\text{unit}}$). Using Eq. (46), which has been proven to hold if the range r_0 of the underlying two-body potential is sufficiently small [183, 198, 206], $E_{\text{tot}}^{\text{unit}}$ and s_ν can be converted into each other.

Figure 14(a) shows the total energy $E_{\text{tot}}^{\text{unit}}$ as a function of N for two-component Fermi gases with $N_1 - N_2 = 0$ or 1 at unitarity, calculated using three different approaches (i.e., a fixed node DMC approach [183], a lattice MC approach [203] and a density functional theory (DFT) approach [207]). These sets of energies have been chosen to illustrate our current understanding (see Refs. [194, 208, 209] for other calculations). The MC and DFT approaches are based on entirely different formulations and the relatively good agreement displayed in Fig. 14(a) is encouraging. To interpret Fig. 14(a), we relate the energies $E_{\text{tot}}^{\text{unit}}$ at unitarity to the energies $E_{\text{tot}}^{\text{NI}}$ of the trapped non-interacting system. Since the system at unitarity is characterized by the same number of length scales as the non-interacting system, the energies have to be directly proportional to each other [39],

$$E_{\text{tot}}^{\text{unit}} = \sqrt{\xi_{\text{tr}}} E_{\text{tot}}^{\text{NI}}, \quad (47)$$

the reason for writing the proportionality factor as a square root will become clear below. The total energy $E_{\text{tot}}^{\text{NI}}$ of the trapped non-interacting system shows shell closures for $N_i = 1, 4, 10, 20, \dots$, i.e., the energy increases by $3\hbar\omega/2$ when the first spin-up fermion and spin-down fermion are added, by $5\hbar\omega/2$ when the second through fourth spin-up and spin-down fermions are added, and so on. The energies at unitarity show—on the scale chosen in Fig. 14(a)—no signature of shell closures but instead odd-even oscillations. Thus, it appears reasonable to determine the proportionality factor $\sqrt{\xi_{\text{tr}}}$ by “smoothing” the non-interacting energies, i.e., by approximating $E_{\text{tot}}^{\text{NI}}$ by the

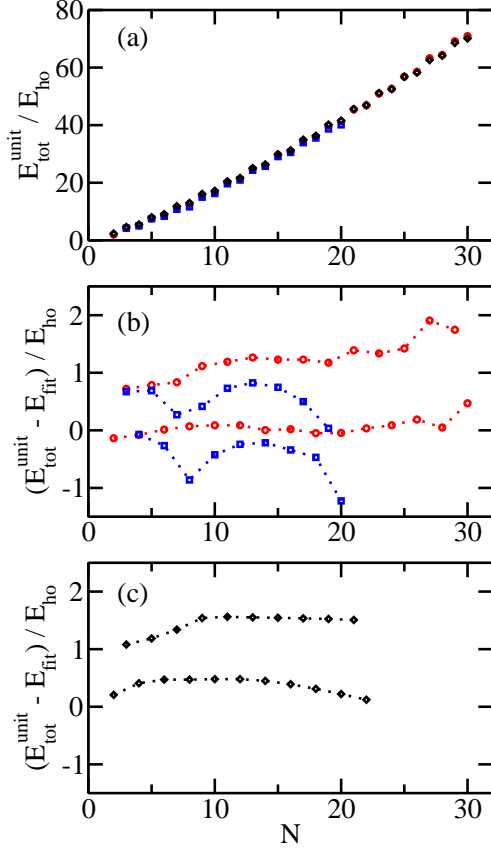


Figure 14. (Color online) Energetics of trapped two-component Fermi gas with $\kappa = 1$ at unitarity as a function of N for $N_1 - N_2 = 0$ or 1. Panel (a) shows the total energy $E_{\text{tot}}^{\text{unit}}$. Panels (b) and (c) show the energy difference $E_{\text{tot}}^{\text{unit}} - E_{\text{fit}}$ using $E_{\text{fit}} = \sqrt{0.467} E_{\text{tot}}^{\text{NI,ETF}}$ (as a guide to the eye, dotted lines connect the data points for even and odd N). Circles, squares, and diamonds show results based on the fixed node DMC energies from Ref. [183], the lattice MC energies from Ref. [203], and the DFT energies from the supplemental material of Ref. [207].

semi-classical extended Thomas Fermi energies $E_{\text{tot}}^{\text{NI,ETF}}$ [210],

$$E_{\text{tot}}^{\text{NI,ETF}} = \frac{1}{4}(3N)^{4/3} \left[1 + c_{\text{ETF}} \frac{1}{2}(3N)^{-2/3} \right] \hbar\omega, \quad (48)$$

where $c_{\text{ETF}} = 1$ (in Subsec. 4.3, we treat c_{ETF} as a fitting parameter). We refer to the energy obtained by fitting the even N energies to Eq. (47) with $E_{\text{tot}}^{\text{NI}}$ replaced by $E_{\text{tot}}^{\text{NI,ETF}}$ as E_{fit} . For the energies for $N = 2 - 30$ of Ref. [183], for example, ξ_{tr} is found to equal 0.465. In the large N limit, the term proportional to c_{ETF} can be neglected and Eq. (48) reduces to the local density approximation (LDA) expression (see below) [39].

Symbols in Figs. 14(b) and (c) show the quantity $E_{\text{tot}}^{\text{unit}} - E_{\text{fit}}$. The energy

difference $E_{\text{tot}}^{\text{unit}} - E_{\text{fit}}$ reveals clear odd-even oscillations for all three data sets. For the fixed node DMC data [circles in Fig. 14(b)], the energy difference $E_{\text{tot}}^{\text{unit}} - E_{\text{fit}}$ is approximately equal to zero for even N and of the order of $\hbar\omega$ (with a slight overall increase with increasing N) for odd N . For the lattice MC data set [squares in Fig. 14(b)], in contrast, $E_{\text{tot}}^{\text{unit}} - E_{\text{fit}}$ shows oscillations that follow the shell structure of the non-interacting system for both even and odd N (recall, the non-interacting system with $N_1 = N_2$ possesses shell closures at $N = 2, 8, 20, \dots$), with a roughly constant offset between the even and odd N data. Thirdly, the DFT data [see Fig. 14(c)] show structure that appears to be independent of the shell structure of the non-interacting system. It is currently not fully clear which of these behaviors can be attributed to numerical artifacts and which reflect genuine physics. We speculate that the data from Ref. [203] overestimate the shell structure but note that further studies are needed to fully understand the energetics of trapped two-component systems at unitarity. We note that modified versions of Eqs. (47) and (48), which are based on a different interpretation of the underlying physics, lead to somewhat different ξ_{tr} values [211].

To further interpret the results of the trapped system at unitarity, we relate the energies of the trapped and homogeneous systems via the LDA. The energy $E_{\text{hom}}^{\text{unit}}$ per particle of the homogeneous system at unitarity is directly proportional to the energy E_{FG} of the non-interacting homogeneous gas, $E_{\text{hom}}^{\text{unit}} = \xi_{\text{hom}} E_{\text{FG}}$. The proportionality constant ξ_{hom} , also referred to as the Bertsch parameter [212], has been determined theoretically and experimentally. The most reliable estimate comes from very recent fixed node DMC calculations, which determine an upper bound for ξ_{hom} , $\xi_{\text{hom}} = 0.383(1)$ [213]. The value of ξ_{hom} is of fundamental importance and enters into effective theories that use the equation of state of the homogeneous system as input. Application of the LDA (see, e.g., Ref. [214]), which treats the trapped Fermi gas as being locally (i.e., at each distance from the trap center) characterized by a constant density, predicts that the energy of the trapped system at unitarity is given by $E_{\text{tot}}^{\text{unit}} = \sqrt{\xi_{\text{hom}}} E_{\text{tot}}^{\text{NI}}$ [39]. Thus, ξ_{tr} (see above) provides an alternative estimate of ξ_{hom} . The fact that the ξ_{tr} obtained by analyzing the energies of the trapped system ($\xi_{\text{tr}} = 0.465$) is larger than the value of $\xi_{\text{hom}} = 0.383(1)$ [213] obtained from recent MC simulations for the homogeneous system may be attributed to the fact that the calculations for the trapped system are restricted to relatively small N and/or that the energies of the trapped system may be slightly too high. The latter may be a consequence of the fixed node approximation employed in Ref. [183].

Another quantity of interest is the excitation gap $\Delta E(N)$, which characterizes the odd-even oscillations of two-component Fermi gases. The excitation gap combines the energies of the imbalanced system with $N_1 - N_2 = 1$ (i.e., $N = 2N_1 - 1$) with the energies of the next smaller and next larger balanced systems [39],

$$\Delta E(N) = \frac{E_{\text{tot}}(N_1, N_1 - 1) - E_{\text{tot}}(N_1 - 1, N_1 - 1) + E_{\text{tot}}(N_1, N_1)}{2}. \quad (49)$$

Figure 15 shows $\Delta E(N)$ as a function of N for two-component Fermi gases at unitarity for the same data sets as shown in Figs. 14(a), 14(b) and 14(c). While the energy difference $E_{\text{tot}}^{\text{unit}} - E_{\text{fit}}$ shows a distinct dependence on the numerical approach employed, the excitation gap determined by the three different methods agrees fairly well. The excitation gap $\Delta E(N)$ increases from about $0.7\hbar\omega$ to about $1.5\hbar\omega$ as N increases from 3 to 29. In the homogeneous system, the excitation gap equals half the energy it takes to brake a pair [39]. In the trapped system, the

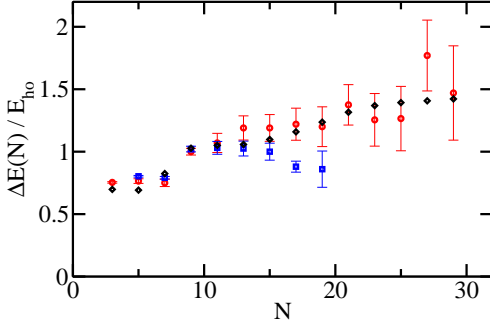


Figure 15. (Color online) Excitation gap $\Delta E(N)$ of trapped two-component Fermi gas with $\kappa = 1$ at unitarity as a function of N for $N_1 - N_2 = 0$ or 1. Circles, squares, and diamonds show results based on the fixed node DMC energies from Ref. [183], the lattice MC energies from Ref. [203], and the DFT energies from the supplemental material of Ref. [207]. For clarity, errorbars are only shown for the fixed node DMC and lattice MC data sets.

interpretation is not quite as straightforward because of the inhomogeneity induced by the confining potential. In particular, the fixed node DMC calculations suggest that the extra particle is located near the edge of the cloud as opposed to the center of the cloud [183, 187]. This finding supports the conclusion put forward by Son [215] that $\Delta E(N)$ scales as $N^{1/9}$ and not as $N^{1/3}$ as would be expected based on the LDA. The microscopic data available to date do not, however, extend to sufficiently large N to unambiguously distinguish between the $N^{1/9}$ and $N^{1/3}$ behaviors. We note that the definition of the excitation gap $\Delta E(N)$, Eq. (49), applies to all interaction strengths, and not just the unitary regime. The excitation gap’s behavior in the weakly-attractive regime has been discussed briefly in the context of Fig. 12.

Lastly, we use the energies $E_{\text{tot}}^{\text{unit}}$ to arrive at an interpretation of the unitary Fermi gas within the hyperspherical framework. The odd-even oscillations of the energies imply odd-even oscillations of the s_ν coefficients that describe the ground state and thus an odd-even staggering of the hyperspherical potential curves $V_{\text{eff}}(R)$ that govern the dynamics at unitarity [41, 187]. Application of the LDA predicts that the s_ν coefficient of the ground state for even N approaches $\sqrt{\xi_{\text{hom}}} E_{\text{tot}}^{\text{NI}} / (\hbar\omega)$ in the large N limit [183].

The microscopic energies as well as structural properties have been used to assess the accuracy of a number of effective approaches, such as those based on fractional exclusion statistics [216], DFT [207, 209, 217, 218, 219, 220] and effective field theory. Lastly, we note that effort has also been devoted to understanding population-imbalanced Fermi gases with $N_1 \gg N_2$ at unitarity within a microscopic framework [221]. In the limit of “extreme” population imbalance, the trapped analog of the fermionic polaron problem is realized [222, 223].

4.3. Mass-imbalanced Fermi gas

This subsection considers s -wave interacting two-component Fermi gases with unequal masses. While equal-mass Fermi gases are, by now, relatively well understood, our

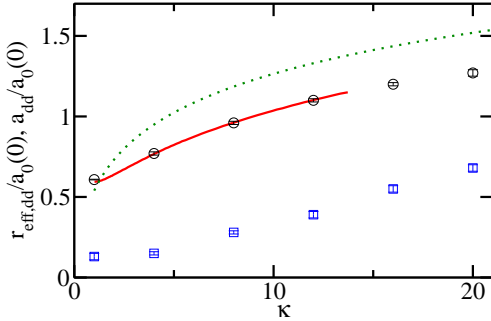


Figure 16. (Color online) Dimer-dimer scattering length a_{dd} and effective range $r_{\text{eff},dd}$ as a function of the mass ratio κ . Solid lines show a_{dd} obtained by solving the free-space Schrödinger equation with zero-range interactions (the results are taken from Fig. 3 of Ref. [99]) while dotted lines show a_{dd} obtained by applying the BO approximation [see Eq. (14) of Ref. [229]]. Circles and squares show a_{dd} and $r_{\text{eff},dd}$ extracted from the energy spectrum of the trapped (2, 2) system (the values of a_{dd} and $r_{\text{eff},dd}$ are taken from Table II of Ref. [187]).

understanding of unequal-mass systems is much less complete. One of the reasons is that experiments on unequal-mass systems are just now becoming available [224, 225, 226, 227, 228]. Dual species experiments can be hampered by large three-body loss rates, which reduce the system's lifetime and thus make it challenging to cool dual-species systems to degeneracy. Trapped dual-species systems with mass ratio κ ($\kappa = m_1/m_2$, where m_i denotes the atom mass of the i^{th} component) are, in general, characterized by two different angular trapping frequencies, i.e., $\omega_1 \neq \omega_2$. If ω_1 and ω_2 differ, the center of mass motion no longer separates. The behavior of the (2, 1) system changes with increasing κ (see Sec. 3): Three-body resonances may occur for $8.619 < \kappa < 13.607$ [41, 161] and Efimov physics plays a role for $\kappa > 13.607$ [48, 49]. The treatment of larger systems with $\kappa \gtrsim 8.619$ thus requires theoretical tools that are capable of accounting for these three-body phenomena and, at the same time, of capturing the new physics introduced by the fourth, fifth, etc. particle.

We first consider unequal-mass Fermi gases with small, positive $a_0(0)$. Assuming that $a_0(0)$ fully characterizes the system dynamics, the perturbative expression Eq. (44) may be generalized to unequal-mass systems [121, 189]. Thus, a natural question is how the atom-dimer and dimer-dimer scattering lengths a_{ad} and a_{dd} vary with κ . For the (2, 1) system, the atom-dimer s -wave scattering length is associated with the $L^\Pi = 0^+$ wave function; for this channel, Efimov physics is absent. The atom-dimer scattering length a_{ad} equals $1.18a_0(0)$ for $\kappa = 1$ and increases with increasing κ [162]. For the (2, 2) system, the s -wave dimer-dimer scattering length was first determined via a free-space calculation that employs a zero-range interaction model and assumes the absence of three-body bound states for $\kappa < 13.607$ [99]. a_{dd} changes monotonically from $0.6a_0(0)$ to $1.14a_0(0)$ as κ increases from 1 to 13.607 [99]. The solid line in Fig. 16 shows the results for a_{dd} . The free-space calculations terminate at $\kappa = 13.607$, where it is known that Efimov physics enters. For $\kappa > 13.607$, the effective dimer-dimer interactions are expected to depend on a three-body or Efimov

parameter.

The dimer-dimer scattering length a_{dd} for unequal-mass systems has also been extracted from the energy spectrum of the trapped $(2, 2)$ system with equal frequencies and finite-range interactions (see circles in Fig. 16) [187, 189]. Figure 16 shows that the two sets of calculations (solid line and circles) are in good agreement for $\kappa \lesssim 13.607$. The latter calculation does not terminate at $\kappa = 13.607$ but goes beyond. In particular, for $\kappa \gtrsim 13.607$, the scattering length a_{dd} is obtained by following the lowest state of the dimer-dimer family, which lies above a subset of states whose energies show a pronounced dependence on the three-body parameter. The dimer-dimer scattering lengths for $\kappa \gtrsim 13.607$ have been confirmed independently by an approximate BO treatment (see dotted line in Fig. 16) [229]. While the scattering lengths derived within the BO framework are larger than those obtained by the more exact treatment, the overall behavior is similar. A more sophisticated BO treatment, referred to as hybrid BO approach, leads to scattering lengths nearly indistinguishable from those shown by the solid line and the symbols in Fig. 16 [229]. The energy spectrum of the trapped four-fermion system additionally allows for the determination of the dimer-dimer effective range $r_{\text{eff,dd}}$ (squares in Fig. 16) [187, 189]. Figure 16 shows that $r_{\text{eff,dd}}$ increases more rapidly with κ than a_{dd} , indicating that finite-range effects for the dimer-dimer system become more important with increasing κ . This implies, e.g., that the validity regime of the dimer-dimer zero-range model decreases with increasing κ . The positive dimer-dimer scattering length suggests that two-component Fermi gases with large mass ratio κ and small atom-atom s -wave scattering length form repulsively interacting metastable molecular Bose gases. Losses due to the formation of Efimov trimers in dimer-dimer collisions are predicted to decrease exponentially with increasing mass ratio [229].

Next, we consider the unitary regime and assume that the angular trapping frequencies ω_i are adjusted such that the harmonic oscillator lengths $a_{\text{ho},i}$, where $a_{\text{ho},i} = \sqrt{\hbar/(m_i\omega_i)}$, are equal. Small trapped two-component systems with equal oscillator lengths, $N \leq 20$ and $1 < \kappa \leq 20$ have been studied by the fixed node DMC method [121, 189]. These fixed node DMC calculations are performed using a guiding function that is constructed from the solution of the two-body problem, a so-called “pairing function”. Since the densities of the two components overlap to a fairly large degree, the fixed node DMC calculations can be used to estimate the dependence of ξ_{tr} on κ . The fixed node DMC energies for $\kappa > 1$ suggest a slightly modified analysis compared to that outlined around Eqs. (47) and (48) for $\kappa = 1$. In particular, E_{fit} is determined by treating the parameter c_{ETF} in Eq. (48) as a fitting parameter and not as a constant [189]. Figure 17 shows that ξ_{tr} (circles in the main figure) and c_{ETF} (squares in the inset) decrease with increasing κ . For comparison, triangles and a diamond show the values of ξ_{hom} for the homogeneous system obtained by performing fixed node DMC calculations [213, 230]. The slight decrease of ξ_{hom} from $\kappa = 1$ to 6.5 (triangles) has been interpreted as providing a measure of non- s -wave contributions for the $\kappa = 6.5$ system compared to the $\kappa = 1$ system [230]. The energy of the trapped system (see circles in Fig. 17) appears to be lowered more than that of the homogeneous system (see triangles in Fig. 17), which might be a consequence of the fact that the trapped system lowers its energy if the densities are slightly mismatched. Other causes for the discrepancy cannot be ruled out and further investigations are needed to clarify this point.

Our discussion thus far has been based on the assumption that trimers are absent. From the zero-range model with infinite $a_0(0)$, however, it is known that three-body

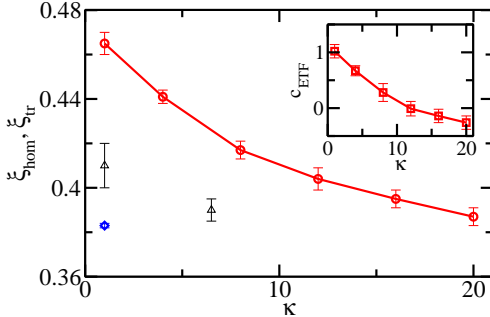


Figure 17. (Color online) Circles (main figure) and squares (inset) show ξ_{tr} and c_{ETF} , respectively, as a function of the mass ratio κ (the values are taken from Fig. 6 of Ref. [189]). For comparison, triangles show ξ_{hom} obtained by the fixed node DMC method [230]; the diamond shows a more recent value for ξ_{hom} for $\kappa = 1$ [213].

bound states may appear for $8.619 < \kappa < 13.607$ [41, 161]. The possibility that three-body physics, and maybe even N -body physics, could play a decisive role in determining the properties of two-component Fermi gases for sufficiently large κ is intriguing and has recently stimulated interest among theorists [161, 163, 164, 165]. In particular, a three-body bound state with $L^{\Pi} = 1^{-}$ symmetry and a four-body bound state with $L^{\Pi} = 1^{+}$ symmetry have been predicted to appear for the FFX systems with $\kappa \approx 12.31$ and the FFFX system with $\kappa \approx 10.4$, respectively [163, 164]. These results are obtained by studying trapped systems with purely attractive short-range Gaussian model interactions using the stochastic variational approach. An independent fixed node DMC study of the free-space system [165], in which the F and X atoms interact through different short-range model potentials, arrives at similar conclusions, and furthermore predicts the existence of a resonance for the (4, 1) system for κ slightly smaller than 10.4. Although the observed resonances depend, at least in principle, on the details of the underlying two-body potential, it has been argued that these resonances occur most likely if $s_{\nu} \approx 1/2$ [163, 164]. The analysis that leads to this speculation is based on the hyperspherical framework, which allows for the dependence of the eigenenergies on the hyperradial boundary condition to be studied. In particular, it was found [163, 164] that the energy-dependence of the transcendental eigenequation is weakest for $s_{\nu} = 1/2$ and that the N -body resonances might thus be most amenable to tuning if $s_{\nu} \approx 1/2$. Although the mass ratio of two-component Fermi gases is fixed by nature (implying a particular s_{ν} value), the effective mass may be tuned by loading the system into an optical lattice [161]. Future work needs to investigate to which extent N -body resonances can be utilized to study or engineer novel many-body phenomena. A first step in this direction was undertaken by Nishida *et al.* [161] who investigated the behavior of many-body systems with two- and three-body resonances and $\kappa \approx 8.619$ and 13.607.

Lastly, we consider the regime where κ is greater than 13.607, i.e., the regime where three-body Efimov physics plays a role (see Subsec. 3.3). While the three-body Efimov effect is quite well understood by now, it is presently an open question to

which extent the behavior of the three-body system is modified due to the presence of other particles. While such modifications due to the “many-body background” are expected to be relatively small for bosons, the situation may be different for fermions due to Pauli blocking. In a lowest order semi-classical WKB treatment, the presence of the fermions that “do not belong to” the Efimov trimer have been accounted for by constraining the momenta $\hbar k$ that contribute to the three-body wave function to $k > k_F$ [231]. As a consequence, the energy spacing between consecutive Efimov states depends, in addition to s_ν , on k_F . While more studies are needed, the outlined example points toward a future frontier, namely the study of few-body phenomena in the presence of a many-body background. In passing, we also mention that a four-body Efimov effect has been predicted to exist for the FFFX system with $13.384 < \kappa < 13.607$ and 1^+ symmetry, i.e., in a regime where the three-body Efimov effect is absent [232].

4.4. Microscopic approach to thermodynamics of equal-mass Fermi gas

So far, this review has focused on the zero-temperature regime. An important question is, however, how the system properties depend on temperature (see Refs. [223, 233] for very recent experiments). Recently, the finite-temperature properties of macroscopic two-component Fermi gases have been examined by employing a high temperature virial expansion approach that uses the two- and three-body energies as input [169, 170].

For concreteness, we consider a spin- and mass-balanced s -wave interacting two-component Fermi gas consisting of N mass m point particles. Since the chemical potential μ diverges logarithmically toward $-\infty$ as the temperature approaches ∞ , the fugacity z , $z = \exp[\mu/(k_B T)]$, can be identified as a small parameter [234, 235, 236]. It has been shown that a cluster expansion in terms of the fugacity provides reliable results for spin- and mass-balanced Fermi gases down to about half the Fermi temperature if the expansion includes the second and third order virial coefficients (i.e., if the two- and three-body clusters are accounted for) [169, 170]. The high-temperature virial expansion approach is equivalent to an expansion in terms of the “diluteness or degeneracy parameter” $n\lambda_{\text{dB}}^3$, where n denotes the density and λ_{dB} the de Broglie wave length [234, 235, 236]. At high temperatures, the degeneracy parameter is small. However, near the transition temperature, i.e., near $T/T_c \approx 1$, the degeneracy parameter is of order one (or $\lambda_{\text{dB}} \approx \langle r \rangle$, where $\langle r \rangle$ denotes the average interparticle spacing). Thus, the applicability of the virial expansion approach is expected to break down in the low-temperature regime.

Following Liu *et al.* [169, 170], we work in the grand canonical ensemble and write the thermodynamic potential Ω in terms of the partition function \mathcal{Z} , $\Omega = -k_B T \ln \mathcal{Z}$ with $\mathcal{Z} = \text{tr} \exp[-(H - \mu N)/(k_B T)]$. Once the thermodynamic potential Ω is known, other thermodynamic observables such as the energy and pressure can be derived from Ω by taking appropriate derivatives. The idea behind the virial expansion is to write the partition function \mathcal{Z} in terms of the partition functions Q_n of the n^{th} cluster, $Q_n = \text{tr}_n \exp[-H_n/(k_B T)]$ and $\mathcal{Z} = 1 + zQ_1 + z^2Q_2^2 + \dots$. Here, H and H_n denote the Hamiltonian of the full N -particle system and the n -particle subsystem or cluster, respectively. The notation tr_n indicates that the trace is taken over the n -particle states. If we denote the eigenenergies of the n^{th} cluster by $E_{n,j}$, then the partition function Q_n becomes $Q_n = \sum_j \exp[-E_{n,j}/(k_B T)]$, where j collectively denotes the set of quantum numbers (i.e., the Q_n are fully determined by the eigenenergies of

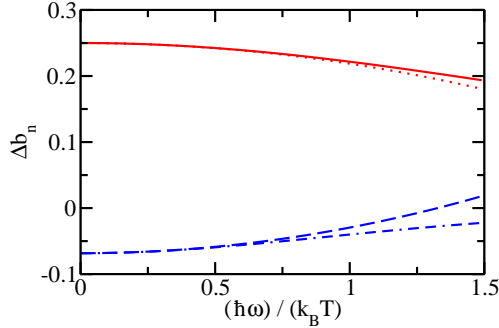


Figure 18. (Color online) Shifted virial coefficients Δb_n as a function of the dimensionless inverse temperature $\tilde{\omega}$, $\tilde{\omega} = \hbar\omega/(k_B T)$, of the trapped equal-mass two-component Fermi gas at unitarity. Solid and dotted lines show respectively the virial coefficient Δb_2 and its Taylor expansion up to order $\tilde{\omega}^2$. Dash-dotted and dashed lines show respectively the virial coefficient Δb_3 [237] and its Taylor expansion up to order $\tilde{\omega}^2$.

the n^{th} cluster). Inserting the expansion for \mathcal{Z} into the thermodynamic potential Ω defines the virial coefficients b_n , $\Omega = -k_B T Q_1(z + b_2 z^2 + b_3 z^3 + \dots)$. The second virial coefficient b_2 , e.g., equals $(Q_2 - Q_1^2/2)/Q_1$ and depends on the s -wave scattering length $a_0(0)$ as well as on the confining geometry and temperature. The expansion of Ω in terms of z shows that, if $|b_n z/b_{n-1}|$ is smaller than one, the n^{th} contribution is suppressed by a factor of $|b_n z/b_{n-1}|$ compared to the $(n-1)^{\text{th}}$ contribution.

We now consider an application to the harmonically trapped two-component Fermi system at unitarity, for which the two- and three-particle energies are known with high precision [104, 158]. It is convenient to express the virial coefficients $b_n(a_0(0))$ of the interacting system relative to the virial coefficients $b_n(a_0(0) = 0)$ of the non-interacting system, i.e., we define $\Delta b_n = b_n(a_0(0)) - b_n(a_0(0) = 0)$. At unitarity, the s -wave two-body energies equal $(2j + 1/2)\hbar\omega + E_{\text{cm}}$ ($j = 0, 1, \dots$) and Δb_2 can be calculated analytically by summing over the quantum numbers associated with the relative and center-of-mass degrees of freedom. The result is $\Delta b_2 = \exp(-\tilde{\omega}/2)/[2(1 + \exp(-\tilde{\omega}))]$ [169], where $\tilde{\omega}$ denotes a dimensionless “inverse temperature” or scaled frequency, $\tilde{\omega} = \hbar\omega/(k_B T)$. The third, shifted virial coefficient Δb_3 requires summing the three-body energies, which can be obtained by solving a transcendental equation [see Subsec. 3.2 and Eq. (7) of Ref. [158]], numerically. The high temperature expansions of Δb_2 and Δb_3 at unitarity are $1/4 - \tilde{\omega}^2/32$ and $-0.06833960 + 0.038867\tilde{\omega}^2$, respectively [169]. Figure 18 shows the shifted virial coefficients Δb_2 and Δb_3 at unitarity as a function of $\tilde{\omega}$. As can be seen, the temperature dependence of the virial coefficients is fairly weak in the high temperature (small $\tilde{\omega}$) regime. The Fermi energy E_F of the harmonically trapped non-interacting two-component Fermi gas, which can be written as $E_F \approx (3N)^{1/3}\hbar\omega$, defines the Fermi temperature T_F , $T_F = E_F/k_B$. For $N = 100$, e.g., one finds $k_B T_F \approx 7\hbar\omega$, i.e., the temperature dependence of the virial coefficients is fairly weak if the temperature T is larger than the Fermi temperature T_F .

Knowing the virial coefficients Δb_2 and Δb_3 , the thermodynamic properties of

the trapped Fermi gas can be calculated. As a first application, Liu *et al.* [169] determined the interaction energy E_{int} , $E_{\text{int}} = E - E_{\text{tot}}^{\text{NI}}$ (here, $E_{\text{tot}}^{\text{NI}}$ denotes the energy of the corresponding non-interacting system), of a trapped two-component lithium mixture at unitarity in the temperature regime $T \gtrsim T_F$. The theoretical predictions connect smoothly to experimental data from the Duke group [238], which cover the temperature regime $T \lesssim T_F$. More recently, the virial expansion approach has been used to determine other observables at and away from unitarity [239, 240].

The virial expansion approach outlined can be extended to the homogeneous system, thereby allowing for comparisons with results obtained by finite temperature MC simulations [241, 242, 243] and effective many-body approaches. To this end, Liu *et al.* [169] applied an “inverse LDA”, which allowed for the determination of the virial coefficients of the homogeneous system from those of the inhomogeneous system. The theoretically determined high-temperature value of the third order virial coefficient has been confirmed experimentally [223]. The examples discussed in this subsection underline that microscopic bottom-up approaches provide, in certain cases, powerful means to predict many-body properties.

5. *s*-wave interacting Bose gas under confinement

This section considers single-component Bose gases under external confinement. Subsection 5.1 introduces the mean-field Gross-Pitaevskii (GP) framework, which assumes that the behavior of weakly-interacting Bose gases is fully governed by the *s*-wave scattering length $a_0(0)$. The validity regimes of the GP equation and a modified GP equation are benchmarked for Bose gases under spherically symmetric harmonic confinement. Subsection 5.2 discusses the mechanical instability that arises for Bose gases with negative *s*-wave scattering lengths. Lastly, Subsec. 5.3 discusses the role of the effective range and the three-body parameter for Bose systems.

5.1. Equation of state of trapped Bose gas: The role of the *s*-wave scattering length

Weakly-interacting Bose gases under external confinement at zero temperature are most commonly described by the non-linear mean-field GP equation [11, 12, 13, 14, 244, 245, 246], which can be derived by approximating the many-body wave function $\Psi(\vec{r}_1, \dots, \vec{r}_N)$ by a product of single-particle orbitals $\Phi(\vec{r}_j)$, $\Psi = \prod_{j=1}^N \Phi(\vec{r}_j)$, where $\int |\Phi(\vec{r})|^2 d^3\vec{r} = 1$ [16, 247]. This product ansatz is fully symmetrized and geared toward the description of the energetically lowest lying gas-like state of the *N*-boson system. Assuming that the interactions can be parameterized through a sum of two-body potentials $V_{\text{tb}}(\vec{r}_{jk})$ and minimizing the total energy $E_{\text{tot}}(N)$ with respect to Φ^* , one obtains the Hartree equation [16, 247]

$$\left[\frac{-\hbar^2}{2m} \nabla_{\vec{r}}^2 + V_{\text{trap}}(\vec{r}) + (N-1) \int V_{\text{tb}}(\vec{r}, \vec{r}') |\Phi(\vec{r}')|^2 d^3\vec{r}' \right] \Phi(\vec{r}) = \epsilon \Phi(\vec{r}). \quad (50)$$

In Eq. (50), m denotes the atom mass, V_{trap} the external confining potential felt by each of the bosons, and ϵ the orbital energy or chemical potential. The integro-differential equation (50), which has to be solved self-consistently for $\Phi(\vec{r})$ and ϵ , describes a trapped “test particle” that moves—just as in atomic structure calculations—in the mean-field [the third term in square brackets on the left hand side of Eq. (50)] created by the other $(N-1)$ atoms.

For ultracold degenerate s -wave interacting Bose gases, the two-body interaction potential V_{tb} with s -wave scattering length $a_0(0)$ is frequently replaced by the Fermi pseudopotential V_F , Eq. (42), for which the integral in Eq. (50) can be evaluated analytically,

$$\left[\frac{-\hbar^2}{2m} \nabla_{\vec{r}}^2 + V_{\text{trap}}(\vec{r}) + (N-1) \frac{4\pi\hbar^2 a_0(0)}{m} |\Phi(\vec{r})|^2 \right] \Phi(\vec{r}) = \epsilon \Phi(\vec{r}). \quad (51)$$

Equation (51) is the GP equation for s -wave interacting systems, sometimes also referred to as non-linear Schrödinger equation. Although the GP equation has been derived by applying the variational principle, the resulting total energy $E_{\text{tot}}(N)$ does not constitute a variational upper bound to the energy of the energetically lowest-lying gas-like state of the many-body system since the true atom-atom potential has been replaced by Fermi's pseudopotential. The GP equation depends on the product $(N-1)a_0(0)$, and not on $(N-1)$ and $a_0(0)$ separately. This implies that the mean-field formulation is only sensitive to the “strength” of the effective interaction and not to its underlying microscopic origin, i.e., whether it is due to, say, large N and small $a_0(0)$ or small N and large $a_0(0)$. An alternative derivation of Eq. (51) is based on a field operator description and results in a factor of N as opposed to $N-1$ (see, e.g., Refs. [15, 248, 249]). While it is justified to replace $N-1$ by N in the large N limit, the factor of $N-1$ should be used in the small N limit where the difference between $N-1$ and N is appreciable. The outlined number conserving microscopic derivation of the GP equation emphasizes that its application is not restricted to large number of particles; in fact, as shown below, the GP equation provides a good description even for dilute two-particle systems.

The solid line in Fig. 19 shows the total energy E_{tot}/N per particle, obtained by solving the GP equation for a spherically symmetric harmonic confinement, as a function of the interaction parameter $(N-1)a_0(0)/a_{\text{ho}}$. The solid line terminates at $(N-1)a_0(0)/a_{\text{ho}} \approx -0.57497$ [247, 250]. For more negative interaction parameters, the GP equation supports a solution whose energy is unbounded from below (i.e., the energy approaches $-\infty$ and the corresponding wave function describes a high density state of size much smaller than a_{ho}). Generally speaking, the validity regime of the GP equation is restricted to dilute systems, i.e., to parameter combinations that fulfill the inequality $n(0)|a_0(0)|^3 \ll 1$ [251], where $n(0)$ denotes the peak density. For $(N-1)a_0(0)/a_{\text{ho}} \gtrsim -0.57497$, the diluteness parameter $n(0)|a_0(0)|^3$ is much smaller than 1, assuming N is not too small. This suggests that the predicted drop of the GP energy (the termination of the solid line in Fig. 19) lies within the validity regime of the mean-field framework. As discussed in Subsec. 5.2, the sudden drop of the GP energy is interpreted as a mechanical instability or collapse.

We now compare the solutions of the GP equation with those obtained by solving the linear Schrödinger equation. Dotted, dashed and dash-dotted lines in Fig. 19 show the total energy E_{tot}/N per particle for two particles under spherically symmetric harmonic confinement interacting through a hard-sphere potential with range $a_0(0)$ [$a_0(0) > 0$], a square well potential with range r_0 and depth V_0 ($r_0 = 0.01a_{\text{ho}}$ and V_0 are chosen such that the potential supports one s -wave bound state in free space), and the pseudopotential V_0^{pp} [see Eq. (4)], respectively. The two-body energies for these potentials are obtained by solving the linear Schrödinger equation analytically (for the treatment of V_0^{pp} , see Sec. 2). For $(N-1)|a_0(0)|/a_{\text{ho}} \lesssim 0.1$, the agreement between the energies obtained by solving the linear and non-linear Schrödinger equations is

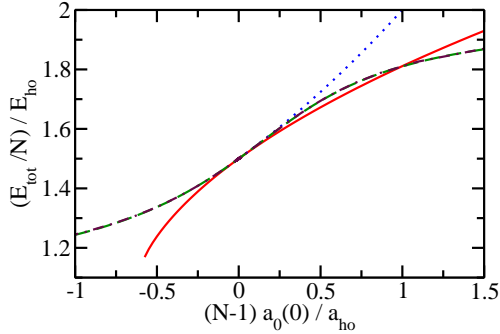


Figure 19. (Color online) Total energy E_{tot}/N per particle of a dilute Bose gas under external spherically symmetric confinement as a function of the “interaction parameter” $(N-1)a_0(0)/a_{\text{ho}}$. The solid line shows the mean-field GP energy. Dotted, dashed and dash-dotted lines show the energies obtained by solving the linear Schrödinger equation for two particles interacting through a hardsphere potential, a square-well potential (with range r_0 , $r_0 = 0.01a_{\text{ho}}$, and depth V_0 adjusted such that the free-space system does support one bound state) and the zero-range pseudopotential V_0^{PP} [Eq. (4)], respectively. Note that the dashed and dash-dotted lines are indistinguishable on the scale shown.

excellent. However, for larger $(N-1)|a_0(0)|/a_{\text{ho}}$ deviations are visible. The energy for two particles interacting through the hardsphere potential increases roughly linearly with $a_0(0)$ and lies above the other energies. The comparatively large increase of the energy for the hardsphere potential can be understood by realizing that the excluded volume increases with increasing $a_0(0)$, resulting in an infinite two-body energy as $a_0(0)$ approaches infinity. This unphysical behavior suggests that the applicability regime of the hardsphere potential is limited to small $a_0(0)$. The GP energy lies below the energies for the zero-range and square-well interaction potentials for $(N-1)a_0(0)/a_{\text{ho}} \lesssim 1$ and above for $(N-1)a_0(0)/a_{\text{ho}} \gtrsim 1$. The discrepancy between the GP energy and the energies for the zero-range and square-well interaction potentials increases as $(N-1)a_0(0)/a_{\text{ho}}$ increases further. In the large interaction parameter regime, the diluteness parameter $n(0)|a_0(0)|^3$ is no longer small compared to one and higher order corrections need to be included in the mean-field description (see below). For negative scattering lengths, the energies obtained by solving the linear Schrödinger equation vary smoothly. In particular, the mechanical instability predicted by the GP equation has no two-body analog; at least three particles are needed to see an analog of the instability predicted by the GP equation within the framework of the linear Schrödinger equation (see also Subsec. 5.2).

For larger number of particles, the determination of the solutions to the linear Schrödinger equation becomes more involved. In addition to the increased number of degrees of freedom, complications arise due to the fact that the N -boson system supports, unlike s -wave interacting two-component Fermi systems, N -body ($N > 2$) bound states even if the underlying two-body potential does not support a two-body bound state. Thus, the energetically lowest lying gas-like state of the Bose gas is a metastable state and not the true ground state of the system. Tightly

bound N -body clusters, whose properties are discussed further in Subsec. 5.3, are absent for systems interacting through purely repulsive two-body potentials such as the hard-sphere potential. Although purely repulsive interaction models exhibit, as discussed exemplarily above for the hard-sphere potential, unphysical behavior for large $a_0(0)$, they provide a quantitatively correct description for small $a_0(0)$ and allow one to estimate model dependent effects for intermediate $a_0(0)$ [252, 253, 254, 255]. Symbols in Fig. 20(a) show the energy E_{tot}/N per particle for N -boson systems, $N = 2 - 50$, with hard-sphere interactions under external spherically symmetric harmonic confinement as a function of the interaction parameter $(N - 1)a_0(0)/a_{\text{ho}}$ [252]. It can be seen clearly that the solutions of the linear Schrödinger equation depend on N and $a_0(0)/a_{\text{ho}}$ separately and not just the product of these two parameters. For comparison, the solid line shows the GP energy per particle. The DMC energies for different number of particles (symbols), obtained by solving the linear Schrödinger by the DMC method [252], lie above the GP energies. Figure 20(b) shows the energy difference $E_{\text{DMC}} - E_{\text{GP}}$. For fixed N , the deviations between the DMC and GP energies increase with increasing interaction parameter. For a fixed interaction parameter, the deviations decrease with increasing N . An improved mean-field description of the hard-sphere equation of state is discussed below.

To investigate the small $|a_0(0)|/a_{\text{ho}}$ behavior in more detail, the N -boson system under external spherically symmetric confinement with two-body zero-range interactions can be treated perturbatively within the framework of linear Schrödinger quantum mechanics. Up to order $[a_0(0)/a_{\text{ho}}]^2$, the perturbative energy of the energetically lowest-lying gas-like state of the N -boson system reads [256]

$$E_{\text{tot}} \approx \frac{3N}{2}\hbar\omega + \binom{N}{2} \sqrt{\frac{2}{\pi}} \frac{a_0(0)}{a_{\text{ho}}} \hbar\omega + \left[\binom{N}{2} \frac{2(1 - \ln(2))}{\pi} - \binom{N}{3} \beta \right] \left[\frac{a_0(0)}{a_{\text{ho}}} \right]^2 \hbar\omega, \quad (52)$$

where

$$\beta = \frac{2}{\pi} \left[4\sqrt{3} - 6 + 6 \ln \left(\frac{4}{2 + \sqrt{3}} \right) \right] \approx 0.8557583 \quad (53)$$

and

$$\binom{N}{n} = \frac{N!}{n!(N-n)!}. \quad (54)$$

The first term on the right hand side is the energy of the non-interacting (unperturbed) N -boson system. The leading order energy shift of the N -particle system is equal to the energy shift that $N(N - 1)/2$ independent two-body systems would experience. The next order shift contains a positive term that scales with the number of pairs and a negative term that scales with the number of trimers. The latter contribution has been interpreted as an effective attractive three-body interaction [160, 256]. This interpretation emerges naturally in an effective field theory treatment [256], which derives an effective low-energy Hamiltonian that contains one-body, two-body and three-body terms. We stress that the effective attractive three-body interaction arises from the pairwise zero-range interactions and not from an explicit three-body potential. The need for and role of an actual three-body potential is discussed in Subsec. 5.3. The effective three-body interaction for the harmonically trapped Bose gas was first predicted by Jonsell *et al.* [160], who employed the BO and

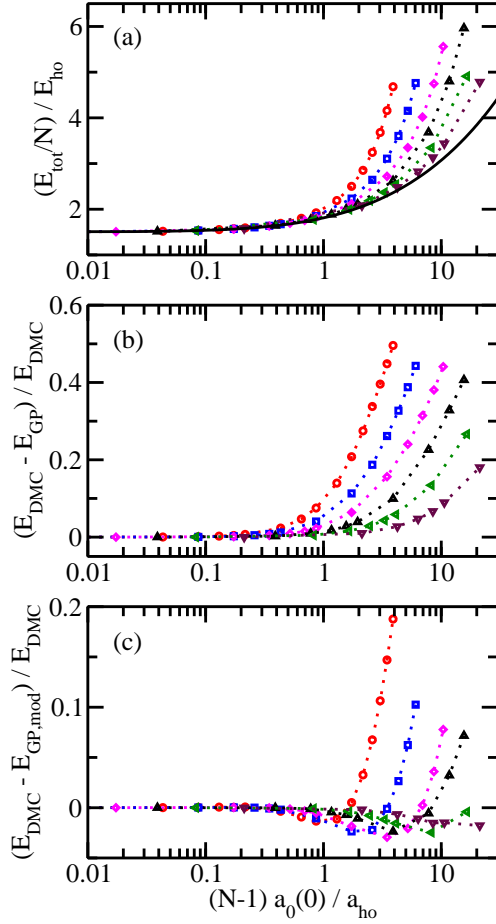


Figure 20. (Color online) Hardsphere equation of state for the Bose gas under spherically symmetric confinement. Symbols in panel (a) show the total energy E_{DMC}/N per particle for the N -particle Bose gas with hardsphere interactions as a function of the interaction parameter $(N-1)a_0(0)/a_{\text{ho}}$ for $N = 2$ (circles), $N = 3$ (squares), $N = 5$ (diamonds), $N = 10$ (up triangles), $N = 20$ (left triangles), and $N = 50$ (down triangles); the energies are obtained by solving the linear Schrödinger equation by the DMC method. For comparison, the solid line shows the total energy per particle E_{GP}/N obtained by solving the mean-field GP equation. Panels (b) and (c) show the scaled energy differences $(E_{\text{DMC}} - E_{\text{GP}})/E_{\text{DMC}}$ and $(E_{\text{DMC}} - E_{\text{GP,mod}})/E_{\text{DMC}}$, respectively, for the same N as panel (a); to guide the eye, dotted lines connect data points for the same N . The figure has been adapted from Ref. [252].

adiabatic approximations within the hyperspherical framework to place bounds on the three-body coefficient. For a Bose gas confined to a box with periodic boundary conditions, the effective three-body interaction has a positive coefficient [81] (see also Refs. [257, 258, 259, 260]), which illustrates that the effective N -body interactions can be tuned by varying the external confinement. The second term on the right hand side of Eq. (52) can also be derived within the GP framework by approximating Φ in Eq. (51) by the non-interacting wave function.

Equation (52) can be viewed as the few-particle trap analog of the low-density expansion of the equation of state of the homogeneous Bose gas with density n [258, 261],

$$\frac{E_{\text{hom}}/N}{\frac{\hbar^2}{2ma_0^3(0)}} \approx 4\pi na_0^3(0) \left[1 + \frac{128}{15\sqrt{\pi}} \sqrt{na_0^3(0)} \right]. \quad (55)$$

Application of the LDA to the first term on the right hand side of Eq. (55) gives the second term on the right hand side of Eq. (52). The next order correction in Eq. (52), in contrast, cannot be determined by applying the LDA to the $\sqrt{na_0^3(0)}$ term in Eq. (55) [160].

Lastly, we comment on the large scattering length regime. The experimental realization of cold atomic gases with large scattering length and sufficiently long lifetimes would open the possibility to study strongly-correlated Bose systems with unprecedented control. Historically [262, 263], the study of liquid helium, which is characterized by a gas parameter $na_0^3(0)$ of about 0.21 and a condensate fraction of about 7% [264, 265, 266], is tremendously important. Liquid helium has an s -wave scattering length that is roughly 10 times larger than the effective range, which in turn is of the order of the interparticle spacing. Although the s -wave scattering length of Bose gases can, for a subset of species such as ^{85}Rb [34], be tuned over a wide range through the application of an external magnetic field in the vicinity of a Fano-Feshbach resonance, Bose gases with large scattering length exhibit detrimental losses since the three-body recombination rate shows an overall $|a_0(0)|^4$ scaling [171, 172, 173, 174, 267]. This is in contrast to two-component Fermi gases with equal masses, which are stabilized by the ‘‘Pauli pressure’’ that results from the Pauli exclusion principle. While it is not clear at present to which extent the equilibrium properties of Bose gases with large scattering length can be probed experimentally [268], several theoretical studies have investigated the properties of Bose gases with large scattering length based on the assumption that the system’s lifetime would be sufficiently long to reach equilibrium. The first studies in this direction were performed for the trapped three-boson system by Jonsell *et al.* [160] and Blume *et al.* [166]. More recent studies have estimated the lifetime of the trapped three-boson system [158, 179]. Extensions to larger systems have also been considered [218, 269, 270, 271, 272, 273]. The work by Song and Zhou [272], e.g., predicts the existence of a fermionized three-dimensional Bose gas with large scattering length (see also Ref. [274]). This is an intriguing prospect since the fermionization of Bose gases has been studied extensively in one-dimensional systems.

If the interaction parameter $(N-1)a_0(0)/a_{\text{ho}}$ becomes appreciable but not too large, corrections to the GP equation can be accounted for by a modified mean-field GP equation [252, 275, 276, 277],

$$\left[\frac{-\hbar^2}{2m} \nabla_{\vec{r}}^2 + V_{\text{trap}}(\vec{r}) + (N-1) \frac{4\pi\hbar^2 a_0(0)}{m} |\Phi(\vec{r})|^2 \right] \times$$

$$\left(1 + \frac{32}{3\sqrt{\pi}}[a_0^3(0)(N-1)]^{1/2}\Phi(\vec{r})\right)\Phi(\vec{r}) = \epsilon\Phi(\vec{r}). \quad (56)$$

The second term in the big round brackets in the second line of Eq. (56) can be derived from the “quantum fluctuation term” of the homogeneous system, i.e., the second term on the right hand side of Eq. (55). Figure 20(c) shows the energy difference $E_{\text{DMC}} - E_{\text{GP,mod}}$, where the energy $E_{\text{GP,mod}}$ has been derived from the orbital energy ϵ that results when solving Eq. (56). A comparison of the vertical scales of Figs. 20(b) and 20(c) shows that the modified GP equation extends the validity regime of the mean-field treatment.

5.2. Bose gas with negative s -wave scattering length

To shed light on the mechanical instability for Bose gases with negative scattering length (i.e., the termination of the solid line in Fig. 19 for negative scattering length), we solve the GP equation for a spherically symmetric harmonic confinement using a variational Gaussian wave function with width b . Writing $\Phi(\vec{r}) = b^{-3/2}\pi^{-3/4}\exp[-r^2/(2b^2)]$, the variational energy becomes [278]

$$\frac{E_{\text{var}}}{N} \approx \left[\frac{3a_{\text{ho}}^2}{4b^2} + \frac{3b^2}{4a_{\text{ho}}^2} + \frac{(N-1)a_0(0)a_{\text{ho}}^2}{\sqrt{\pi}b^3} \right] \hbar\omega, \quad (57)$$

where the first, second and third terms on the right hand side are the kinetic, trap and interaction energies, respectively. Since the interaction energy varies as b^{-3} while the kinetic and potential energies vary as b^{-2} and b^2 , respectively, it is clear that there exists a critical negative interaction parameter beyond which the variational energy possesses a global minimum for $b = 0$ but not a local minimum [278]. Similar conclusions have been drawn in related studies [279, 280, 281]. Lines in Fig. 21(a) show the variational energy per particle as a function of b/a_{ho} for various interaction parameters $(N-1)|a_0(0)|/a_{\text{ho}}$. For small $(N-1)|a_0(0)|/a_{\text{ho}}$, the variational energy shows a minimum around $b/a_{\text{ho}} \approx 1$. As $(N-1)|a_0(0)|/a_{\text{ho}}$ increases [$a_0(0)$ negative], the energy minimum moves to smaller b/a_{ho} and the barrier that separates the local and global energy minima decreases. At the critical value of $(N-1)a_0(0)/a_{\text{ho}} \approx -0.67051$ [see dashed line in Fig. 21(a)], the barrier disappears, suggesting that the Bose gas can lower its energy—without having to “tunnel” through an “energy barrier”—by shrinking toward (or collapsing into) a so-called high density “snowflake state”. The variational Gaussian approach describes the onset of the mechanical instability quite well, i.e., it predicts a slightly more negative critical interaction parameter than the full solution to the GP equation [$(N-1)a_0(0)/a_{\text{ho}} \approx -0.67051$ compared to -0.57497]. Furthermore, it highlights that the trapped Bose gas is, for sufficiently small $(N-1)|a_0(0)|/a_{\text{ho}}$ [$a_0(0) < 0$], stabilized by the positive energy contributions that arise due to the presence of the trap. If the system was homogeneous, an infinitesimally small $|a_0(0)|$ [$a_0(0) < 0$] would induce collapse. While it is suggestive to interpret the energy curves shown in Fig. 21(a) as effective potentials, it must be kept in mind that the width b corresponds to a variational parameter and not to an actual spatial coordinate.

The collapse dynamics of Bose gases with negative $a_0(0)$ has also been investigated by solving the linear Schrödinger equation with zero-range interactions within the BO hyperspherical approximation [149]. For a variational wave function that is written as the product of a constant hyperangular piece and a hyperradial function

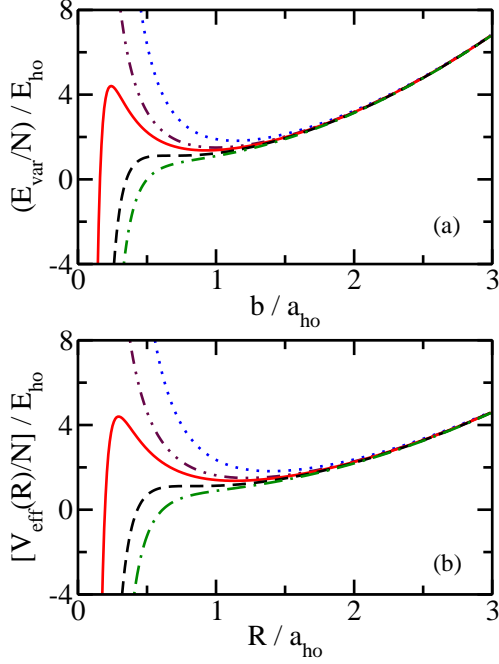


Figure 21. (Color online) Mechanical instability of Bose gases with negative scattering length. (a) Dotted, dash-dot-dotted, solid, dashed and dash-dotted lines show the variational energy E_{var}/N per particle, Eq. (57), as a function of b/a_{ho} for $(N-1)a_0(0)/a_{\text{ho}} = 1, 0, -0.3, -0.67$ and -1 , respectively. (b) Dotted, dash-dot-dotted, solid, dashed and dash-dotted lines show the effective potential curve $V_{\text{eff}}(R)/N$, Eq. (58), as a function of R/a_{ho} for $(N-1)a_0(0)/a_{\text{ho}} = 1, 0, -0.3, -0.67$ and -1 , respectively (N is fixed, $N = 1000$).

$R^{-(3N-1)/2}F(R)$, the effective hyperradial potential curve $V_{\text{eff}}(R)$ takes the form [149]

$$V_{\text{eff}}(R) = \frac{\hbar^2(3N-1)(3N-3)}{8NmR^2} + \frac{1}{2}Nm\omega^2R^2 + \sqrt{\frac{1}{2\pi}} \frac{\hbar^2(N-1)a_0(0)}{m} \frac{\Gamma(3N/2)}{\Gamma((3N-3)/2)N^{3/2}} \frac{N}{R^3}, \quad (58)$$

where $NR^2 = \sum_i \vec{r}_i^2$. The effective potential $V_{\text{eff}}(R)$ enters into the hyperradial equation $-\hbar^2/(2Nm)F'' + V_{\text{eff}}F = E_{\text{tot}}F$, which can be solved readily. In Eq. (58), the first, second and third terms on the right hand side arise due to the kinetic energy operator, the external confinement, and the pairwise interactions, respectively. Lines in Fig. 21(b) show $V_{\text{eff}}(R)/N$ for various interaction parameters $(N-1)a_0(0)/a_{\text{ho}}$ and $N = 1000$. We note that the curves $V_{\text{eff}}(R)/N$ depend only weakly on N [149]. A comparison of Figs. 21(a) and 21(b) [and, equivalently, of Eqs. (57) and (58)] shows that b plays a role similar to that played by R . The key difference is that b is a variational parameter while the hyperradius R is a spatial coordinate. Physically, the small R region describes a system in which the atom-atom distances are small, i.e., where the system is self-bound. Using the effective potential curves V_{eff} , tunneling

from the region where the potential exhibits a local minimum to the small R region where the effective potential is unbounded from below has been estimated within the WKB approximation [149]. The conclusions discussed here have been confirmed for the three-body system by performing an analysis that goes beyond the variational treatment and furthermore accounts for the coupling between channels [166]. For larger systems, confirmation comes from treatments that explicitly account for two-body correlations [282] and experiments [283, 284].

5.3. Beyond the s -wave scattering length: Effective range and three-body parameter

The previous two subsections assumed that the equation of state of trapped Bose gases is fully determined by the s -wave scattering length $a_0(0)$. However, atom-atom potentials possess a finite range, which induces range-dependent corrections to the equation of state. Furthermore, the properties of Bose gases may additionally depend on a three-body parameter whose role for the three-boson system with large s -wave scattering length has already been discussed in Subsec. 3.3. In the following, we present simple arguments that illustrate at which order these corrections appear in the equation of state.

To account for the finite range of the underlying atom-atom potential, we resort to the effective range expansion, Eq. (3). The effective range r_{eff} is determined by the shape and range of the two-body potential. For the hardsphere potential, e.g., the effective range r_{eff} is directly proportional to $a_0(0)$ [i.e., $r_{\text{eff}} = 2a_0(0)/3$]. For the van der Waals potential with r^{-6} tail, the effective range r_{eff} is, in the low-energy regime, also determined by the scattering length $a_0(0)$ [285]. To estimate the order at which finite range effects occur, we replace the s -wave scattering length $a_0(0)$ in the leading order term of Eq. (52) by $a_0(E)$ and, in a second step, approximate $a_0(E)$ by Eq. (3). A simple calculation shows that finite range corrections enter, according to this estimate, at order $r_{\text{eff}}a_0^2(0)/a_{\text{ho}}^3$. Thus, finite range effects are, assuming that $|r_{\text{eff}}|$ is smaller than a_{ho} , suppressed compared to the effective three-body interaction [see Eq. (52) in Subsec. 5.1], which scales as $[a_0(0)/a_{\text{ho}}]^2$, by a factor of $r_{\text{eff}}/a_{\text{ho}}$. The calculation could be made rigorous by carrying out a perturbative analysis for a sum of zero-range two-body potentials that account for finite-range effects through derivative operators [81] [i.e., that depend on $a_0(0)$ and r_{eff}]. Within the mean-field framework, effective range corrections have been accounted for by adding a gradient term that is proportional to $g_2(N-1)\nabla^2|\Phi(\vec{r})|^2$ to the mean-field potential of the GP equation [286]. To determine this modified mean-field term and the constant g_2 , Fu *et al.* derived a pseudopotential that reproduces the real part of the scattering amplitude up to order k^2 [286] and then used this revised pseudopotential in the Hartree framework (see Subsec. 5.1).

The role of the three-body parameter has previously been discussed in Subsec. 3.3 for the three-boson system with infinitely large two-body scattering length $a_0(0)$. We now consider the small $a_0(0)$ regime and estimate at which order the three-body parameter enters into the equation of state. As already discussed, an imaginary s_ν gives rise for the need of a three-body parameter. For small $|a_0(0)|$, Fig. 5 shows that there exists an imaginary root for sufficiently small R . This implies that the sum of zero-range two-body potentials has to be complemented by a hyperradial three-body potential V_3 or, equivalently, a three-body boundary condition in the hyperradial coordinate. While this boundary condition does not, as in the large $|a_0(0)|$ limit, lead to the appearance of an infinite ladder of geometrically spaced finite energy states, it

does have an effect on the energy spectrum.

To estimate the effect of V_3 on the energy spectrum of the trapped three-boson system, we perform a perturbative analysis. We assume that V_3 is proportional to $(\hbar^2 A^4(k)/m)\delta(\vec{r}_1 - \vec{r}_2)\delta(\vec{r}_2 - \vec{r}_3)$, where $A^4(k)$ denotes the generalized energy-dependent three-body scattering length. Dimensional analysis shows that $A^4(k)$ has units of (length)⁴. This three-body pseudopotential can alternatively be written in terms of a δ -function in the hyperradius. The quantity $A^4(0)$ conveniently parameterizes the three-body parameter in the weakly-interacting regime and is related to the hypervolume D defined by Tan [260]. In first order perturbation theory, this pseudopotential leads to an energy shift proportional to $[A(k)/a_{\text{ho}}]^4 \hbar\omega$. For the N -boson system, this energy correction gets multiplied by the number of trimers. This analysis reveals that the three-body potential introduces an energy shift of higher order in the inverse harmonic oscillator length than both the effective three-body interaction and the two-body effective range correction. We note that the effect of the three-body parameter on the energy spectrum of the weakly-interacting N -boson system in a box with periodic boundary conditions has been discussed in Refs. [259, 260].

We now turn to the large $a_0(0)$ regime and ask two questions: (i) Does the description of successively larger Bose systems require a new parameter for each successively larger weakly-bound Bose system? (ii) What are the imprints of the three-body parameter on the N -body ($N > 3$) spectrum? The first question has been studied extensively ever since Efimov’s work from the early seventies [45, 46, 47, 287, 288, 289]. It is fairly well established by now that the treatment of the low-energy physics of N -body ($N > 3$) Bose systems does not require additional parameters, i.e., the low-energy properties of the N -body system are believed to be determined by $a_0(0)$ and a three-body parameter [289, 291, 292]. A consequence of the absence of four- and higher-body parameters is that there exists no four- or higher-body Efimov effect for Bose systems with 0^+ symmetry, i.e., there exists no infinite sequence of N -body bound states whose geometric spacing is determined by an N -body parameter ($N > 3$). Other interpretations do, however, exist [290]. The second question has been studied extensively over the past five years or so, mostly but not exclusively in the context of the four-body system in free space [291, 292]. For each Efimov trimer, there exist two universal four-body states whose properties are determined by those of the Efimov trimer that the four-body states are “attached to”. These four-body states are, in fact, resonance states with finite lifetime [295]. The energies of the tetramer “ground state” and “first excited state” in free space are about 4.58 and 1.01 times larger than the binding energy of the respective trimer [291, 292]. The factor of 4.58 can be rationalized by realizing that the tetramer can be thought of as consisting of four trimers. In addition to the energy spectrum, other observables—such as the scattering lengths for which the tetramers become unbound and dissociate into four free atoms—obey universal relations [293, 294, 295, 296, 54]. At present, the study of larger systems is still in its infancy. Initial predictions that relate the N -body energies to those of the trimer have been made [289, 297, 298, 299] and it is expected that this research area will flourish in the years to come.

6. Summary and Outlook

Trapped ultracold atomic and molecular gases present a research area that is blossoming and whose future looks bright. This area has attracted the attention of researchers from diverse areas, including those with backgrounds in atomic physics,

nuclear physics, few-body physics, quantum optics, condensed matter physics and high energy physics. One attractive aspect of this research area is that experimental and theoretical efforts go hand in hand, with experiments being motivated by theoretical work and theoretical work being motivated by experimental progress.

This review provides an introduction to trapped atomic and molecular physics following a bottom-up approach. Building on a detailed discussion of two-body and three-body systems, the properties of trapped fermionic and bosonic systems with varying number of particles have been investigated. The discussions and examples presented are meant to give the reader a flavor of this rich and rapidly developing interdisciplinary field. In the following, we comment on selected present and future frontiers that have only been touched upon or not been covered at all in this review.

Other mixtures: This review focused primarily on the properties of two-component Fermi gases and single-component Bose gases. Extensions of these studies to other mixtures, such as Bose-Fermi or Bose-Bose mixtures, introduce additional degrees of freedom (i.e., another scattering length and possibly another confining length and/or mass ratio) and will allow one to investigate the interplay between interactions and symmetry in more depth. Studies along these lines may, e.g., lead to a bottom-up understanding of induced interactions (see, e.g., Ref. [300]).

Multi-component Fermi gases: While two-component Fermi gases are stable for essentially any interaction strength, Fermi gases with more than two components are not necessarily stable against collapse. In fact, the phase diagram of multi-component Fermi gases is currently being debated [301, 302, 303, 304, 305]. Bosenova-type collapse, BCS-type phases and phases whose properties are governed by competing dimer and trimer formation have been suggested. Studies of trapped multi-component Fermi gases may shed light on the effective interactions between two trimers and its connections to Efimov physics.

p-wave Fermi gases: This review focused almost exclusively on *s*-wave interacting systems in the vicinity of broad Fano-Feshbach resonances. While present experiments on higher partial wave resonances are plagued by detrimental losses, it seems feasible that these losses could be suppressed by loading the gas into an optical lattice or by utilizing atomic species for which dipolar relaxation rates can be suppressed [306]. Some theoretical few-body studies on *p*-wave interacting systems have been performed [307, 308, 309, 310], and it is anticipated that additional studies will further clarify questions related to the system's lifetime and address which aspects of higher partial wave systems are universal and which ones are not.

Dipolar systems: Much progress has been made in trapping and cooling systems with magnetic and electric dipoles. While weakly-interacting dipolar Bose gases have been modeled quite successfully using a mean-field description, the study of strongly-interacting dipolar systems is still in its infancy. The three-body system has been investigated for a few limiting scenarios within a microscopic framework [311, 312] but little has been done yet for larger systems. One possible approach is to pursue a description that is based on an effective Hamiltonian, which incorporates our understanding gained from microscopic two- and three-body studies.

Extended Efimov scenario and N -body parameter: The Efimov effect, in its original formulation, applies to three-body systems in free-space. Ever since Efimov's papers from the early 1970s, researchers have asked whether or not the Efimov effect generalizes to larger systems. Although much progress has been made, there are still open questions. Future studies of free-space and trapped four-, five- and higher-body systems will address in more detail how the energy spectrum of the N -body

system ($N > 3$) depends on the three-body parameter and how finite-range corrections enter. It is anticipated that answers to these questions will be found by combining the insights gained from microscopic and effective approaches applied to systems of varying symmetry and size.

Systems with two- and/or three-body resonances: This review discussed how two- and three-body interactions can be tuned by varying the trapping frequency of the harmonic confinement, by taking advantage of the optical lattice structure, or by inducing tunable effective three-body interactions that correspond to varying short-range hyperradial boundary conditions. For example, the scattering properties of three- and four-body systems in effectively one- and two-dimensional confining geometries have been analyzed in some detail [313, 314]. Another intriguing example is the appearance of resonances in mixed dimensional systems [315, 316]. It is expected that future work will uncover other means to manipulate the interactions. The resulting effective interactions are expected to open unique opportunities for designing larger systems with exotic properties. This is a research branch that appears to be equally intriguing to few- and many-body physicists.

Input for Hubbard Hamiltonian: Any type of effective Hamiltonian such as the Bose or Fermi Hubbard Hamiltonian depends on effective parameters such as the tunneling amplitude and on-site interactions. As experiments are being refined and many-body simulation techniques advance, it is paramount to refine the determination of the effective parameters that define a given effective Hamiltonian [317, 318]. Studies of trapped few-body systems are expected to contribute to this endeavor.

Beyond the LDA: Connections between inhomogeneous and homogeneous systems are often made through the LDA. While this approach has been tremendously successful, several limitations of this approach are known. A future goal of trapped atom and molecule studies should be to develop alternative approaches. These could involve pushing microscopic calculations of trapped atom systems to larger number of particles and extending condensed matter techniques to trapped systems.

Time-dependent dynamics of Bose gases: Although this review focused primarily on time-independent studies, it should be noted that much progress has been made over the past few years in solving the time-dependent many-body Schrödinger equation. One-dimensional Bose gases, e.g., have been treated by various variants of the multi-configurational approach [319] (borrowed from quantum chemistry) and the time-evolving block decimation or density-matrix renormalization group approaches [320, 321, 322] (borrowed from condensed matter physics). From a fundamental as well as an experimental point of view, the emergence of fragmented states of Bose gases is particularly interesting. Another intriguing set of studies addresses the tunneling dynamics in double-well geometries. In particular, the interplay between single particle and pair tunneling has been investigated [323]. It is expected that studies along these lines will be extended to higher-dimensional systems in the future.

Finite-temperature physics: Except for Subsec. 4.4, this review considered system properties at zero-temperature. Many features, such as the shell structure of two-component Fermi gases [324] and peaks in the loss rate due to Efimov resonances [325], become smeared out as the temperature increases. At the microscopic level, few studies to date have considered thermally averaged quantities, despite the fact that thermometry in optical lattice systems is currently a hot topic [326]. It is expected that the few-body community will push to develop the machinery that allows for the treatment of trapped systems at finite-temperature.

Non-equilibrium few-body dynamics: One of the key advantages of small trapped systems is that their entire excitation spectrum is, in certain cases, amenable to analytical or numerical treatments. This opens the possibility to prepare a system in a given initial state and to then follow the dynamics in response to a slow variation of a system parameter or a rapid quench. Initial studies along these lines have been performed [72, 188]. It is expected that this area of research will further intensify as studies of the non-equilibrium dynamics of optical lattice systems are progressing dramatically. Answers related to equilibration times, entanglement dynamics, and critical behavior are expected to emerge. For example, it is anticipated that few-body studies will address what happens when two initially separated optical lattice sites or plaquettes are being merged.

Acknowledgments

The author has benefitted greatly from close collaborations with M. Asad-uz-Zaman, Kevin Daily, Krittika Goyal, Chris Greene, Gabriel Hanna, Debraj Rakshit, Seth Rittenhouse, and Javier von Stecher on topics covered in or related to this review. The author thanks K. Daily for comments on the manuscript, and for providing the full temperature dependent Δb_3 data shown in Fig. 18. Support by the NSF through grant PHY-0855332 is gratefully acknowledged.

References

- [1] C. C. Bradley, C. A. Sackett, J. J. Tollett, and R. G. Hulet. Evidence of Bose-Einstein condensation in an atomic gas with attractive interactions. *Phys. Rev. Lett.*, 75:1687, 1995.
- [2] A. G. Truscott, K. E. Strecker, W. I. McAlexander, G. B. Partridge, and R. G. Hulet. Observation of Fermi pressure in a gas of trapped atoms. *Science*, 291:2570, 2002.
- [3] K. B. Davis, M.-O. Mewes, M. R. Andrews, N. J. van Druten, D. S. Durfee, D. M. Kurn, and W. Ketterle. Bose-Einstein condensation in a gas of sodium atoms. *Phys. Rev. Lett.*, 75:3969, 1995.
- [4] B. DeMarco and D. S. Jin. Onset of Fermi degeneracy in a trapped atomic gas. *Science*, 285:1703, 1999.
- [5] G. Modugno, G. Ferrari, G. Roati, R. J. Brecha, A. Simoni, and M. Inguscio. Bose-Einstein condensation of potassium atoms by sympathetic cooling. *Science*, 294:1320, 2001.
- [6] M. H. Anderson, J. R. Ensher, M. R. Matthews, C. E. Wieman, and E. A. Cornell. Observation of Bose-Einstein condensation in a dilute atomic vapor. *Science*, 269:198, 1995.
- [7] S. L. Cornish, N. R. Claussen, J. L. Roberts, E. A. Cornell, and C. E. Wieman. Stable Rb-85 Bose-Einstein condensates with widely tunable interactions. *Phys. Rev. Lett.*, 85:1795, 2000.
- [8] T. Weber, J. Herbig, M. Mark, H.-C. Nägerl, and R. Grimm. Bose-Einstein condensation of cesium. *Science*, 299:232, 2003.
- [9] L. Pitaevskii and S. Stringari. *Bose-Einstein Condensation*. New York, Oxford University Press, 2003.
- [10] C. J. Pethick and H. Smith. *Bose-Einstein Condensation in Dilute Gases*. Cambridge, Cambridge University Press, 2002.
- [11] V. L. Ginzburg and L. P. Pitaevskii. [*Sov. Phys. JETP*, 7:858, 1958] *Zh. Eksp. Teor. Fiz.*, 34:1240, 1958.
- [12] E. P. Gross. Structure of a quantized vortex in boson systems. *Nuovo Cimento*, 20:454, 1961.
- [13] E. P. Gross. Hydrodynamics of a Superfluid Condensate. *J. Math. Phys.*, 4:195, 1963.
- [14] L. P. Pitaevskii. Vortex Lines in an Imperfect Bose Gas. *J. Exptl. Theoret. Phys. (U.S.S.R.)*, 40:646, 1961.
- [15] F. Dalfovo, S. Giorgini, L. P. Pitaevskii, and S. Stringari. Theory of Bose-Einstein condensation in trapped gases. *Rev. Mod. Phys.*, 71:463, 1999.
- [16] B. D. Esry. Hartree-Fock theory for Bose-Einstein condensates and the inclusion of correlation effects. *Phys. Rev. A*, 55:1147, 1997.
- [17] S. Kraft, F. Vogt, O. Appel, F. Riehle, and U. Sterr. Bose-Einstein Condensation of Alkaline Earth Atoms: Ca-40. *Phys. Rev. Lett.*, 130401:103, 2009.

- [18] A. Robert, O. Sirjean, A. Browaeys, J. Poupard, S. Nowak, D. Boiron, C. I. Westbrook, and A. Aspect. A Bose-Einstein condensate of metastable atoms. *Science*, 292:461, 2001.
- [19] F. P. Dos Santos, J. Leonard, J. M. Wang, C. J. Barrelet, F. Perales, E. Rasel, C. S. Unnikrishnan, M. Leduc, and C. Cohen-Tannoudji. Bose-Einstein condensation of metastable helium. *Phys. Rev. Lett.*, 86:3459, 2001.
- [20] A. Griesmaier, J. Werner, S. Hensler, J. Stuhler, and T. Pfau. Bose-Einstein condensation of chromium. *Phys. Rev. Lett.*, 94:160401, 2005.
- [21] T. Fukuhara, Y. Takasu, Y. M. Kumakura, and Y. Takahashi. Degenerate Fermi gases of ytterbium. *Phys. Rev. Lett.*, 98:030401, 2007.
- [22] T. Fukuhara, S. Sugawa, S., and Y. Takahashi. Bose-Einstein condensation of an ytterbium isotope. *Phys. Rev. A*, 76:051604, 2009.
- [23] S. Stellmer, M. K. Tey, B. Huang, R. Grimm, and F. Schreck. Bose-Einstein Condensation of Strontium. *Phys. Rev. Lett.*, 103:200401, 2009.
- [24] Y. N. M. de Escobar, P. G. Mickelson, M. Yan, B. J. DeSalvo, S. B. Nagel, and T. C. Killian. Bose-Einstein Condensation of Sr-84. *Phys. Rev. Lett.*, 103:200402, 2009.
- [25] M. A. Baranov. Theoretical progress in many-body physics with ultracold dipolar gases. *Physics Reports*, 464:71, 2008.
- [26] T. Lahaye, C. Menotti, L. Santos, M. Lewenstein, and T. Pfau. The physics of dipolar bosonic quantum gases. *Rep. Prog. Phys.*, 72:126401, 2009.
- [27] F. Serwane, G. Zürn, T. Lompe, T. B. Ottenstein, A. N. Wenz, and S. Jochim. Deterministic Preparation of a Tunable Few-Fermion System. *Science*, 332:336, 2011.
- [28] M. Greiner, O. Mandel, T. Esslinger, T. W. Hänsch, and I. Bloch. Quantum phase transition from a superfluid to a Mott insulator in a gas of ultracold atoms. *Nature*, 415:39, 2002.
- [29] M. Köhl, H. Moritz, T. Stöferle, K. Günter, and T. Esslinger. Fermionic Atoms in a Three Dimensional Optical Lattice: Observing Fermi Surfaces, Dynamics, and Interactions. *Phys. Rev. Lett.*, 94:080403, 2005.
- [30] G. Thalhammer, K. Winkler, F. Lang, S. Schmid, R. Grimm, and J. Hecker Denschlag. Long-Lived Feshbach Molecules in a Three-Dimensional Optical Lattice. *Phys. Rev. Lett.*, 96:050402, 2006.
- [31] C. Chin, R. Grimm, P. Julienne, and E. Tiesinga. Feshbach resonances in ultracold gases. *Rev. Mod. Phys.*, 82:1225, 2010.
- [32] S. Inouye, M. R. Andrews, J. Stenger, H. J. Miesner, D. M. Stamper-Kurn, and W. Ketterle. Observation of Feshbach resonances in a Bose-Einstein condensate. *Nature*, 392:151, 1998.
- [33] P. Courteille, R. S. Freeland, D. J. Heinzen, F. A. van Abeelen, and B. J. Verhaar. Observation of a Feshbach resonance in cold atom scattering. *Phys. Rev. Lett.*, 81:69, 1998.
- [34] J. L. Roberts, N. R. Claussen, J. P. Burke, C. H. Greene, E. A. Cornell, and C. E. Wieman. Resonant magnetic field control of elastic scattering in cold ^{85}Rb . *Phys. Rev. Lett.*, 81:5109, 1998.
- [35] G. A. Baker, Jr. Neutron matter model. *Phys. Rev. C*, 60:054311, 1999.
- [36] H. Heiselberg. Fermi systems with long scattering lengths. *Phys. Rev. A*, 63:043606, 2001.
- [37] J. Carlson, S. Y. Chang, V. R. Pandharipande, and K. E. Schmidt. Superfluid Fermi gases with large scattering length. *Phys. Rev. Lett.*, 91:050401, 2003.
- [38] G. E. Astrakharchik, J. Boronat, J. D. Casulleras, and S. Giorgini. Equation of state of a Fermi gas in the BEC-BCS crossover: A quantum Monte Carlo study. *Phys. Rev. Lett.*, 93:200404, 2004.
- [39] S. Giorgini, L. P. Pitaevskii, and S. Stringari. Theory of ultracold atomic Fermi gases. *Rev. Mod. Phys.*, 80:1215, 2008.
- [40] S. Tan. Short Range Scaling Laws of Quantum Gases With Contact Interactions. *arXiv:0412764v2*.
- [41] F. Werner and Y. Castin. Unitary gas in an isotropic harmonic trap: Symmetry properties and applications. *Phys. Rev. A*, 74:053604, 2006.
- [42] S. Tan. Energetics of a strongly correlated Fermi gas. *Ann. Phys.*, 323:2952, 2008.
- [43] S. Tan. Large momentum part of a strongly correlated Fermi gas. *Ann. Phys.*, 323:2971, 2008.
- [44] S. Tan. Generalized virial theorem and pressure relation for a strongly correlated Fermi gas. *Ann. Phys.*, 323:2987, 2008.
- [45] V. Efimov. Energy levels arising from resonant 2-body forces in a 3-body system. *Phys. Lett.*, 33B:563, 1970.
- [46] V. Efimov. Weakly Bound States of Three Resonantly Interacting Particles. [*Sov. J. Nucl. Phys.* 12:598, 1971] *Yad. Fiz.*, 12:1080, 1970.
- [47] V. N. Efimov. Energy levels of three resonantly interacting particles. *Nucl. Phys. A*, 210:157, 1973.

- [48] E. Braaten and H.-W. Hammer. Universality in few-body systems with large scattering length. *Phys. Rep.*, 428:259, 2006.
- [49] E. Braaten and H.-W. Hammer. Efimov physics in cold atoms. *Ann. Phys.*, 322:120, 2007.
- [50] R. Brühl, A. Kalinin, O. Kornilov, J. P. Toennies, G. C. Hegerfeldt, and M. Stoll. Matter wave diffraction from an inclined transmission grating: Searching for the elusive He-4 trimer Efimov state. *Phys. Rev. Lett.*, 95:063002, 2005.
- [51] I. Mazumdar, A. R. P. Rau, and D. Uskov. Efimov states and their Fano resonances in a neutron-rich nucleus. *Phys. Rev. Lett.*, 97:062503, 2006.
- [52] T. Kraemer, M. Mark, P. Waldburger, J. G. Danzl, C. Chin, B. Engeser, A. D. Lange, K. Pilch, A. Jaakkola, H.-C. Nägerl, and R. Grimm. Evidence for Efimov quantum states in an ultracold gas of caesium atoms. *Nature*, 440:315, 2006.
- [53] G. Barontini, C. Weber, F. Rabatti, J. Catani, G. Thalhammer, M. Inguscio, and F. Minardi. Observation of Heteronuclear Atomic Efimov Resonances. *Phys. Rev. Lett.*, 103:043201, 2009.
- [54] S. E. Pollack, D. Dries, and R. G. Hulet. Universality in Three- and Four-Body Bound States of Ultracold Atoms. *Science*, 326:1683, 2009.
- [55] N. Gross, Z. Shotan, S. Kokkelmans, L. Khaykovich. Observation of Universality in Ultracold ^7Li Three-Body Recombination. *Phys. Rev. Lett.* 103:163202, 2009.
- [56] S. Knoop, F. Ferlaino, M. Mark, M. Berninger, H. Schobel, H.-C. Nägerl, and R. Grimm. Observation of an Efimov-like trimer resonance in ultracold atom-dimer scattering. *Nat. Phys.* 5:227, 2009.
- [57] M. Zaccanti, B. Dreissler, C. D'Errico, M. Fattori, M. Jona-Lasinio, S. Müller, G. Roati, M. Inguscio, and M. Modugno. Observation of an Efimov spectrum in an atomic system. *Nat. Phys.*, 5:586, 2009.
- [58] J. R. Williams, E. L. Hazlett, J. H. Huckans, R. W. Stites, Y. Zhang, and K. M. O'Hara. Evidence for an Excited-State Efimov Trimer in a Three-Component Fermi Gas. *Phys. Rev. Lett.*, 103:130404, 2009.
- [59] T. Lompe, T. B. Ottenstein, F. Serwane, A. N. Wenz, G. Zurn, and S. Jochim. Radio-Frequency Association of Efimov Trimers. *Science*, 330:940, 2010.
- [60] J. Weiner, V. S. Bagnato, S. Zilio, and P. S. Julienne. Experiments and theory in cold and ultracold collisions. *Rev. Mod. Phys.*, 71:1, 1999.
- [61] T. Köhler, K. Goral, and P. S. Julienne. Production of cold molecules via magnetically tunable Feshbach resonances. *Rev. Mod. Phys.*, 78:1311, 2006.
- [62] K. M. Jones, E. Tiesinga, P. D. Lett, and P. S. Julienne. Ultracold photoassociation spectroscopy: Long-range molecules and atomic scattering. *Rev. Mod. Phys.*, 78:483, 2006.
- [63] F. Ferlaino and R. Grimm. Trends: Forty years of Efimov physics: How a bizarre prediction turned into a hot topic. *Physics*, 3:9, 2010.
- [64] C. H. Greene. Universal insights from few-body land. *Physics Today*, 63:40, 2010.
- [65] I. Bloch, J. Dalibard, and W. Zwerger. Many-body physics with ultracold gases. *Rev. Mod. Phys.*, 80:885, 2008.
- [66] A. S. Jensen, K. Riisager, D. V. Fedorov, and E. Garrido. Structure and reactions of quantum halos. *Rev. Mod. Phys.*, 76:215, 2004.
- [67] J. Carlson and R. Schiavilla. Structure and dynamics of few-nucleon systems. *Rev. Mod. Phys.*, 70:743, 1998.
- [68] H. Saarikoski, S. M. Reimann, A. Harju, and M. Manninen. Vortices in quantum droplets: Analogies between boson and fermion systems. *Rev. Mod. Phys.*, 82:2785, 2010.
- [69] E. Nielsen, D. V. Fedorov, A. S. Jensen, and E. Garrido. The three-body problem with short-range interactions. *Phys. Rep.*, 347:374, 2001.
- [70] C. D. Lin. Hyperspherical Coordinate Approach to Atomic and other Coulombic 3-Body Systems. *Phys. Rep.*, 257:2, 1995.
- [71] S. T. Rittenhouse, J. von Stecher, J. P. D'Incao, N. P. Mehta, and C. H. Greene. The hyperspherical four-fermion problem. *J. Phys. B*, 44:172001, 2011.
- [72] F. H. Mies, E. Tiesinga, and P. S. Julienne. Manipulation of Feshbach resonances in ultracold atomic collisions using time-dependent magnetic fields. *Phys. Rev. A*, 61:022721, 2000.
- [73] D. B. Kaplan, M. J. Savage, and M. B. Wise. Two-nucleon systems from effective field theory. *Nucl. Phys. B*, 534:329, 1998.
- [74] M. Lüscher. Volume dependence of the energy-spectrum in massive quantum-field theories. 2. Scattering states. *Commun. Math. Phys.*, 105:153, 1986.
- [75] M. Lüscher. 2-particle states on a torus and their relation to the scattering matrix. *Nucl. Phys.*, B354:531, 1991.
- [76] S. R. Beane, P. F. Bedaque, A. Parreno, and M. J. Savage. Two nucleons on a lattice. *Phys.*

- Lett. B*, 585:106, 2004.
- [77] E. Braaten and M. Kusunoki. Low-energy universality and the new charmonium resonance at 3870 MeV. *Phys. Rev. D*, 69:074005, 2004.
- [78] E. Fermi. Sopra lo spostamento per pressione delle righe elevate delle serie spettrali. *Nuovo Cimento*, 11:157, 1934.
- [79] R. G. Taylor. *Scattering Theory of Waves and Particles, Second Edition*. Dover Publications, Inc., Mineola and New York, 2002.
- [80] G. Breit and P. R. Zitsel. The Scattering of Slow Neutrons by Bound Protons. II. Harmonic Binding – Neutrons of Zero Energy. *Phys. Rev.*, 71:232, 1947.
- [81] K. Huang and C. N. Yang. Quantum-Mechanical Many-Body Problem with Hard-Sphere Interaction. *Phys. Rev.*, 105:767, 1957.
- [82] M. J. Seaton. Quantum defect theory. *Rep. Prog. Phys.*, 46:167, 1983.
- [83] B. Borca, D. Blume, and C. H. Greene. A two-atom picture of coherent atom-molecule quantum beats. *New J. Phys.*, 5:111, 2003.
- [84] G. Peach, I. B. Whittingham, and T. J. Beams. Ultracold atomic collisions in tight harmonic traps: Quantum-defect model and application to metastable helium atoms. *Phys. Rev. A*, 70:032713, 2004.
- [85] E. P. Wigner. Über die Streuung von Neutronen an Protonen. *Z. für Physik*, 83:253, 1933.
- [86] H. A. Bethe and R. Peierls. Quantum Theory of the Dipion. *Proc. Roy. Soc.*, 148:146, 1935.
- [87] D. Blume and C. H. Greene. Fermi pseudopotential approximation: Two particles under external confinement. *Phys. Rev. A*, 65:043613, 2002.
- [88] E. L. Bolda, E. Tiesinga, and P. S. Julienne. Effective-scattering-length model of ultracold atomic collisions and Feshbach resonances in tight harmonic traps. *Phys. Rev. A*, 66:013403, 2002.
- [89] A. Omont. Theory of collisions of atoms in Rydberg states with neutral particles. *Journal de Physique*, 38:1343, 1977.
- [90] Yu N. Demkov and V. N. Ostrovskii. *Zero-range potentials and their applications in atomic physics*. New York, Plenum, 1988.
- [91] K. Kanjilal and D. Blume. Nondivergent pseudopotential treatment of spin-polarized fermions under one- and three-dimensional harmonic confinement. *Phys. Rev. A*, 70:042709, 2004.
- [92] R. Stock, A. Silberfarb, E. L. Bolda, and I. H. Deutsch. Generalized Pseudopotentials for higher Partial Wave Scattering. *Phys. Rev. Lett.*, 94:023202, 2005.
- [93] A. Derevianko. Revised Huang-Yang multipolar pseudopotential. *Phys. Rev. A*, 72:044701, 2005.
- [94] Z. Idziaszek and T. Calarco. Pseudopotential method for higher partial wave scattering. *Phys. Rev. Lett.*, 96:013201, 2006.
- [95] L. Pricoupenko. Pseudopotential in resonant regimes. *Phys. Rev. A*, 73:012701, 2006.
- [96] M. Holland, S. J. J. M. F. Kokkelmans, M. L. Chiofalo, and R. Walser. Resonance superfluidity in a quantum degenerate Fermi gas. *Phys. Rev. Lett.*, 87:120406, 2001.
- [97] J. W. Dunn, D. Blume, B. Borca, B. E. Granger, and C. H. Greene. Feshbach resonance cooling of trapped atom pairs. *Phys. Rev. A*, 71:033402, 2005.
- [98] G. M. Bruun and C. J. Pethick. Effective Theory of Feshbach Resonances and Many-Body Properties of Fermi Gases. *Phys. Rev. Lett.*, 92:140404, 2004.
- [99] D. S. Petrov, C. Salomon, and G. V. Shlyapnikov. Diatomic molecules in ultracold Fermi gases—Novel composite bosons. *J. Phys. B*, 38:S645, 2005.
- [100] R. B. Diener and T.-L. Ho. The Condition for Universality at Resonance and Direct Measurement of Pair Wavefunctions Using rf Spectroscopy. *arXiv:cond-mat/0405174*, 2004.
- [101] D. S. Petrov. Three-Boson Problem near a Narrow Feshbach Resonance. *Phys. Rev. Lett.*, 93:143201, 2004.
- [102] V. Gurarie and L. Radzihovsky. Resonantly paired fermionic superfluids. *Ann. Phys.*, 322:2, 2007.
- [103] *Handbook of Mathematical Functions With Formula, Graphs, and Mathematical Tables; Ed. by M. Abramowitz and I. E. Stegun (10th printing)*. U.S. Department of Commerce, National Bureau of Standards, Applied Mathematics Series 55, 1972.
- [104] T. Busch, B.-G. Englert, K. Rzazewski, and M. Wilkens. Two cold atoms in a harmonic trap. *Foundations of Phys.*, 28:549, 1998.
- [105] Y. Chen and B. Gao. Multiscale quantum-defect theory for two interacting atoms in a symmetric harmonic trap. *Phys. Rev. A*, 75:053601, 2007.
- [106] I. Reichenbach, A. Silberfarb, R. Stock, and I. H. Deutsch. Quasi-Hermitian pseudo-potential for higher partial wave scattering. *Phys. Rev. A*, 74:042724, 2006.
- [107] L. Pricoupenko. Modeling Interactions for Resonant p -Wave Scattering. *Phys. Rev. Lett.*,

- 96:050401, 2006.
- [108] M. Olshanii. Atomic scattering in the presence of an external confinement and a gas of impenetrable bosons. *Phys. Rev. Lett.*, 81:938, 1998.
- [109] T. Bergeman, M. G. Moore, and M. Olshanii. Atom-atom scattering under cylindrical harmonic confinement: Numerical and analytic studies of the confinement induced resonance. *Phys. Rev. Lett.*, 91:163201, 2003.
- [110] D. S. Petrov and G. V. Shlyapnikov. Interatomic collisions in a tightly confined Bose gas. *Phys. Rev. A*, 64:012706, 2001.
- [111] E. L. Bolda, E. Tiesinga, and P. S. Julienne. Pseudopotential model of ultracold atomic collisions in quasi-one- and two-dimensional traps. *Phys. Rev. A*, 68:032702, 2003.
- [112] B. E. Granger and D. Blume. Tuning the interactions of spin-polarized fermions using quasi-one-dimensional confinement. *Phys. Rev. Lett.*, 92:133202, 2004.
- [113] Z. Idziaszek and T. Calarco. Analytical solutions for the dynamics of two trapped interacting ultracold atoms. *Phys. Rev. A*, 74:022712, 2006.
- [114] Z. Idziaszek. Analytical solutions for two atoms in a harmonic trap: p-wave interactions. *Phys. Rev. A*, 79:062701, 2009.
- [115] K. Kanjilal, J. L. Bohn, and D. Blume. Pseudopotential treatment of two aligned dipoles under external harmonic confinement. *Phys. Rev. A*, 75:052705, 2007.
- [116] R. B. Diener and T.-L. Ho. Fermions in Optical Lattices Swept across Feshbach Resonances. *Phys. Rev. Lett.*, 96:010402, 2006.
- [117] J.-J. Liang and C. Zhang. Two ultracold atoms in a completely anisotropic trap. *Phys. Scr.*, 77:025302, 2008.
- [118] S.-G. Peng, S. S. Bohloul, X.-J. Liu, H. Hu, and P. D. Drummond. Confinement-induced resonance in quasi-one-dimensional systems under transversely anisotropic confinement. *Phys. Rev. A*, 82:063633, 2010.
- [119] F. Deuretzbacher, K. Plassmeier, D. Pfannkuche, F. Werner, C. Ospelkaus, S. Ospelkaus, K. Sengstock, and K. Bongs. Heteronuclear molecules in an optical lattice: Theory and experiment. *Phys. Rev. A*, 77:032726, 2008.
- [120] S. Grishkevich and A. Saenz. Theoretical description of two ultracold atoms in a single site of a three-dimensional optical lattice using realistic interatomic interaction potentials. *Phys. Rev. A*, 80:013403, 2009.
- [121] D. Blume. Small mass- and trap-imbalanced two-component Fermi systems. *Phys. Rev. A*, 78:013613, 2008.
- [122] X. Feng, X. Li, and C. Liu. Two particles in an asymmetric box and the elastic scattering phases. *Phys. Rev. D*, 70:014505, 2004.
- [123] E. H. Lieb and W. Liniger. Exact analysis of an interacting bose gas. I. The general solution and the ground state. *Phys. Rev.*, 130:1605, 1963.
- [124] E. H. Lieb. Exact analysis of an interacting bose gas. II. The excitation spectrum. *Phys. Rev.*, 130:1616, 1963.
- [125] M. Gaudin. Un système a une dimension de fermions en interaction. *Phys. Lett.*, 24A:55, 1967.
- [126] C. N. Yang. Some Exact Results for the Many-Body Problem in one Dimension with Repulsive Delta-Function Interaction. *Phys. Rev. Lett.*, 19:1312, 1967.
- [127] T. Kinoshita, T. Wenger, and D. S. Weiss. A quantum Newton's cradle. *Nature*, 440:900, 2006.
- [128] M. Rigol, V. Dunjko, Y. Yurovsky, and M. Olshanii. Relaxation in a completely integrable many-body quantum system: An ab initio study of the dynamics of the highly excited states of 1D lattice hard-core bosons. *Phys. Rev. Lett.*, 98:050405, 2007.
- [129] M. Rigol, V. Dunjko, and M. Olshanii. Thermalization and its mechanism for generic isolated quantum systems. *Nature*, 452:854, 2008.
- [130] V. A. Yurovsky, A. Ben-Reuven, and M. Olshanii. One-dimensional Bose chemistry: Effects of nonintegrability. *Phys. Rev. Lett.*, 96:163201, 2006.
- [131] I. E. Mazets, T. Schumm, and J. Schmiedmayer. Breakdown of integrability in a quasi-1D ultracold bosonic gas. *Phys. Rev. Lett.*, 100:210403, 2008.
- [132] R. C. Ashoori. Electrons in artificial atoms. *Nature*, 379:413, 1996.
- [133] S. M. Reimann and M. Manninen. Electronic structure of quantum dots. *Rev. Mod. Phys.*, 74:1283, 2002.
- [134] M. Rontani, J. R. Armstrong, Y. Yu, S. Aberg, and S. M. Reimann. Cold Fermionic Atoms in Two-Dimensional Traps: Pairing versus Hund's Rule. *Phys. Rev. Lett.*, 102:060401, 2009.
- [135] P. O. Fedichev, M. J. Bijlsma, and P. Zoller. Extended molecules and geometric scattering resonances in optical lattices. *Phys. Rev. Lett.*, 92:080401, 2004.

- [136] M. Wouters and G. Orso. Two-body problem in periodic potentials. *Phys. Rev. A*, 73:012707, 2006.
- [137] M. Grupp, R. Walser, W. P. Schleich, A. Maramatsu, and M. Weitz. Resonant Feshbach scattering of fermions in one-dimensional optical lattices. *J. Phys. B*, 40:2703, 2007.
- [138] X. L. Cui, Y. P. Wang, and F. Zhou. Resonance Scattering in Optical Lattices and Molecules: Interband versus Intraband Effects. *Phys. Rev. Lett.*, 104:153201, 2010.
- [139] H. W. Hamber, E. Marinari, G. Parisi, and C. Rebbi. Considerations on numerical analysis of QCD. *Nucl. Phys. B*, 225:475, 1983.
- [140] M. Marinescu and L. You. Controlling Atom-Atom Interaction at Ultralow Temperatures by dc Electric Fields. *Phys. Rev. Lett.*, 81:4596, 1998.
- [141] S. Yi and L. You. Trapped atomic condensates with anisotropic interactions. *Phys. Rev. A*, 61:041604(R), 2000.
- [142] B. Deb and L. You. Low-energy atomic collision with dipole interactions. *Phys. Rev. A*, 64:022717, 2002.
- [143] C. Ticknor and J. L. Bohn. Long-range scattering resonances in strong-field-seeking states of polar molecules. *Phys. Rev. A*, 72:032717, 2005.
- [144] K. Kanjilal and D. Blume. Low-energy resonances and bound states of aligned bosonic and fermionic dipoles. *Phys. Rev. A*, 78:040703(R), 2008.
- [145] V. Roudnev and M. Cavagnero. Universal resonant ultracold molecular scattering. *Phys. Rev. A*, 79:014701, 2009.
- [146] V. Roudnev and M. Cavagnero. Resonance phenomena in ultracold dipole-dipole scattering. *Phys. Rev. A*, 42:044017, 2009.
- [147] J. Macek. Properties of autoionizing states of He. *J. Phys. B*, 1:831, 1968.
- [148] J. Avery. *Hyperspherical Harmonics: Applications in Quantum Theory*. Kluwer Academic Publishers, Dordrecht, Boston, London, 1989.
- [149] J. L. Bohn, B. D. Esry, and C. H. Greene. Effective potentials for dilute Bose-Einstein condensates. *Phys. Rev. A*, 58:584, 1998.
- [150] U. Fano, D. Green, J. L. Bohn, and T. A. Heim. Geometry and symmetries of multi-particle systems. *J. Phys. B*, 32:R1, 1999.
- [151] S. T. Rittenhouse, M. J. Cavagnero, J. von Stecher, and C. H. Greene. Hyperspherical description of the degenerate Fermi gas: s -wave interactions. *Phys. Rev. A*, 74:053624, 2006.
- [152] B. D. Esry and C. H. Greene. Validity of the shape-independent approximation for Bose-Einstein condensates. *Phys. Rev. A*, 60:1451, 1999.
- [153] D. V. Fedorov and A. S. Jensen. Efimov effect in coordinate space Faddeev equations. *Phys. Rev. Lett.*, 71:4103, 1993.
- [154] A. F. Starace and G. L. Webster. Atomic hydrogen in a uniform magnetic field: Low-lying energy levels for fields below 10^9 G. *Phys. Rev. A*, 19:1629, 1979.
- [155] H. T. Coelho and J. E. Hornos. Proof of basic inequalities in the hyperspherical formalism for the N -body problem. *Phys. Rev. A*, 43:6379, 1991.
- [156] S. T. Rittenhouse, N. P. Mehta, and C. H. Greene. Greens functions and the adiabatic hyperspherical method. *Phys. Rev. A*, 82:022706, 2010.
- [157] O. I. Kartavtsev and A. V. Malykh. Low-energy three-body dynamics in binary quantum gases. *J. Phys. B*, 40:1429, 2007.
- [158] F. Werner and Y. Castin. Unitary Quantum Three-Body Problem in a Harmonic Trap. *Phys. Rev. Lett.*, 97:150401, 2006.
- [159] O. I. Kartavtsev and J. H. Macek. Low-Energy Three-Body Recombination Near a Feshbach Resonance. *Few-Body Systems*, 31:249, 2002.
- [160] S. Jonsell, H. Heiselberg, and C. J. Pethick. Universal Behavior of the Energy of Trapped Few-Boson Systems with Large Scattering Length. *Phys. Rev. Lett.*, 98:250401, 2002.
- [161] Y. Nishida, D. T. Son, and S. Tan. Universal Fermi Gas with Two- and Three-Body Resonances. *Phys. Rev. Lett.*, 100:090405, 2008.
- [162] D. S. Petrov. Three-body problem in Fermi gases with short-range interparticle interaction. *Phys. Rev. A*, 67:010703(R), 2003.
- [163] D. Blume and K. M. Daily. Breakdown of Universality for Unequal-Mass Fermi Gases with Infinite Scattering Length. *Phys. Rev. Lett.*, 105:170403, 2010.
- [164] D. Blume and K. M. Daily. Few-body resonances of unequal-mass systems with infinite interspecies two-body s -wave scattering length. *Phys. Rev. A*, 82:063612, 2010.
- [165] S. Gandolfi and J. Carlson. Heavy-Light Few Fermion Clusters at Unitarity. *arXiv:1006.5186*, 2010.
- [166] D. Blume and C. H. Greene. Three particles in an external trap: Nature of the complete $J = 0$

- spectrum. *Phys. Rev. A*, 66:013601, 2002.
- [167] K. M. Daily and D. Blume. Energy spectrum of harmonically trapped two-component Fermi gases: Three- and four-particle problem. *Phys. Rev. A*, 81:053615, 2010.
- [168] The lowest s_ν value for $L = 0$ derived within the “atom-dimer” picture differs from that derived using the semi-classical framework; the atom-dimer picture gives 2 in this case, which should be compared with the semi-classically derived result of 3 and the exact result of 2.166.
- [169] X.-J. Liu, H. Hu, and P. D. Drummond. Virial Expansion for a Strongly Correlated Fermi Gas. *Phys. Rev. Lett.*, 102:160401, 2009.
- [170] X.-J. Liu, H. Hu, and P. D. Drummond. Three attractively interacting fermions in a harmonic trap: Exact solution, ferromagnetism, and high-temperature thermodynamics. *Phys. Rev. A*, 82:023619, 2010.
- [171] B. D. Esry, C. H. Greene, and J. P. Burke Jr. Recombination of Three Atoms in the Ultracold Limit. *Phys. Rev. Lett.*, 83:1751, 1999.
- [172] E. Nielsen and J. H. Macek. Low-Energy Recombination of Identical Bosons by Three-Body Collisions. *Phys. Rev. Lett.*, 83:1566, 1999.
- [173] P. F. Bedaque, E. Braaten, and H.-W. Hammer. Three-body Recombination in Bose Gases with Large Scattering Length. *Phys. Rev. Lett.*, 85:908, 2000.
- [174] E. Braaten and H.-W. Hammer. Three-Body Recombination into Deep Bound States in a Bose Gas with Large Scattering Length. *Phys. Rev. Lett.*, 87:160407, 2001.
- [175] V. Efimov. Effective interaction of three resonantly interacting particles and the force range. *Phys. Rev. C*, 47:1876, 1993.
- [176] L. Platter, C. Ji, and D. R. Phillips. Range corrections to three-body observables near a Feshbach resonance. *Phys. Rev. A*, 79:022702, 2009.
- [177] M. Thøgersen, D. V. Fedorov, A. S. Jensen, B. D. Esry, and Y. Wang. Conditions for Efimov physics for finite-range potentials. *Phys. Rev. A*, 80:013608, 2009.
- [178] M. Stoll and T. Köhler. Production of three-body Efimov molecules in an optical lattice. *Phys. Rev. A*, 72:022714, 2005.
- [179] J. Portegies and S. Kokkelmans. Efimov Trimers in a Harmonic Potential. *arXiv:1101.0696*, 2011.
- [180] G. V. Skorniakov and K. A. Ter-Martirosian. Three body problem for short range forces. I. Scattering of low energy neutrons by deuterons. [*Sov. Phys. JETP*, 4:648, 1957] *Zh. Eksp. Teor. Fiz.*, 31:775, 1956.
- [181] S. Y. Chang, V. R. Pandharipande, J. Carlson, and K. E. Schmidt. Quantum Monte Carlo studies of superfluid Fermi gases. *Phys. Rev. A*, 70:043602, 2004.
- [182] D. S. Petrov, C. Salomon, and G. V. Shlyapnikov. Weakly Bound Dimers of Fermionic Atoms. *Phys. Rev. Lett.*, 93:090404, 2004.
- [183] D. Blume, J. von Stecher, and C. H. Greene. Universal properties of a trapped two-component Fermi gas at unitarity. *Phys. Rev. Lett.*, 99:233201, 2007.
- [184] B. M. Fregoso and G. Baym. Stability of trapped fermionic gases with attractive interactions. *Phys. Rev. A*, 73:043616, 2006.
- [185] J. P. Kestner and L. M. Duan. Level crossing in the three-body problem for strongly interacting fermions in a harmonic trap. *Phys. Rev. A*, 76:033611, 2007.
- [186] I. Stetcu, B. R. Barrett, U. van Kolck, and J. P. Vary. Effective theory for trapped few-fermion systems. *Phys. Rev. A*, 76:063613, 2007.
- [187] J. von Stecher, C. H. Greene, and D. Blume. Energetics and structural properties of trapped two-component Fermi gases. *Phys. Rev. A*, 77:043619, 2008.
- [188] J. von Stecher and C. H. Greene. Spectrum and Dynamics of the BCS-BEC Crossover from a Few-Body Perspective. *Phys. Rev. Lett.*, 99:090402, 2007.
- [189] J. von Stecher, C. H. Greene, and D. Blume. BEC-BCS crossover of a trapped two-component Fermi gas with unequal masses. *Phys. Rev. A*, 76:053613, 2007.
- [190] A. Bulgac, P. F. Bedaque, and A. C. Fonseca. A dilute atomic Fermi system with a large positive scattering length. *cond-mat/0306302*, 2003.
- [191] I. V. Brodsky, A. V. Klaptsov, M. Yu. Kagan, R. Combescot, and X. Leyronas. Bound States of Three and Four Resonantly Interacting Particles. *JETP Lett.*, 82:273, 2005.
- [192] J. Levensen and V. Gurarie. Properties of strongly paired fermionic condensates. *Phys. Rev. A*, 73:053607, 2006.
- [193] J. P. D’Incao, S. T. Rittenhouse, N. P. Mehta, and C. H. Greene. Dimer-dimer collisions at finite energies in two-component Fermi gases. *Phys. Rev. A*, 79:030501(R), 2009.
- [194] R. Jáuregui, R. Paredes, and G. Toledo Sánchez. BEC-BCS crossover of a trapped Fermi gas without using the local density approximation. *Phys. Rev. A*, 76:011604(R), 2007.
- [195] P. J. Reynolds, D. M. Ceperley, B. J. Alder, and W. A. Lester, Jr.. Fixed-node quantum Monte

- Carlo for molecules. *J. Chem. Phys.*, 77: 5593, 1982.
- [196] D. Blume and K. M. Daily. Trapped two-component Fermi gases with up to six particles: Energetics, structural properties, and molecular condensate fraction. *C. R. Physique*, 12:86, 2011.
- [197] Y. Suzuki and K. Varga. *Stochastic Variational Approach to Quantum Mechanical Few-Body Problems*. Springer Verlag, Berlin, 1998.
- [198] D. Blume and K. M. Daily. Universal relations for a trapped four-fermion system with arbitrary s -wave scattering length. *Phys. Rev. A*, 80:053626, 2009.
- [199] J. Rotureau, I. Stetcu, B. R. Barrett, M. C. Birse, U. van Kolck, and J. P. Vary. Three and four harmonically trapped particles in an effective-field-theory framework. *Phys. Rev. A*, 82:032711, 2010.
- [200] S. Tölle, H.-W. Hammer, and B. C. Metsch. Universal few-body physics in a harmonic trap. *C. R. Physique*, 12:59, 2011.
- [201] Y. Alhassid, G. F. Bertsch, and L. Fang. New Effective Interaction for the Trapped Fermi Gas. *Phys. Rev. Lett.*, 100:230401, 2008.
- [202] M. G. Endres, D. B. Kaplan, J.-W. Lee, and A. N. Nicholson. A new approach for studying large numbers of fermions in the unitary regime. *PoS Lattice*, 2010:182, 2010.
- [203] A. N. Nicholson, M. G. Endres, D. B. Kaplan, and J.-W. Lee. Lattice study of trapped fermions at unitarity. *PoS Lattice*, 2010:206, 2010.
- [204] Y. Castin. Exact scaling transform for a unitary quantum gas in a time dependent harmonic potential. *C. R. Phys.*, 5:407, 2004.
- [205] J. von Stecher and C. H. Greene. Correlated Gaussian hyperspherical method for few-body systems. *Phys. Rev. A*, 80:022504, 2009.
- [206] F. Werner. Virial theorems for trapped cold atoms. *Phys. Rev. A*, 78:025601, 2008.
- [207] A. Bulgac. Local-density-functional theory for superfluid fermionic systems: The unitary gas. *Phys. Rev. A*, 76:040502(R), 2007.
- [208] S. Y. Chang and G. F. Bertsch. Unitary Fermi gas in harmonic trap. *Phys. Rev. A*, 76:021603(R), 2007.
- [209] A. L. Zubarev and M. Zoubarev. On the kinetic energy of unitary Fermi gas in a harmonic trap. *EPL*, 87:33001, 2009.
- [210] M. Brack and R. K. Bhaduri. *Semiclassical Physics*. Addison-Wesley, Reading, MA, 1997.
- [211] G. Rupak and T. Schäfer. Density functional theory for non-relativistic fermions in the unitarity limit. *Nucl. Phys. A*, 816:52, 2009.
- [212] G. F. Bertsch proposed the problem of determining the ground state of a two-component Fermi gas with large scattering length at a conference in 1999.
- [213] M. M. Forbes, S. Gandolfi, and A. Gezerlis. Resonantly Interacting Fermions In a Box. *Phys. Rev. Lett.*, 106:235303, 2011.
- [214] C. Menotti, P. Pedri, and S. Stringari. Expansion of an Interacting Fermi Gas.
- [215] D. T. Son. Three comments on the Fermi gas at unitarity in a harmonic trap. *arXiv:0707.1851v1*, 2007.
- [216] R. K. Bhaduri, M. V. N. Murthy, and M. Brack. Fermionic ground state at unitarity and Haldane Exclusion Statistics. *J. Phys. B*, 41:115301, 2008.
- [217] L. Salasnich and F. Toigo. Extended Thomas-Fermi density functional for the unitary Fermi gas. *Phys. Rev. A*, 78:053626, 2008.
- [218] S. K. Adhikari. Nonlinear Schrödinger equation for a superfluid Fermi gas in the BCS-BEC crossover. *Phys. Rev. A*, 77:045602, 2008.
- [219] A. L. Zubarev. Weizsacker energy of unitary Fermi gas in a harmonic trap. *J. Phys. B*, 42:011001, 2009.
- [220] A. Bulgac, M. M. Forbes, and P. Magierski. The Unitary Fermi Gas: From Monte Carlo to Density Functionals. *arXiv:1008.3933*, 2010. to be published as a chapter in BCS-BEC Crossover and the Unitary Fermi Gas (Lecture Notes in Physics), edited by W. Zwerger (Springer, 2011).
- [221] D. Blume. Trapped polarized Fermi gas at unitarity. *Phys. Rev. A*, 78:013635, 2008.
- [222] A. Schirotzek, C.-H. Wu, A. Sommer, and M. W. Zwierlein. Observation of Fermi Polarons in a Tunable Fermi Liquid of Ultracold Atoms. *Phys. Rev. Lett.*, 102:230402, 2009.
- [223] S. Nascimbene, N. Navon, K. J. Jiang, F. Chevy, and C. Salomon. Exploring the thermodynamics of a universal Fermi gas. *Nature*, 463:1057, 2010.
- [224] M. Taglieber, A.-C. Vogt, F. Henkel, S. Fray, T. W. Hänsch, and K. Dieckmann. Simultaneous magneto-optical trapping of three atomic species. *Phys. Rev. A*, 73:011402(R), 2006.
- [225] M. Taglieber, A.-C. Vogt, T. Aoki, T. W. Hänsch, and K. Dieckmann. Quantum degenerate two-species Fermi-Fermi mixture coexisting with a Bose-Einstein condensate. *Phys. Rev.*

- Lett.*, 100:010401, 2008.
- [226] F. M. Spiegelhalder, A. Trenkwalder, D. Naik, G. Hendl, F. Schreck, and R. Grimm. Collisional Stability of ^{40}K Immersed in a Strongly Interacting Fermi Gas of ^6Li . *Phys. Rev. Lett.*, 103:223203, 2009.
- [227] F. M. Spiegelhalder, A. Trenkwalder, D. Naik, G. Kerner, E. Wille, G. Hendl, F. Schreck, and R. Grimm. All-optical production of a degenerate mixture of Li-6 and K-40 and creation of heteronuclear molecules. *Phys. Rev. A*, 81:043637, 2010.
- [228] A. Trenkwalder, C. Kohstall, M. Zaccanti, D. Naik, A. I. Sidorov, F. Schreck, and R. Grimm. Hydrodynamic Expansion of a Strongly Interacting Fermi-Fermi Mixture. *Phys. Rev. Lett.*, 106:115304, 2011.
- [229] B. Marcellis, S. J. J. M. F. Kokkelmans, G. V. Shlyapnikov, and D. S. Petrov. Collisional properties of weakly bound heteronuclear dimers. *Phys. Rev. A*, 77:032707, 2008.
- [230] A. Gezerlis, S. Gandolfi, K. E. Schmidt, and J. Carlson. Heavy-Light Fermion Mixtures at Unitarity. *Phys. Rev. Lett.*, 103:060403, 2009.
- [231] D. J. MacNeill and F. Zhou. Pauli Blocking Effect on Efimov States Near Feshbach Resonance. *Phys. Rev. Lett.*, 106:145301, 2010.
- [232] Y. Castin, C. Mora, and L. Pricoupenko. Four-Body Efimov Effect for Three Fermions and a Lighter Particle. *Phys. Rev. Lett.*, 105:223201, 2010.
- [233] M. Horikoshi, S. Nakajima, M. Ueda, and T. Mukaiyama. Measurement of Universal Thermodynamic Functions for a Unitary Fermi Gas. *Science*, 327:442, 2010.
- [234] T.-L. Ho and E. J. Mueller. High Temperature Expansion Applied to Fermions near Feshbach Resonance. *Phys. Rev. Lett.*, 92:160404, 2004.
- [235] G. Rupak. Universality in a 2-Component Fermi System at Finite Temperature. *Phys. Rev. Lett.*, 98:090403, 2007.
- [236] K. Huang. *Statistical Mechanics*. New York, Wiley, 1987.
- [237] The data for Δb_3 were provided by K. M. Daily.
- [238] L. Luo, B. Clancy, J. Joseph, J. Kinast, and J. E. Thomas. Measurement of the Entropy and Critical Temperature of a Strongly Interacting Fermi Gas. *Phys. Rev. Lett.*, 98:080402, 2007.
- [239] H. Hu, X.-J. Liu, and P. D. Drummond. Dynamic response of strongly correlated Fermi gases in the quantum virial expansion. *Phys. Rev. A*, 81:033630, 2010.
- [240] X.-J. Liu and H. Hu. Virial expansion for a strongly correlated Fermi gas with imbalanced spin populations. *Phys. Rev. A*, 82:043626, 2010.
- [241] A. Bulgac, J. E. Drut, and P. Magierski. Spin 1/2 Fermions in the Unitary Regime: A Superfluid of a New Type. *Phys. Rev. Lett.*, 96:090404, 2006.
- [242] E. Burovski, N. Prokof'ev, B. Svistunov, and M. Troyer. Critical Temperature and Thermodynamics of Attractive Fermions at Unitarity. *Phys. Rev. Lett.*, 96:160402, 2006.
- [243] V. K. Akkineni, D. M. Ceperley, and N. Trivedi. Pairing and superfluid properties of dilute fermion gases at unitarity. *Phys. Rev. B*, 76:165116, 2007.
- [244] P. A. Ruprecht, M. J. Holland, K. Burnett, and M. Edwards. Time-dependent solution of the nonlinear Schrödinger equation for Bose-condensed trapped neutral atoms. *Phys. Rev. A*, 51:4704, 1995.
- [245] G. Baym and C. J. Pethick. Ground-State Properties of Magnetically Trapped Bose-Condensed Rubidium Gas. *Phys. Rev. Lett.*, 76:6, 1996.
- [246] F. Dalfovo, L. P. Pitaevskii, and S. Stringari. Order parameter at the boundary of a trapped Bose gas. *Rev. Phys. A*, 54:4213, 1996.
- [247] B. D. Esry. *Ph. D. thesis, University of Colorado, Boulder (unpublished)*, 1997.
- [248] A. Fetter. Ground state and excited states of a confined condensed Bose gas. *Phys. Rev. A*, 53:4245, 1996.
- [249] A. J. Leggett. Bose-Einstein condensation in the alkali gases: Some fundamental concepts. *Rev. Mod. Phys.*, 73:307, 2001.
- [250] R. J. Dodd, M. Edwards, C. J. Williams, C. W. Clark, M. J. Holland, P. A. Ruprecht, and K. Burnett. Role of attractive interactions on Bose-Einstein condensation. *Phys. Rev. A*, 54:661, 1996.
- [251] N. N. Bogoliubov. On the theory of superfluidity. *J. Phys. USSR*, 11:23, 1947.
- [252] D. Blume and C. H. Greene. Quantum corrections to the ground-state energy of a trapped Bose-Einstein condensate: A diffusion Monte Carlo calculation. *Phys. Rev. A*, 63:063601, 2001.
- [253] M. Holzmann, W. Krauth, and M. Naraschewski. Precision Monte Carlo test of the Hartree-Fock approximation for a trapped Bose gas. *Phys. Rev. A*, 59:2956, 1999.
- [254] J. L. DuBois and H. R. Glyde. Bose-Einstein condensation in trapped bosons: A variational

- Monte Carlo analysis. *Phys. Rev. A*, 63:023602, 2001.
- [255] J. L. DuBois and H. R. Glyde. Natural orbitals and Bose-Einstein condensates in traps: A diffusion Monte Carlo analysis. *Phys. Rev. A*, 68:033602, 2003.
- [256] P. R. Johnson, E. Tiesinga, J. V. Porto, and C. J. Williams. Effective three-body interactions of neutral bosons in optical lattices. *New J. Phys.*, 11:093022, 2009.
- [257] T. T. Wu. Ground State of a Bose System of Hard Spheres. *Phys. Rev.*, 115:1390, 1959.
- [258] T. D. Lee, K. Huang, and C. N. Yang. Eigenvalues and Eigenfunctions of a Bose System of Hard Spheres and Its Low-Temperature Properties. *Phys. Rev.*, 106:1135, 1957.
- [259] S. R. Beane, W. Detmold, and M. J. Savage. n -Boson Energies at Finite Volume and Three-Boson Interactions. *Phys. Rev. D*, 76:074507, 2007.
- [260] S. Tan. Three-boson problem at low energy and implications for dilute Bose-Einstein condensates. *Phys. Rev. A*, 78:013636, 2008.
- [261] T. D. Lee and C. N. Yang. Many-Body Problem in Quantum Mechanics and Quantum Statistical Mechanics. *Phys. Rev.*, 105:1119, 1957.
- [262] F. London. On the Bose-Einstein Condensation. *Phys. Rev.*, 54:947, 1938.
- [263] F. London. The λ -phenomenon of liquid helium and the Bose-Einstein degeneracy. *Nature*, 141:643, 1938.
- [264] D. M. Ceperley. Path integrals in the theory of condensed helium. *Rev. Mod. Phys.*, 67:279, 1995.
- [265] S. Moroni, G. Senatore, and S. Fantoni. Momentum distribution of liquid helium. *Phys. Rev. B*, 55:1040, 1997.
- [266] H. R. Glyde, R. T. Azuah, and W. G. Stirling. Condensate, momentum distribution, and final-state effects in liquid ^4He . *Phys. Rev. B*, 62:14337, 2000.
- [267] P. O. Fedichev, M. W. Reynolds, and G. V. Shlyapnikov. Three-Body Recombination of Ultracold Atoms to a Weakly Bound s Level. *Phys. Rev. Lett.*, 77:2921, 1996.
- [268] S. B. Papp, J. M. Pino, R. J. Wild, S. Ronen, C. E. Wieman, D. S. Jin, and E. A. Cornell. Bragg Spectroscopy of a Strongly Interacting ^{85}Rb Bose-Einstein Condensate. *Phys. Rev. Lett.*, 101:135301, 2008.
- [269] S. Cowell, H. Heiselberg, I. E. Mazets, J. Morales, V. R. Pandharipande, and C. J. Pethick. Cold Bose Gases with Large Scattering Lengths. *Phys. Rev. Lett.*, 88:210403, 2002.
- [270] H. Heiselberg. Bosons and fermions near Feshbach resonances. *J. Phys. B*, 37:S141, 2004.
- [271] M. Thøgersen, D. V. Fedorov, and A. S. Jensen. Trapped Bose gases with large positive scattering length. *Europhysics Letters*, 79:40002, 2007.
- [272] J. L. Song and F. Zhou. Ground State Properties of Cold Bosonic Atoms at Large Scattering Lengths. *Phys. Rev. Lett.*, 103:025302, 2009.
- [273] Y.-I. Lee and Y.-W. Lee. Universality and stability for a dilute Bose gas with a Feshbach resonance. *Phys. Rev. A*, 81:063613, 2010.
- [274] T.-L. Ho. Universal Thermodynamics of Degenerate Quantum Gases in the Unitarity Limit. *Phys. Rev. Lett.*, 92:090402, 2004.
- [275] E. Braaten and A. Nieto. Quantum corrections to the ground state of a trapped Bose-Einstein condensate. *Phys. Rev. B*, 56:14745, 1997.
- [276] E. Timmermans, P. Tommasini, and K. Huang. Variational Thomas-Fermi theory of a nonuniform Bose condensate at zero temperature. *Phys. Rev. A*, 55:3645, 1997.
- [277] A. Fabrocini and A. Polls. Beyond the Gross-Pitaevskii approximation: Local density versus correlated basis approach for trapped bosons. *Phys. Rev. A*, 60:2319, 1999.
- [278] V. Pérez-García, H. Michinel, J. I. Cirac, M. Lewenstein, and P. Zoller. Dynamics of Bose-Einstein condensates: Variational solutions of the Gross-Pitaevskii equation. *Phys. Rev. A*, 56:1424, 1997.
- [279] Yu. Kagan, G. V. Shlyapnikov, and J. T. M. Walraven. Bose-Einstein Condensation in Trapped Atomic Gases. *Phys. Rev. Lett.*, 76:2670, 1996.
- [280] E. V. Shuryak. Metastable Bose condensate made of atoms with attractive interaction. *Phys. Rev. A*, 54:3151, 1996.
- [281] H. T. C. Stoof. Macroscopic quantum tunneling of a Bose condensate. *J. Stat. Phys.*, 87:1353, 1997.
- [282] O. Sørensen, D. V. Fedorov, and A. S. Jensen. Correlated N -boson systems for arbitrary scattering length. *Phys. Rev. A*, 68:063618, 2003.
- [283] C. C. Bradley, C. A. Sackett, and R. G. Hulet. Bose-Einstein condensation of lithium: Observation of limited condensate number. *Phys. Rev. Lett.*, 78:985, 1997.
- [284] J. L. Roberts, N. R. Claussen, S. L. Cornish, E. A. Donley, E. A. Cornell, and C. E. Wieman. Controlled Collapse of a Bose-Einstein Condensate. *Phys. Rev. Lett.*, 86:4211, 2001.
- [285] B. Gao. Quantum-defect theory of atomic collisions and molecular vibration spectra. *Phys.*

- Rev. A*, 58:4222, 1998.
- [286] H. Fu, Y. Wang, and B. Gao. Beyond the Fermi pseudopotential: A modified Gross-Pitaevskii equation. *Phys. Rev. A*, 67:053612, 2003.
- [287] R. D. Amado and F. C. Greenwood. There Is No Efimov Effect for Four or More Particles. *Phys. Rev. D*, 7:2517, 1973.
- [288] H. W. L. Naus and J. A. Tjon. The Efimov effect in a four-body system. *Few-Body Systems*, 2:121, 1987.
- [289] L. Platter, H. W. Hammer, and U. G. Meissner. Four-boson system with short-range interactions. *Phys. Rev. A*, 70:052101, 2004.
- [290] M. T. Yamashita, L. Tomio, A. Delfino, and T. Frederico. Four-boson scale near a Feshbach resonance. *Europhys. Lett.*, 75:555, 2006.
- [291] H. W. Hammer and L. Platter. Universal properties of the four-body system with large scattering length. *Eur. Phys. J. A*, 32:113, 2007.
- [292] J. von Stecher, J. P. D’Incao, and C. H. Greene. Signatures of universal four-body phenomena and their relation to the Efimov effect. *Nature Phys.*, 5:417, 2009.
- [293] J. P. D’Incao, J. von Stecher, and C. H. Greene. Universal Four-Boson States in Ultracold Molecular Gases: Resonant Effects in Dimer-Dimer Collisions. *Phys. Rev. Lett.*, 103:033004, 2009.
- [294] A. Deltuva. Efimov physics in bosonic atom-trimer scattering. *Phys. Rev. A*, 82:063612, 2010.
- [295] A. Deltuva. Shallow Efimov tetramer as inelastic virtual state and resonant enhancement of the atom-trimer relaxation. *EPL*, 95:43002, 2011.
- [296] F. Ferlaino, S. Knoop, M. Berninger, W. Harm, J. P. D’Incao, H.-C. Nägerl, and R. Grimm. Evidence for Universal Four-Body States Tied to an Efimov Trimer. *Phys. Rev. Lett.*, 102:140401, 2009.
- [297] G. J. Hanna and D. Blume. Energetics and structural properties of three-dimensional bosonic clusters near threshold. *Phys. Rev. A*, 74:063604, 2006.
- [298] J. von Stecher. Weakly bound cluster states of Efimov character. *J. Phys. B*, 43:101002, 2010.
- [299] M. T. Yamashita, D. V. Fedorov, and A. S. Jensen. Universality of Brunnian (N-body Borromean) four- and five-body systems. *Phys. Rev. A*, 81:063607, 2010.
- [300] H. Heiselberg, C. J. Pethick, H. Smith, and L. Viverit. Influence of Induced Interactions on the Superfluid Transition in Dilute Fermi Gases. *Phys. Rev. Lett.*, 85:2418, 2000.
- [301] C. Honerkamp and W. Hofstetter. BCS pairing in Fermi systems with N different hyperfine states. *Phys. Rev. B*, 70:094521, 2004.
- [302] H. Zhai. Superfluidity in three-species mixtures of Fermi gases across Feshbach resonances. *Phys. Rev. A*, 75:031603(R), 2007.
- [303] T. Paananen, P. Törmä, and J.-P. Martikainen. Coexistence and shell structures of several superfluids in trapped three-component Fermi mixtures. *Phys. Rev. A*, 75:023622, 2007.
- [304] R. W. Cherng, G. Refael, and E. Demler. Superfluidity and magnetism in multicomponent ultracold fermions. *Phys. Rev. Lett.*, 99:130406, 2007.
- [305] D. Blume, S. T. Rittenhouse, J. von Stecher, and C. H. Greene. Stability of inhomogeneous multicomponent Fermi gases. *Phys. Rev. A*, 77:033627, 2008.
- [306] J. P. Gaebler, J. T. Stewart, J. L. Bohn, and D. S. Jin. p -Wave Feshbach Molecules. *Phys. Rev. Lett.*, 98:200403, 2007.
- [307] J. Levinsen, N. R. Cooper, and V. Gurarie. Strongly Resonant p -Wave Superfluids. *Phys. Rev. Lett.*, 99:210402, 2007.
- [308] J. Levinsen, N. R. Cooper, and V. Gurarie. Stability of fermionic gases close to a p -wave Feshbach resonance. *Phys. Rev. A*, 78:063616, 2008.
- [309] M. Jona-Lasinio, L. Pricoupenko, and Y. Castin. Three fully polarized fermions close to a p -wave Feshbach resonance. *Phys. Rev. A*, 77:043611, 2008.
- [310] J. P. D’Incao, B. D. Esry, and C. H. Greene. Ultracold atom-molecule collisions with fermionic atoms. *Phys. Rev. A*, 77:052709, 2008.
- [311] C. Ticknor and S. T. Rittenhouse. Three Body Recombination of Ultracold Dipoles to Weakly Bound Dimers. *Phys. Rev. Lett.*, 105:013201, 2010.
- [312] Y. Wang, J. P. D’Incao, and C. H. Greene. Efimov Effect for Three Interacting Bosonic Dipoles. *Phys. Rev. Lett.*, 106:233201, 2011.
- [313] C. Mora, R. Egger, and A. O. Gogolin. Three-body problem for ultracold atoms in quasi-one-dimensional traps. *Phys. Rev. A*, 71:052705, 2005.
- [314] C. Mora, A. Komnik, R. Egger, and A. O. Gogolin. Four-Body Problem and BEC-BCS Crossover in a Quasi-One-Dimensional Cold Fermion Gas. *Phys. Rev. Lett.*, 95:080403, 2005.
- [315] Y. Nishida and S. Tan. Universal Fermi Gases in Mixed Dimensions. *Phys. Rev. Lett.*,

- 101:170401, 2008.
- [316] G. Lamporesi, J. Catani, G. Barontini, Y. Nishida, M. Inguscio, and F. Minardi. Scattering in Mixed Dimensions with Ultracold Gases. *Phys. Rev. Lett.*, 104:153202, 2010.
 - [317] S. Will, T. Best, U. Schneider, L. Hackermüller, D.-S. Lühmann, and I. Bloch. Time-resolved observation of coherent multi-body interactions in quantum phase revivals. *Nature (London)*, 465:197, 2010.
 - [318] S. Will, T. Best, S. Braun, U. Schneider, and I. Bloch. Coherent Interaction of a Single Fermion with a Small Bosonic Field. *Phys. Rev. Lett.*, 106:115305, 2011.
 - [319] O. E. Alon, A. I. Streltsov, and L. S. Cederbaum. Multiconfigurational time-dependent Hartree method for bosons: Many-body dynamics of bosonic systems. *Phys. Rev. A*, 77:033613, 2008.
 - [320] G. Vidal. Efficient Classical Simulation of Slightly Entangled Quantum Computations. *Phys. Rev. Lett.*, 91:147902, 2003.
 - [321] U. Schollwöck. The density-matrix renormalization group. *Rev. Mod. Phys.*, 77:259, 2005.
 - [322] B. Bauer1, L. D. Carr, H. G. Evertz, A. Feiguin, J. Freire, S. Fuchs, L. Gamper, J. Gukelberger, E. Gull, S. Guertler, A. Hehn, R. Igarashi, S. V. Isakov, D. Koop, P. N. Ma, P. Mates, H. Matsuo, O. Parcollet, G. Pawłowski, J. D. Picon, L. Pollet, E. Santos, V. W. Scarola, U. Schollwöck, C. Silva, B. Surer, S. Todo, S. Trebst, M. Troyer, M. L. Wall, P. Werner, and S. Wessel. The ALPS project release 2.0: open source software for strongly correlated systems. *J. Stat. Mech.*, 2011:P05001, 2011.
 - [323] S. Zöllner, H.-D. Meyer, and P. Schmelcher. Few-Boson Dynamics in Double Wells: From Single-Atom to Correlated Pair Tunneling. *Phys. Rev. Lett.*, 100:040401, 2008.
 - [324] P. Dyke, E. D. Kuhnle, S. Whitlock, H. Hu, M. Mark, S. Hoinka, M. Lingham, P. Hannaford, and C. J. Vale. Crossover from 2D to 3D in a Weakly Interacting Fermi Gas. *Phys. Rev. Lett.*, 106:105304, 2011.
 - [325] J. P. D’Incao, H. Suno, and B. D. Esry. Limits on Universality in Ultracold Three-Boson Recombination. *Phys. Rev. Lett.*, 93:123201, 2004.
 - [326] D. C. McKay and B. DeMarco. Cooling in strongly correlated optical lattices: prospects and challenges. *Rep. Prog. Phys.*, 74:054401, 2010.